

1-1-2008

Experimental and theoretical control of a smart projectile fin using piezoelectric bimorph actuator

Venkat R Mudupu

University of Nevada, Las Vegas

Follow this and additional works at: <https://digitalscholarship.unlv.edu/rtds>

Repository Citation

Mudupu, Venkat R, "Experimental and theoretical control of a smart projectile fin using piezoelectric bimorph actuator" (2008). *UNLV Retrospective Theses & Dissertations*. 2849.

<http://dx.doi.org/10.25669/47i6-4jr2>

This Dissertation is protected by copyright and/or related rights. It has been brought to you by Digital Scholarship@UNLV with permission from the rights-holder(s). You are free to use this Dissertation in any way that is permitted by the copyright and related rights legislation that applies to your use. For other uses you need to obtain permission from the rights-holder(s) directly, unless additional rights are indicated by a Creative Commons license in the record and/or on the work itself.

This Dissertation has been accepted for inclusion in UNLV Retrospective Theses & Dissertations by an authorized administrator of Digital Scholarship@UNLV. For more information, please contact digitalscholarship@unlv.edu.

EXPERIMENTAL AND THEORETICAL CONTROL OF A SMART
PROJECTILE FIN USING PIEZOELECTRIC BIMORPH
ACTUATOR

by

Venkat R. Mudupu

Bachelor of Technology
Jawaharlal Nehru Technological University, India
2001

Master of Science
Osmania University, India
2004

A dissertation submitted in partial fulfillment
of the requirements for the

Doctor of Philosophy Degree in Mechanical Engineering
Department of Mechanical Engineering
Howard R. Hughes College of Engineering

Graduate College
University of Nevada, Las Vegas
December 2008

UMI Number: 3352181

INFORMATION TO USERS

The quality of this reproduction is dependent upon the quality of the copy submitted. Broken or indistinct print, colored or poor quality illustrations and photographs, print bleed-through, substandard margins, and improper alignment can adversely affect reproduction.

In the unlikely event that the author did not send a complete manuscript and there are missing pages, these will be noted. Also, if unauthorized copyright material had to be removed, a note will indicate the deletion.

UMI[®]

UMI Microform 3352181

Copyright 2009 by ProQuest LLC.

All rights reserved. This microform edition is protected against unauthorized copying under Title 17, United States Code.

ProQuest LLC
789 E. Eisenhower Parkway
PO Box 1346
Ann Arbor, MI 48106-1346



Dissertation Approval
The Graduate College
University of Nevada, Las Vegas

November 13, 2008

The Dissertation prepared by

Venkat R. Mudupu

Entitled

Experimental and Theoretical Control of a Smart Projectile
Fin Using Piezoelectric Bimorph Actuator

is approved in partial fulfillment of the requirements for the degree of

Doctor of Philosophy in Engineering

Examination Committee Co-Chair

Examination Committee Member

Examination Committee Member

Examination Committee Member

Graduate College Faculty Representative

Examination Committee Chair

Dean of the Graduate College

ABSTRACT

Experimental and Theoretical Control Of A Smart Projectile Fin Using Piezoelectric Bimorph Actuator

by

Venkat R. Mudupu

Woosoon Yim, Examination Committee Chair
Professor of Mechanical Engineering
University of Nevada, Las Vegas

and

Mohamed B. Trabia, Examination Committee Chair
Professor of Mechanical Engineering
University of Nevada, Las Vegas

The goal of this work is to develop efficient control algorithms for the control of a smart projectile fin. Smart fins are deployed as soon as the projectile reaches the apogee and are used to steer the projectile towards its target by controlling the rotation angle of the fin. The fin is actuated using the piezoelectric macro-fiber composite (MFC) bimorph actuator which is completely enclosed within the aero-shell. The actuator is composed of two Macro Fiber Composites (MFC's), manufactured by Smart Material Co. The presented smart fin design minimizes the volume and weight of the unit.

Two different models of the smart fin are developed. One is mathematical model that uses finite element approach to describe dynamics of the smart fin system. This model includes the aerodynamic moment which is a function of the angle of attack of the projectile. Second model is based on system identification approach. A linear model of the actuator and fin is identified experimentally by exciting the system using a chirp signal. Comparison is done

between these two models based on open-loop step response of the smart fin system.

In this dissertation, five kinds of control systems based on fuzzy logic, inverse dynamics and adaptive structure theory are developed. The aerodynamic disturbances and parameter uncertainties are considered in these controllers. The simulation results illustrate that asymptotic trajectory tracking of the fin angle is achieved, in spite of uncertainties in the system parameters and presence of aerodynamic disturbance. A prototype model of the projectile fin is developed in the laboratory for real-time control. The designed controllers are validated using the subsonic wind tunnel at University of Nevada, Las Vegas (UNLV) for various wind speeds. Experimental results show that the designed controllers accomplish fin angle control.

TABLE OF CONTENTS

ABSTRACT	iii
LIST OF FIGURES	viii
LIST OF TABLES	ix
ACKNOWLEDGMENTS	x
CHAPTER 1 INTRODUCTION	1
1.1 Review of Literature	2
1.2 Objectives of Research Work	10
1.3 Overview of the Dissertation	11
CHAPTER 2 PIEZOELECTRIC MACRO FIBER COMPOSITE ACTUATOR	13
2.1 Macro Fiber Composite	13
2.2 Bimorph Actuator: Principle of Operation	14
2.2.1 Mechanics of Bimorph Actuator	15
2.3 Configurations of MFC Actuator	16
CHAPTER 3 CONFIGURATION OF SMART FIN	19
3.1 Configuration	19
3.2 Prototype of Smart Fin	19
3.3 Encoder	20
3.4 Test Setup	21
CHAPTER 4 MODEL DEVELOPMENT	25
4.1 Mathematical Model	26
4.1.1 Finite Element Approach	26
4.1.2 Aerodynamic Moment	31
4.2 Model Identification	34
4.3 Comparison: Mathematical Model and Identified Model	36
CHAPTER 5 FUZZY LOGIC CONTROL	38
5.1 A Structure for the Fuzzy Logic Controller	38
5.2 GA-Based Fuzzy Logic Control	38
5.2.1 Rules for the Controller	39
5.2.2 Tuning of the Fuzzy Controller Using Genetic Algorithm	40
5.2.3 Tuning the Smart Fin Fuzzy Controller Using Hybrid Fuzzy Simplex Genetic Algorithm (HFSGA)	43

5.2.4	Simulation Results	44
5.2.5	Experimental Results	44
5.2.6	Conclusions	47
5.3	Inverse Dynamics based Fuzzy Controller	48
5.3.1	Rules for the Fuzzy Logic Controller	48
5.3.2	Gaussian Membership Functions	49
5.3.3	Defining the Ranges of the Variables using Inverse Dynamics	51
5.3.4	Simulation Example	56
5.3.5	Robustness of the Controller	59
5.3.6	Conclusions	59
CHAPTER 6 ADAPTIVE CONTROL		67
6.1	State Variable Representation	67
6.2	Adaptive Control: Nussbaum Gain Based	69
6.2.1	Control Law	69
6.2.2	Digital Simulation Results	75
6.2.3	Experimental Results	76
6.2.4	Summary: Digital Simulation Results and Wind Tunnel Test Results	80
6.2.5	Conclusions	80
6.3	Adaptive Control: Servoregulator	81
6.3.1	Control Law	82
6.3.2	Simulation Results	87
6.3.3	Experimental Results	88
6.3.4	Conclusions	89
6.4	Adaptive Control: Fin Angle Feedback	89
6.4.1	Control Law	90
6.4.2	Simulation Results	97
6.4.3	Experimental Results	98
6.4.4	Conclusions	100
CHAPTER 7 SALIENT FEATURES OF DEVELOPED ALGORITHMS		101
7.1	Comparative Analysis of the Fin Angle Response of Fuzzy Logic and Adaptive Controllers	103
CHAPTER 8 CONCLUSIONS		106
CHAPTER 9 FUTURE WORK		109
BIBLIOGRAPHY		111
VITA		116

LIST OF FIGURES

1.1	Schematic of a Projectile with Smart Fin	10
1.2	Smart Fin Components	11
2.1	Layers of Macro-Fiber Composite [54]	14
2.2	Arrangement of Electrodes in d_{33} MFC Actuator [56]	14
2.3	Cross-section of the Piezoelectric Bimorph Actuator	15
2.4	Cross-section of the Piezoelectric Bimorph Actuator without substrate	16
2.5	Various MFC Actuator configurations	17
3.1	Schematic Diagram of the Smart Fin	20
3.2	Piezoelectric Bimorph Actuator	20
3.3	Smart Fin Prototype	21
4.1	Hinge location and Schematic of tapered fin	26
4.2	Canard normal force versus canard deflection angle, Mach 0.5, $-10^\circ \leq \alpha \leq 10^\circ$	27
4.3	Canard hinge moment versus canard deflection angle, Mach 0.5, $-10^\circ \leq \alpha \leq 10^\circ$	29
4.4	Excitation Signal	31
4.5	Fin Angle Output	32
4.6	Zoomed view of 4.4 and 4.5	34
4.7	Bode plot of the identified smart fin model	35
4.8	Comparison between measured and simulated data	36
4.9	Open-loop Step Response of Smart Fin	37
5.1	Structure of the Smart Fin Fuzzy Logic Controller	39
5.2	Block Diagram of the Algorithm used for Tuning Membership functions of Fuzzy Controllers	40
5.3	Membership Functions, e_β	41
5.4	Membership Functions, $e_{d\beta}$	42
5.5	Membership Functions, Δu	43
5.6	Surface of the Fuzzy Output Variables, Δu	44
5.7	Simulated Fin Angle Response	45
5.8	Simulated Effective Voltages to the MFC's	46
5.9	Fin Angle Response under No-Wind Conditions	47
5.10	Effective Voltages to the MFC's under No-Wind Conditions	48
5.11	Top View of the Disturbance Test Setup	49
5.12	Fin Angle Response under Disturbance	50
5.13	Effective Voltages to the MFC's under Disturbance	51
5.14	Fin Angle Response at Angle of Attack 0° and 40.23 m/s Wind Velocity	52
5.15	Effective Voltage to the MFC's under Angle of Attack 0° and 40.23 m/s Wind Velocity	53
5.16	Fin Angle Response under negative Angles of Attack and 40.23 m/s Wind Velocity	54

5.17	Effective Voltage to the MFC's under negative Angles of Attack and 40.23 m/s Wind Velocity	55
5.18	Fin Angle Response under positive Angles of Attack and 40.23 m/s Wind Velocity	56
5.19	Effective Voltage to the MFC's under positive Angles of Attack and 40.23 m/s Wind Velocity	57
5.20	Membership Functions of Δu	58
5.21	Control Surface Case C	59
5.22	Control Surface Case F	60
5.23	Results for Case C	61
5.24	Results for Case F	62
5.25	Results for Case C (Length of fifth element=10 mm)	63
5.26	Results for Case C when Subjected to External Disturbance	64
6.1	Structure of the Adaptive Control System	70
6.2	Fin Angle= -2° , Angle of Attack= 5°	77
6.3	Fin Angle= -2° , Angle of Attack= -5°	78
6.4	Experimental Results at zero Wind Speed	80
6.5	Fin Angle Response under Various Angles of Attack at Wind Speed 13.4 m/s .	81
6.6	Structure of the Adaptive Servoregulator	82
6.7	Simulation Results at zero Wind Speed	87
6.8	Experimental Results at zero Wind Speed	89
6.9	Fin Angle Response under Various Angles of Attack at Wind Speed 40.23 m/s	90
6.10	Effective Voltages to the MFC's under positive Angles of Attack and 40.23 m/s Wind Velocity	91
6.11	Simulated Fin Angle Response under no disturbance	93
6.12	Simulated Fin Angle Response at Angle of Attack= -5°	95
6.13	Fin Angle Response under No-Wind Conditions	96
6.14	Fin Angle Response under Various Angles of Attack at Wind Speed 40.23 m/s	97
6.15	Effective Voltage to the MFC's under various Angles of Attack and 40.23 m/s Wind Velocity	98
6.16	Comparison: Fin Angle Responses at No Disturbance	99
7.1	Fin Angle Responses for the Controllers (FLC-GA, Adaptive Servo, Adaptive Feedback) for Various Angles of Attack ($\alpha = 0^\circ, -5^\circ, -10^\circ$) at 40.23 m/s Wind Velocity	104
9.1	Hysteresis of smart fin. The plot shows sinusoidal response of the System with 0.5Hz frequency voltage signal	110

LIST OF TABLES

3.1	Characteristics of the Piezoelectric Bimorph Actuator	24
4.1	Characteristics of the Excitation Signal	37
5.1	Rules for the fin fuzzy controller	60
5.2	Rules for the fin fuzzy controller	65
5.3	Characteristics of the Smart Fin Actuator	65
5.4	Characteristics of the Glass Fiber	65
5.5	Typical Case Studies	65
5.6	Results of the Case Studies	66

ACKNOWLEDGMENTS

I would like to thank my advisors, Dr. Woosoon Yim and Dr. Mohamed B. Trabia, for all their help and support in my pursuit of a Doctorates degree. Throughout this process they have provided support and encouragement in my research and my studies. Their advice and their enthusiasm were critical to the success of this effort. I would also like to thank Dr. Sahjendra N. Singh for serving on my advisory committee, as well as his help, advice and guidance during my dissertation work.

I would also like to thank Dr. Brenden J. O'Toole, Dr. George F. Mauer, Dr. Samir Moujaes for their time in reviewing the prospectus, participation of defense, and counseling of the thesis as the committee members.

I thank Jan Kunzmann and Thomas Daue, Smart Material Co., for their help for providing more information on MFC actuator during my research work. A special thanks to them for their patience to answer my emails.

I would also like to thank Mr. Vijay Vatti whose suggestions and advices have been great help for me. Vijay is an individual with highly talented; he can motivate other individuals and I am so proud to have a friend like him.

I would also like to express my heartiest gratitude to my parents and my fiancée, Swetha, for their unconditional support, love, and affection. A special thanks to my friends Shivakanth Gutta, Jagadeep Thota, Venkat Kondur, Madhavan, Kumarswamy Karpanan, Sreenivas Kohir, Srujan Sridharala, Kiran Kondal, Harish Gona, Arun Toomu and Vinod K. Chakka for their unrelenting support and motivation throughout this research activity.

The financial support provided by the Army Research laboratory (ARL), under project SM2 is thankfully acknowledged.

Finally, I would like to thank Joan Conway, staff of the Mechanical Engineering department, for providing me with all resources for my defence.

CHAPTER 1

INTRODUCTION

The use of smart materials has become commonly accepted for the actuation and control of a broad range of structural elements. Once the smart material is embedded or mounted on the outer surface of the host structure, it provides the ability of electrically sensing or inducing strains via the piezoelectric effect. The combination of the sensing and the actuating abilities yields an 'intelligent' structure that can both evaluate its structural state and response with an adequate actuation. This feature makes the intelligent structure an attractive solution to applications associated with dynamic actuation, vibration control, or attenuation of acoustical noise, as well as applications that involve deflection control of structural elements such as beams, plates, or shells.

The advantages of using smart materials in such applications are mainly due to their dual structural functioning. On one hand, the smart material functions as an embedded actuator that responds to electric loads and generate strains, deformations, and forces. On the other hand, it functions as an integrated part of the structural skeleton and contributes to the mechanical load carrying mechanism. This advantage is even more significant in the design and construction of subscale aircraft such as unmanned aerial vehicles, small missiles, guided munitions, and projectiles. In these cases, the active structural skeleton avoids the usage of servomotors, force transmissions, or hydraulic systems, saves the space required for installation of these systems, and reduces the overall weight of the vehicle.

For conventional projectiles, electric or hydraulic actuators are mounted inside the projec-

tile fuselage to activate the aerodynamic control surfaces. These internally mounted actuators occupy considerable volume which otherwise can be used for payload or additional fuel. Reducing the size of the internal actuators and hence lowering the total actuator weight may improve the overall performance of projectile significantly. The goal of this research is to develop a light-weight, low cost smart missile fin capable of surviving the subsonic operating environment while providing necessary performance comparable to existing projectile fins.

The use of intelligent materials in aircraft structural elements mainly focuses on bending or twisting actuation of the structural skeleton of wings, fins, canards, stabilizers, or rotor blades. Piezoelectric twist actuation that is based on anisotropic straining of the host structure can be achieved using directionally attached isotropic actuators or, alternatively, using piezoelectric fibers integrated into the composite structural member. The smart material actuator concept allows the actuator to be incorporated into the control surface structure minimizing volume intrusion and weight within the munition body. Over the past several years, several design concepts have been developed and analyzed and limited bench top testing has been performed. Based on success of previous work, recently, the development of a smart fin has been considered.

The goal of this work is to enhance accuracy of extend range of smart munitions and guided projectiles by providing real-time servo control capability of smart fin on a projectile airframe.

1.1 Review of Literature

The use of surface-mounted or bonded piezoelectric actuators for shape control of intelligent structures has increased due to the low-cost and flexibility of a new generation of composite piezoelectric actuators. Piezoelectric fiber composite actuators were originally de-

veloped as a means of overcoming many of the practical difficulties associated with using monolithic piezoceramic actuators in structural control applications [1]. These actuators use inter-digitated electrodes for poling and subsequent actuation of an internal layer of machined piezoceramic fibers. The fiber sheets are formed from monolithic piezoceramic wafers and conventional computer-controlled wafer-dicing methods. This actuator retains most of the advantageous features of the early piezocomposite actuators, namely, high strain energy density, directional actuation, conformability and durability, yet incorporates several new features, chief among these being the use of low-cost fabrication processes that are uniform and repeatable. The complete delineation of the piezoelectric actuator used in this work can be found in [2].

The use of piezoceramic (PZT) elements as sensors and actuators to control the deflection of the centroid of a rectangular plate suddenly subjected to a uniformly distributed load is studied in [3].

The most current trends in piezoelectric actuation architectures have been discussed in [4]. A new integrated grasping tool for minimally invasive surgery has been designed consisting of two piezoelectric bimorph actuators in [5]. The design of a novel smart actuator with controllable characteristics based on a magnetorheological elastomer (MRE) is introduced in [6]. This actuator is composed of a piezoelectric layer bonded cantilever, whose free end is attached to a MRE layer .

A finite element model for the analysis on deflection control of plates with piezoelectric actuators has been presented in [7]. This model includes an eight-node isoparametric plate element with shear deformation, a 16-node adhesive interface element, and a proposed actuator element. The first-order shear deformation theory is used in conjunction with the eight-node isoparametric element in the proposed actuator element. The capability of FE to accurately

model the behavior of two piezoelectric devices is investigated in [8]. In this, the details of how an FE model for piezoelectric material is constructed are explained. Finite-element modeling and design of piezoelectric flap actuators are discussed in [9]. In this work, two different finite element models are developed. One is a beam model that assumes a perfect bond exists between the piezo and shim, and second extends the perfect bond model by incorporating a shear element for the bond layer. Finite element formulations for the modeling of a laminated composite plate with distributed piezoelectric sensors/actuators are presented in [10]. This formulation is based on the first-order shear deformation laminated plate theory. The stiffness and mass effects of the piezoelectric sensors and actuators are also considered in the formulation.

A procedure for modeling structures containing piezoelectric actuators using MSC/NASTRAN and MATLAB is presented in [11]. It also describes the utility and functionality of one set of validated modeling tools. The tools described herein use MSC/NASTRAN to model the structure with piezoelectric actuators and a thermally induced strain to model staining of the actuators due to an applied field. The modeling of a non-symmetric bimorph constituted by a piezoelectric material deposited on an alumina substrate and used either as an actuator or a sensor is presented in [12]. Theoretical modeling based on the flexural modes of the structure is carried out in [12] and the influence of the electrode characteristics (geometrical dimensions and elastic parameters) is introduced in the modeling for calculating the bimorph bending displacement. Piezoelectric heterogeneous bimorphs have extensive applications in the MEMS area. In order to formulate their displacement more conveniently, a concise analytical solution is described in [13]. The method is subsequently shown to be capable of quickly estimating the displacement in a bimorph beam, making it a useful tool for designing piezoelectric structures. The numerical modeling of a plate structure containing

bonded piezoelectric material is described in [14]. In this work, Hamilton's principle is employed to derive the finite element equations using the mechanical energy of the structure and the electrical energy of the piezoelectric material.

The properties of directionally attached piezoelectric (DAP) elements and a low aspect ratio DAP torque-plate wing is investigated in [15]. A servoflap that uses a piezoelectric bender to deflect a trailing edge flap for use on helicopter rotor blade was designed, built, and tested in [16]. This design utilizes a new flexure mechanism to connect the piezoelectric bender to the control surface. The preliminary design of aeroelastically tailored adaptive missile fins for supersonic speeds is presented in [17]. A systematic approach for the design of a active piezoelectric fins developed for a small-scale flight vehicle is presented in [18]. This proposed design approach uses analytical and computational tools that are based on the high-order theory and provides a graphical representation of the response spectrum of the active fin. A numerical study of a twist-actuated smart fin is also presented. An experimental, theoretical and computational evaluation of a remote control morphing wing aircraft using smart materials is discussed in [19]

A position tracking control of a smart flexible structure with a piezo film actuator is presented in [20]. The research presented in [21] includes robust force tracking control of a flexible gripper driven by piezoceramic actuator characterizing its durability and quick response time. A new type of an optical pick-up for CD-RIM drive feeding system is proposed in [22]. This optical pick-up is activated by a pair of bimorph piezoceramic actuators in order to achieve fine motion control of the objective lens. Following the derivation of the governing equation of motion, a control model, which takes into account the hysteresis behavior of the actuator and also parameter variation such as frequency changes, is established in a state space form. A robust controller is then formulated and experimentally realized.

A new tracking control method for piezoelectric actuators is dealt in [23]. When actuating in an open-loop manner, in order to compensate for the creep effect of the piezoelectric transducer as well as hysteresis, a new concept of 'voltage creep' is proposed. Finally, a tracking control experiment of piezoelectric actuators for an arbitrary desired trajectory is performed giving greatly improved results compared to other open-loop actuating methods. Genetic algorithm is used to optimize the membership functions of a fuzzy logic controller for smart structure systems. The effectiveness of the genetic algorithm is demonstrated with a cantilever beam attached with piezoelectric materials in [24]. An active flow control concept utilizing miniature deployable structures for advanced weapons control is presented in [25]. The ultimate goal is to provide pitch and yaw control to weapons (slender bodies) that operate at low angles of attack, where the baseline control is primarily provided by tail-fins. The analysis of a closed-loop control law for vibration reduction in helicopter blades using piezoelectric fiber composites that provide both bending and torsional actuation capabilities is presented in [26]. A simple aeroelastic model incorporating lead-lag, flapping and torsional degrees of freedom is chosen to evaluate a reduced-state sequential velocity feedback law.

Lyapunov's second method for distributed-parameter systems was used to design a control algorithm for the damper in [27]. The study in [28] deals with the utilization of piezoelectric actuators in controlling the structural vibrations of the flexible beams. A Modified Independent Modal Space Control (MIMSC) method is presented to select the optimal location, control gains and excitation voltage of the piezoelectric actuators.

The fuzzy-logic based vibration suppression control of active structures equipped with piezoelectric sensors and actuators is discussed in [29]. The control methodology is based on the fuzzy logic control of the variable structure system type. A neural network control system based on experimental data was designed and simulated for vibration suppression of a flexible

fin with piezoelectric actuators in [30].

An adaptive force trajectory control of a flexible beam using a piezoceramic actuator is discussed in [31]. An adaptive control scheme based on a fuzzy-logic algorithm and its application in vibration suppression of smart structures is discussed in [32]. Here, a fuzzy-based adaptive controller is considered due to its simplicity and the fact that it does not require expression of the controller in terms of the system parameters, as is necessary in the case of self-tuning regulators.

Active control via fuzzy logic is assessed as a means to suppress the elastic transverse bending vibration of a slider crank mechanism in [33]. Several pairs of piezoelectric elements are used to provide the control action. Sensor output of deflection is fed to the fuzzy controller, which determines the voltage input to the actuator. A three mode approximation is utilized in the simulation study. Computer simulation shows that fuzzy control can be used to suppress bending vibrations at high speeds. A new discrete-time, fuzzy-sliding-mode controller with application to vibration control of a smart structure featuring a piezofilm actuator is presented in [34]. The investigation in [35] deals with the application of an Adaptive Fuzzy Control Algorithm for active vibration control of an experimental flexible beam. However, the uniqueness of this approach is that the damping parameters of the emulated absorber are continuously varied by means of a fuzzy logic control algorithm to provide near minimum-time suppression of vibration. It is demonstrated that application of this methodology allows for its real-time implementation and provides relatively quick settling times in the closed-loop. In [36], the shape control of curved beams using symmetric surface bonded piezoelectric actuators, excited out of phase, is studied. To predict the deflections accurately, a finite element model using a three-noded isoparametric curved beam element has been implemented. To model the piezoelectric layers, coupled finite element equations have been used and solved

using iterative approach.

Fuzzy logic based velocity feedback control for active vibration control of beams is presented in [37]. The controller is first developed for a single degree of freedom spring mass system. Rule base consisting of three simple rules based on velocity is used. The feasibility of using piezoelectric actuator and fuzzy logic control to create a smart fin is thoroughly studied in [38]. Most of the fuzzy logic controllers proposed in most of these publications are valid only for specific system parameters and/or motion variables. This is obviously a severe restriction on general implementation of these controllers since extensive re-tuning will be required whenever there is a change in the specifications of the fin, actuator, and/or motion parameters. A novel hybrid genetic algorithm that has the ability of the genetic algorithms to avoid being trapped at local minimum while accelerating the speed of local search by using the fuzzy simplex algorithm is developed in [39]. The new algorithm is labeled the hybrid fuzzy simplex genetic algorithm (HFSGA). [40] proposes to replace fixed parameters of search strategy by adaptive ones to make the search more responsive to changes in the problem by incorporating fuzzy logic in optimization algorithms. The proposed ideas are used to develop a new adaptive form of the simplex search algorithm whose objective is to minimize a function of n variables. The new algorithm is labeled Fuzzy Simplex. The search starts by generating a simplex with $n + 1$ vertices. The algorithm then repeatedly replaces the point with the highest function value by a new point. This process has three components: reflecting the point with the highest function value, expanding, and contracting the simplex. These operations use fuzzy logic controllers whose inputs incorporate the relative weights of the functions values at the simplex points. Genetic Algorithms (GAs) have been successfully used to eliminate the vibration of beams and plates by several investigators. In addition to proposing fuzzy rules and formulas for spacing the fuzzy variables, [41] also presents a novel method for calculating

the ranges of the variables of the controller based on the inverse dynamics of the smart fin and the parameters of its desired motion. The proposed control strategy can thus be easily modified to work with any modification of desired or system parameters.

The feasibility of using smart material to control the rotation angle of a subsonic projectile fin during flight is studied in [42]. A feedback linearizing adaptive control system is designed for the trajectory control of the fin angle. The controller consists of an inverse system and a high-gain observer. Simulation results are presented which show the fin control is accomplished in spite of uncertainties in the system. The necessary development of systematic modeling and design tools for the active control of large space structures (LSS) that has occurred over the past decade is focussed in [43]. First reviewed are the aspects of the model formulation, model implication, and system identification that form the basis for the control design activities.

The models of flexible structures are generally obtained by solving the eigenvalue problem resulting from finite element methods. However, it is well known that the resulting fidelity of model parameters degrades drastically for higher modes. Researchers have considerable effort to design controllers for the control of flexible structures. A good review of literature is provided in [43] in which readers will find several references for controller designs. For flexible structures, controller designs based on feedback linearization, passivity concepts and adaptive techniques have been attempted by [44], [45], [46], [47], [48], [49]. An adaptive controller has been designed in [50], based on command generator tracker concept. In order to synthesize of this controller, adaptive loop tunes three parameters and requires sigma or dead-zone modification of the adaptation rule in order to avoid parameter divergence. Modifying the adaptation law may give terminal tracking error.

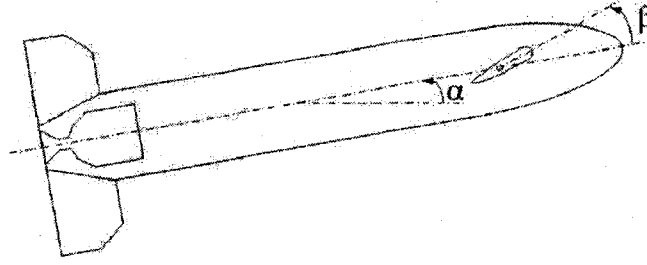


Figure 1.1: Schematic of a Projectile with Smart Fin

1.2 Objectives of Research Work

The U.S. Army Research Laboratory is investigating the feasibility of smart materials for use as actuators and/or aerodynamic control surfaces for smart munition guidance and control. The smart material actuator concept allows the actuator to be incorporated into the control surface structure minimizing volume intrusion and weight within the munition body. The performance of a smart materials canard actuator has been investigated using a multi-disciplinary design approach.

A schematic of a projectile with a smart fin is shown in Fig. 1.1. The smart fins are deployed as soon as the projectile reaches the apogee. These fins are used to steer the projectile toward its target. The smart fin contains a rigid hollow aero-shell that rotates about a rotational hinge that is attached to the projectile body and smart fin as shown in Fig. 1.2, [51] and [52]. The hinge is strategically located to minimize the hinge moments.

The specific objectives of this research work are:

- to obtain a swing angle of ± 10 degrees of smart fin.
- to develop efficient control algorithms to control the rotation angle of the smart fin.
- to validate the developed control algorithms at different angle of attack and for different wind speed.

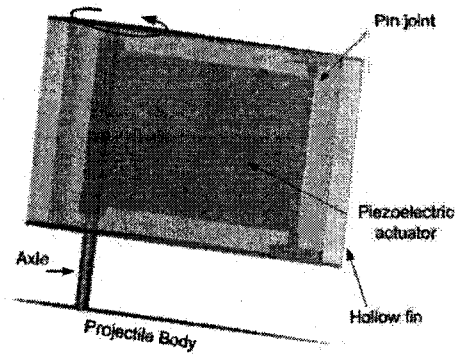


Figure 1.2: Smart Fin Components

1.3 Overview of the Dissertation

This dissertation is organized as follows to present the details of design, dynamic modeling, development, and validation of the control algorithms for a smart projectile fin and conclusions of the current research.

Chapter 2 provides an introduction to piezoelectric macro fiber composite(MFC) actuator and different configurations of the actuator which is used in this work. This chapter also includes the mechanics of the actuator.

Chapter 3 presents the configuration of the smart fin. It also includes experimental setup for the real-time tests in the laboratory and in the subsonic wind tunnel.

Chapter 4 discusses two different ways of modeling of smart fin system. One is based on finite element approach. This model also includes aerodynamic moment which is based on CFD analysis in [53]. Second model is based on experimental data using MATLAB System Identification Techniques. The obtained linear model is compared with the mathematical model.

Chapter 5 describes two kinds of fuzzy logic controllers for the smart fin. The results are

also included in this chapter. This chapter also includes a method for tuning the controller using a hybrid fuzzy simplex genetic algorithm and defining the ranges of the variables using inverse dynamics.

Chapter 6 provides three different adaptive controllers, which are used to control the rotation angle of the smart fin. Simulation results are presented in this chapter along with experimental validation done using the subsonic wind tunnel.

The salient features of developed control algorithms are discussed in Chapter 7. Conclusions of the present work are summarized in Chapter 8 and some recommendations for future work are discussed in Chapter 9.

CHAPTER 2

PIEZOELECTRIC MACRO FIBER COMPOSITE ACTUATOR

2.1 Macro Fiber Composite

The Macro Fiber Composite (MFC) was developed at NASA Langley Research Center [2]. The MFC is layered, planar actuation device that employs rectangular cross-section, unidirectional piezoceramic fibers (PZT 5A) embedded in a thermosetting polymer matrix. This active, fiber reinforced layer is then sandwiched between copper-clad Kapton film layers that have an interdigitated electrode pattern. Figure 2.1 shows an exploded view of the MFC layers, where the PZT fibers are aligned in the 3-direction and the copper electrode fingers are parallel to 1-direction, according to standard piezoelectric notation [54].

A comprehensive manufacturing manual for the MFC can be found in [2]. The in-plane poling and subsequent voltage actuation allows the MFC to utilize the d_{33} piezoelectric effect, Fig. 2.2, which is much stronger than the d_{31} effect used by traditional PZT actuators with through-the-thickness poling [55]. MFC has a uniform geometry, including PZT fiber and electrode spacing and continuity, as well as the absence of air voids or particulate inclusions. The use of rectangular fibers also promotes improved contact between the piezoceramic and adjacent electrode finger, thus ensuring more efficient transfer of electric field into the fibers.

There has been extensive analytical and experimental research focused on utilizing MFC as an actuator (or sensor) for structural control. Applications for the MFC range from vibration reduction to shape-changing structures, from micropositioning to dynamic structural health monitoring or force-sensor applications. The benefits of MFC include flexible, durable,

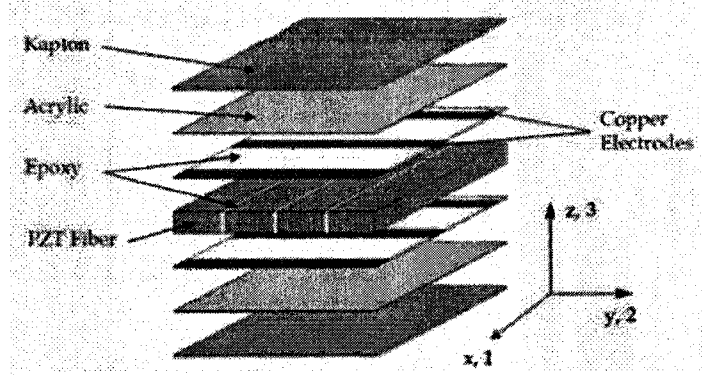


Figure 2.1: Layers of Macro-Fiber Composite [54]

increased strain actuator efficiency, directional actuation/sensing, damage tolerant, conforms to surfaces, readily embeddable, environmentally sealed package, demonstrated performance.

2.2 Bimorph Actuator: Principle of Operation

The piezoelectric bimorph actuator is completely enclosed within the shell. One MFC is activated in tension by applying positive voltage (along the fiber axis) while other MFC is activated in compression by applying negative voltage (against the fiber axis). The tensile and

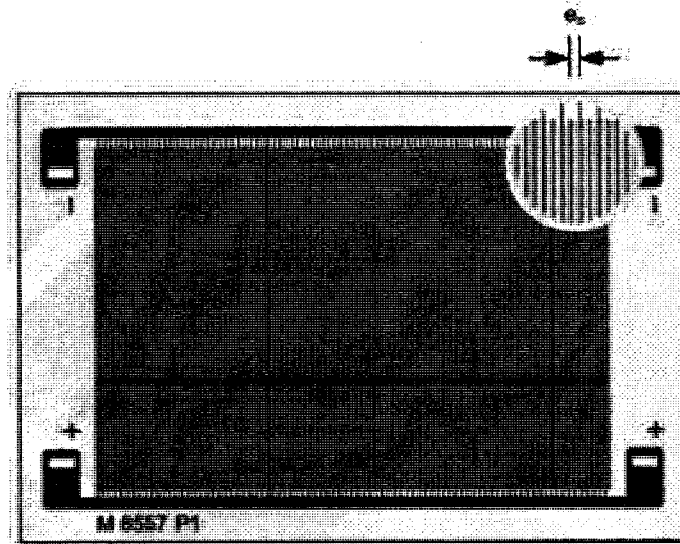


Figure 2.2: Arrangement of Electrodes in d_{33} MFC Actuator [56]

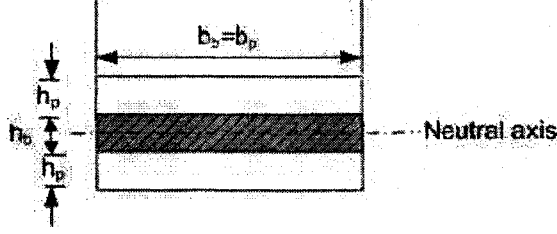


Figure 2.3: Cross-section of the Piezoelectric Bimorph Actuator

compressive strains induce a distributed couple that causes the actuator to bend and rotate the fin at the same time. The fin can be rotated in the opposite direction by changing the polarity of the voltage.

2.2.1 Mechanics of Bimorph Actuator

The strain induced by the bimorph actuator when a control voltage $u(x, t)$ being applied, is given by

$$\varepsilon_p = d_{33}u_f(x, t) \quad (2.1)$$

where ε_p is the piezoelectric strain and d_{33} is the piezoelectric strain constant. $u_f(x, t)$ can be expressed in terms of the voltage applied to the two individual MFC actuators, $u_1(x, t)$ and $u_2(x, t)$, as follows,

$$u_f(x, t) = \frac{u_e(x, t)}{e_s} \quad (2.2)$$

where e_s is the electrode spacing within the actuator and u_e is an effective voltage, which is the average of absolute sum of two individual voltages u_1 and u_2 . The above induced strain generates the bending moment m that is expressed [21] as

$$m = cu_f(x, t) \quad (2.3)$$

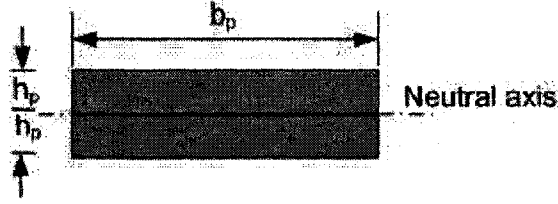


Figure 2.4: Cross-section of the Piezoelectric Bimorph Actuator without substrate

The constant c can be obtained by considering geometrical and mechanical properties of the piezoelectric bimorph actuator. Considering the cross-sectional geometry ,Fig. 2.3, and force equilibrium equation along the axial direction, the constant c can be expressed as [18]

$$c = d_{33} \frac{E_p h_p b_p}{2e_s} (h_p + h_b) \quad (2.4)$$

where E_p is the elastic modulus of the macro fiber composite, h_p is the thickness of MFC, h_b is the thickness of the substrate and b_p is the width of the actuator. The constant c in case of bimorph actuator without substrate is $d_{33} \frac{E_p h_p b_p}{2e_s} h_p$. The cross-section area of the bimorph actuator with no substrate is shown in Fig. 2.4. The analytical deflection of cantilevred piezoelectric bimorph is estimated using the expression

$$\delta = \frac{ML^2}{2EI} \quad (2.5)$$

where L is length of the actuator and EI is the stiffness of the actuator.

2.3 Configurations of MFC Actuator

One of the objectives of this work is to increase the rotation angle of the smart fin or increase the deflection of the actuator. Various configurations of actuator are considered in this work as shown in Figure. 2.5 to increase the deflection of the actuator. Based on analytical

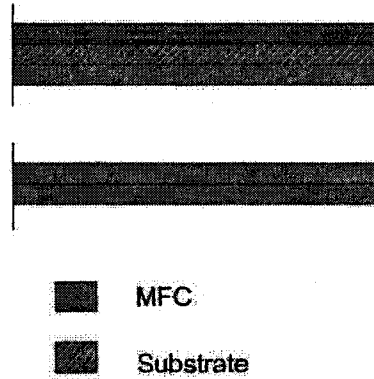
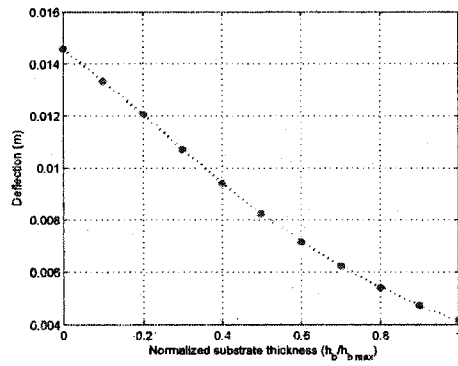
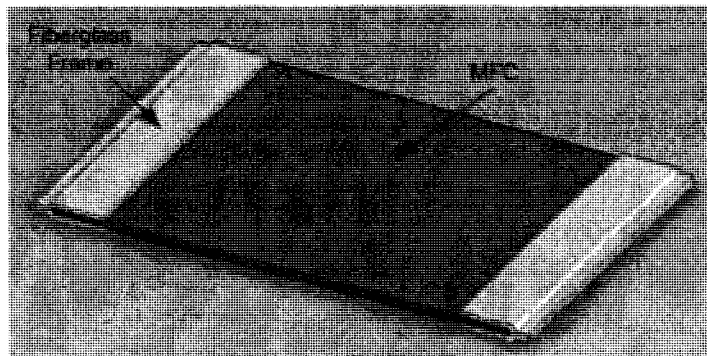


Figure 2.5: Various MFC Actuator configurations

deflection, Eq. 2.5, the effect of substrate on the deflection of actuator is shown in 2.6(a). The maximum thickness value of the substrate is chosen here as 0.5 mm. Earlier studies and analytical solution suggested that using a substrate under two actuators decreases the flexibility, therefore it decreases the fin rotation angle. In this study, it was found that gluing the two MFC's directly increases the resulting displacement of the actuator by reducing its rigidity. The actuators are supported by gluing them to a fiber glass frame at either end of the actuator to mount it within the fin aero-shell. The resulting actuator is shown in Fig. 2.6(b).



(a) Fin Angle Vs Substrate Thickness



(b) Schematic of the Piezoelectric Bimorph Actuator

CHAPTER 3

CONFIGURATION OF SMART FIN

This chapter deals with the configuration of smart projectile's fin. It also presents the experimental setup for the laboratory tests and also for the wind tunnel tests.

3.1 Configuration

The smart fin is actuated using cantilevered piezoelectric bimorph actuator, Fig. 3.2. The discussion about this actuator is found in chapter 2. The fin and the right end of the actuator are connected using a hinged connection, as shown in Fig. 3.1. This figure also shows the placement of the actuator within the aero-shell.

3.2 Prototype of Smart Fin

A prototype of the smart fin is developed as shown in Fig. 3.3. The aero-shell of the fin is created using a rapid prototyping machine. It has a *NACA0026* profile with a chord length and a span of 177.8 mm and 106.7 mm respectively. Two MFCs (Model No. *M8557P1-5H2*) [56] are bonded using adhesive epoxy (3M's DP 460 Epoxy). The actuators are attached to two strips of fiber glass on either side. Table 3.1 summarizes the geometrical properties of the actuator as shown in Fig. 3.4(a). The MFC can operate between -500 V to +1500 V. Two differential amplifiers, which can supply -1000 V to +1000 V, are used to apply the voltages to MFC's. Due to symmetry, V_2 is set to be equal to $-V_1$ in Eq. (2.2).

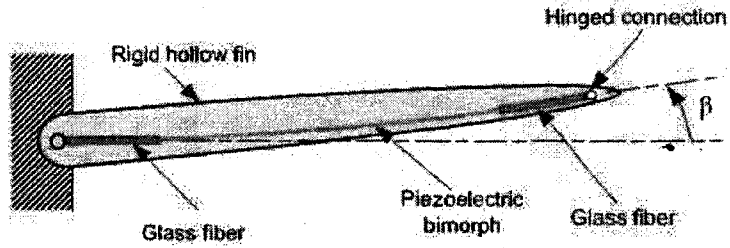


Figure 3.1: Schematic Diagram of the Smart Fin

3.3 Encoder

A through-shaft incremental encoder, Fig. 3.4(c), (15T-05SB-2500N5QHV-F03, Encoder Product Co.), is used to measure the rotation angle of the smart fin. This encoder requires external hardware to setup home position of the smart fin. The encoder gives a quadrature signal with 2500 counts of pulses per quadrature, which gives a resolution of 0.036 degrees for angular measurements.

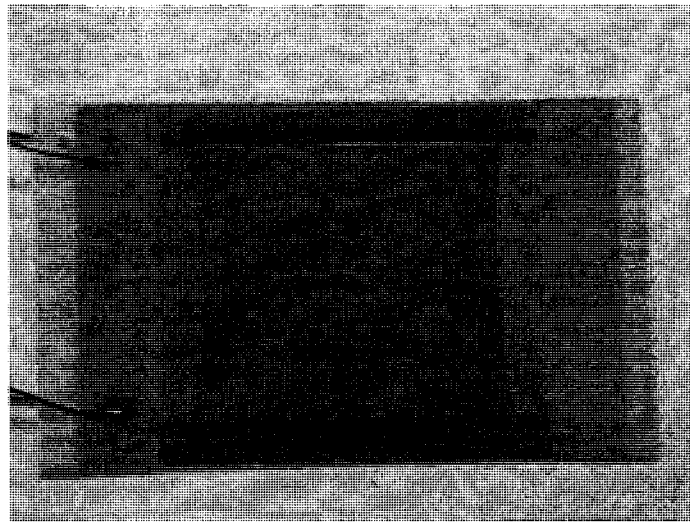


Figure 3.2: Piezoelectric Bimorph Actuator

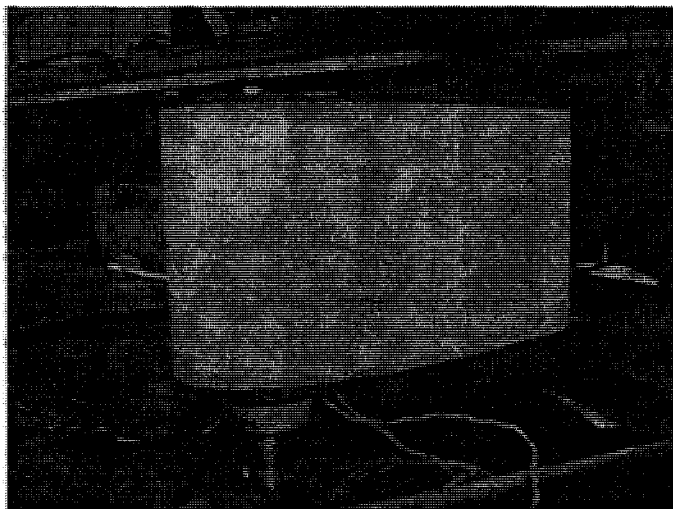
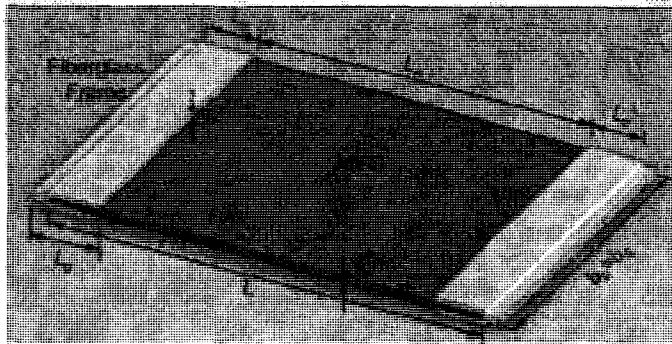


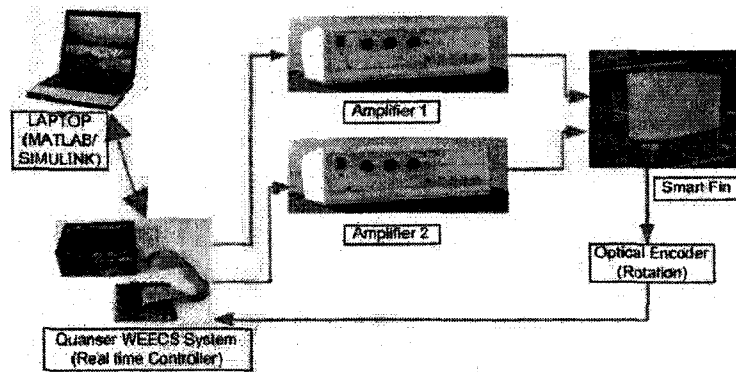
Figure 3.3: Smart Fin Prototype

3.4 Test Setup

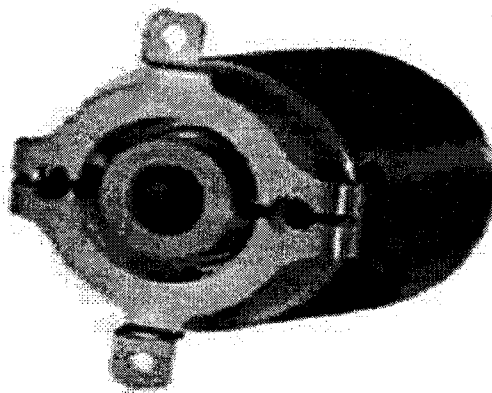
Real-time control software (*Quanser WINCON4.1*, *Multi – Q3 Terminal board*) is used to control the smart fin. The layout of the experiment is shown in Fig. 3.4(b). In addition to conducting bench-top experiments as shown in Fig. 3.3, testing is also conducted inside the UNLV subsonic wind tunnel, Fig. 3.4(d). This wind tunnel can generate wind speed up to 100 *mph*. A metric rotary stage, shown in Fig. 3.4(e), is used in this case to change the angle of attack (α) of the fin inside the wind tunnel. Figure 3.4(f) shows a detailed view of the setup.



(a) Geometry of the Piezoelectric Bimorph Actuator



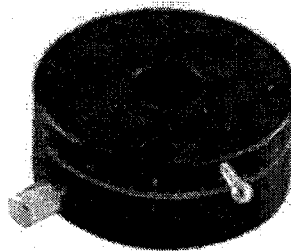
(b) Overall Setup for Experiment



(c) Through-Shaft Incremental Encoder



(d) Experimental Setup inside the Wind Tunnel



(e) Metric Rotary Stage



(f) Detailed View of the Experimental Setup

Table 3.1: Characteristics of the Piezoelectric Bimorph Actuator

Variable	Glass fiber	MFC
Length (mm)	$L_b = 17$	$L = 110$
Active Length (mm)	N/A	$L_a = 85$
Active Width (mm)	N/A	$L_p = 12.5$
Width (mm)	$b_b = 75$	$b_p = 75$
Height (mm)	$h_b = 0.5$	$h_p = 0.3$
Modulus of Elasticity (GPa)	$E_b = 0.3$	$E_p = 0.3$
Piezoelectric strain constant (m/V)	N/A	$d_{33} = 427.5 \times 10^{-12}$
Electrode Spacing (mm)	N/A	$e_s = 0.5$

CHAPTER 4

MODEL DEVELOPMENT

There are basically two ways of building models of systems— the mathematical modeling approach and the identification approach.

Mathematical modeling is the most common and conventional method in Western science and technology. By this approach one starts with decomposing the system into its subsystems, and subsystems into their elements; then one writes down the equations for each element based on first principles, e.g., physical laws; and finally one forms the system model by putting the equations together according to the interrelations between the elements and the subsystems. Some people also call this approach physical modeling. From the methodological point of view, this is typically a reductional, rational and analytical approach.

System identification can be defined as driving system models from observations and measurements. In this approach, the system is viewed as a whole; there is perhaps no need or intention to analyze each element of the system; the system's behavior is observed by measuring some relevant variables; and a model is chosen such that the behavior fits best the measurement. By this approach one does not attempt to go deep into the system, the precise physical knowledge of the system elements and their interrelations is not necessary; therefore identification is also called black-box modeling. Identification is a new branch in the field of dynamic systems and control; and is formally founded about 25 years ago.

This chapter includes the modeling of the smart fin using mathematical and system identification approaches and comparison between these two models with experimental results is

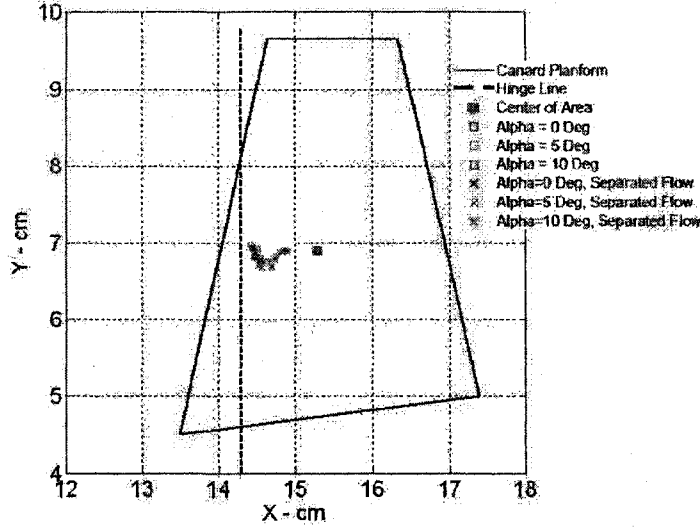


Figure 4.1: Hinge location and Schematic of tapered fin

also included in this chapter.

4.1 Mathematical Model

This section deals with the mathematical modeling of the smart fin system. As shown in Fig. 3.1, the fin is free to rotate about the hinge joint fixed to the projectile body and one end of the actuator is fixed to the projectile body and the other end is connected to the fin using another hinge joint fixed to the tail side of the fin. The fin is considered as rigid and its rotation angle is assumed to be small and planar.

4.1.1 Finite Element Approach

The dynamics of the flexible bimorph is described by using the finite element approach, which is considered as composed of finite elements satisfying Euler-Bernoulli's theorem. The beam is divided into n elements with equal length of $L_i, (i = 1, \dots, n)$. The displacement w of any point on the element i is described in terms of nodal displacement, w_i , and slope, ϕ_i , at

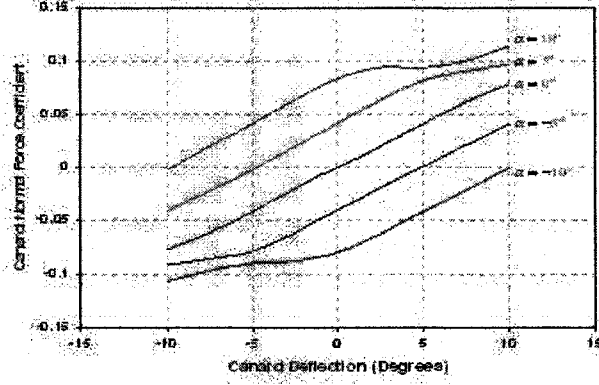


Figure 4.2: Canard normal force versus canard deflection angle, Mach 0.5, $-10^\circ \leq \alpha \leq 10^\circ$

node i and $i + 1$, respectively and is expressed as

$$w = Nq_i \quad (4.1)$$

where $q_i = (w_i, \phi_i, w_{i+1}, \phi_{i+1})^T$ and $N = (N_1, N_2, N_3, N_4)$ is the shape function with

$$\begin{aligned} N_1 &= \frac{1}{L_i^3}(2x_i^3 - 3x_i^2L_i + L_i^3) \\ N_2 &= \frac{1}{L_i^3}(x_i^3L_i - 2x_i^2L_i^2 + x_iL_i^3) \\ N_3 &= \frac{1}{L_i^3}(-2x_i^3 + 3x_i^2L_i) \\ N_4 &= \frac{1}{L_i^3}(x_i^3L_i - 2x_i^2L_i^2) \end{aligned} \quad (4.2)$$

where x_i is the element local coordinate variable defined along the bimorph neutral axis. The velocity of any point in element i can be expressed as

$$\dot{P} = [N]\dot{q}_i \quad (4.3)$$

and the kinetic energy of an element is

$$KE_i = \frac{1}{2} \int_0^{L_i} \rho_i \dot{P}^T \dot{P} dx_i = \frac{1}{2} \dot{q}_i^T m_i \dot{q}_i \quad (4.4)$$

where, ρ_i is the combined density of the beam and piezoelectric film per unit length of element i and the mass matrix m_i becomes

$$m_i = \int_0^{L_i} \rho_i N^T N dx_i \quad (4.5)$$

The complete 2D beam element mass matrix is [57]

$$m_i = \begin{bmatrix} \frac{13}{35} \rho_i L_i & \frac{11}{210} \rho_i L_i^2 & \frac{9}{70} \rho_i L_i & \frac{-13}{420} \rho_i L_i^2 \\ \frac{11}{210} \rho_i L_i^2 & \frac{1}{105} \rho_i L_i^3 & \frac{13}{420} \rho_i L_i^2 & \frac{-1}{140} \rho_i L_i^3 \\ \frac{9}{70} \rho_i L_i & \frac{13}{420} \rho_i L_i^2 & \frac{13}{35} \rho_i L_i & \frac{-11}{210} \rho_i L_i^2 \\ \frac{-13}{420} \rho_i L_i^2 & \frac{-1}{140} \rho_i L_i^3 & \frac{-11}{210} \rho_i L_i^2 & \frac{1}{105} \rho_i L_i^3 \end{bmatrix} \quad (4.6)$$

The kinetic energy of the fin is

$$KE_f = \frac{1}{2} \dot{w}_{N+1}^T \frac{J_f}{L^2} \dot{w}_{N+1} \quad (4.7)$$

where, J_f is the mass moment of inertia of the fin.

The potential energy of an element is

$$PE_i = \frac{1}{2} \int_0^{L_i} \frac{1}{EI_i} (EI_i \frac{\partial^2 w}{\partial x^2} + cu(x, t))^T (EI_i \frac{\partial^2 w}{\partial x^2} + cu(x, t)) dx_i \quad (4.8)$$

where EI_i is the product of Young's modulus of elasticity by the cross-sectional area moment

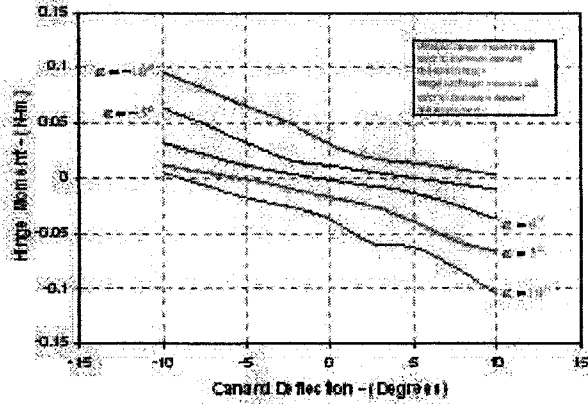


Figure 4.3: Canard hinge moment versus canard deflection angle, Mach 0.5, $-10^\circ \leq \alpha \leq 10^\circ$

of inertia for the equivalent beam for an element i in the x-y plane respectively. If the piezoelectric actuator has a uniform voltage is applied along it's length, $u(x, t)$ can be assumed to be function of time only. The potential energy of an element can be further expressed as,

$$PE_i = \frac{1}{2} q_i^T k_i q_i + q_i \left(\int_0^{L_i} \left(\frac{\partial^2 N}{\partial x_i^2} \right) dx_i \right) cu(t) + \frac{1}{2} \frac{1}{EI_i} c^2 u^2(t) \quad (4.9)$$

where, stiffness matrix of element i , k_i is represented as

$$k_i = \int_0^{L_i} EI_i \left(\frac{\partial^2 N}{\partial x_i^2} \right)^T \left(\frac{\partial^2 N}{\partial x_i^2} \right) dx_i \quad (4.10)$$

The complete 2D beam element stiffness matrix is , [57]

$$k_i = \begin{bmatrix} \frac{12EI_i}{L_i^3} & \frac{6EI_i}{L_i^2} & \frac{-12EI_i}{L_i^3} & \frac{6EI_i}{L_i^2} \\ \frac{6EI_i}{L_i^2} & \frac{4EI_i}{L_i} & \frac{-6EI_i}{L_i^2} & \frac{2EI_i}{L_i} \\ \frac{-12EI_i}{L_i^3} & \frac{-6EI_i}{L_i^2} & \frac{12EI_i}{L_i^3} & \frac{-6EI_i}{L_i^2} \\ \frac{6EI_i}{L_i^2} & \frac{2EI_i}{L_i} & \frac{-6EI_i}{L_i^2} & \frac{4EI_i}{L_i} \end{bmatrix} \quad (4.11)$$

Using Lagrangian dynamics, the equations of motion for an element, i , are

$$\frac{d(\frac{\partial KE_i}{\partial \dot{q}_i})}{dt} - (\frac{\partial KE_i}{\partial q_i}) + (\frac{\partial PE_i}{\partial q_i}) = 0 \quad (4.12)$$

The terms with u are moved to the right hand side of the equation. They correspond to the force matrix of a distributed moment that is replaced by two concentrated moments at the two nodes. The equation can be expressed in matrix form as

$$M_i \ddot{q}_i + K_i q_i = B_i(-cu(t)), i = 1, \dots, n-1 \quad (4.13)$$

where $B_i = (0, -1, 0, -1)^T$ which represents two concentrated moments at two nodes of the element i and M_i is the mass matrix. The equation of motion including the mass of the rigid fin for the last element is

$$M_n \ddot{q}_n + \begin{bmatrix} 0 & 0 & 0 & 0 \\ 0 & 0 & 0 & 0 \\ 0 & 0 & \frac{J_f}{L^2} & 0 \\ 0 & 0 & 0 & 0 \end{bmatrix} q_n = B_n(-cu(t)), i = 1, \dots, n-1 \quad (4.14)$$

where J_f is the mass moment of inertia of the fin. The equations derived for each element

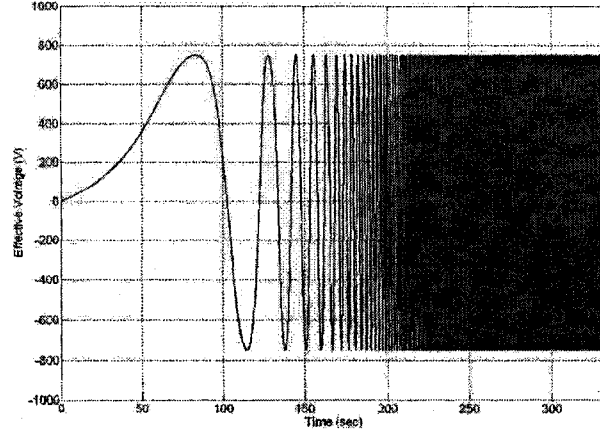


Figure 4.4: Excitation Signal

can be agglomerated after expansion and matrix reduction from the boundary conditions of cantilever beam as follows:

$$M\ddot{q} + Kq = B_0 u(t) \quad (4.15)$$

where $q = (w_2, \phi_2, \dots, w_{n+1}, \phi_{n+1})^T \in \mathbb{R}^{2n}$, $M \in \mathbb{R}^{2n \times 2n}$, $K \in \mathbb{R}^{2n \times 2n}$, $B_0 \in \mathbb{R}^{2n \times 1}$, $w_1 = 0$ and $\phi_1 = 0$. Considering the hinge connection between the bimorph and the aero-shell, the fin angle can be expressed as

$$\beta = \tan^{-1}\left(\frac{\delta_t}{L}\right) \quad (4.16)$$

where L is the total length of the beam and $\delta_t = w_{n+1}$ is the tip displacement of the beam. It can be approximated as $\beta = \delta_t/L$ for small fin angle.

4.1.2 Aerodynamic Moment

The fin is subjected to an external aerodynamic moment induced by the incidence angle of attack, α , and the fin deflection angle, β . Predictions of the external aerodynamic moment have been made using computational fluid dynamics techniques to determine the entire flow field over a generic smart projectile configuration, [53]. This allows a realistic determination

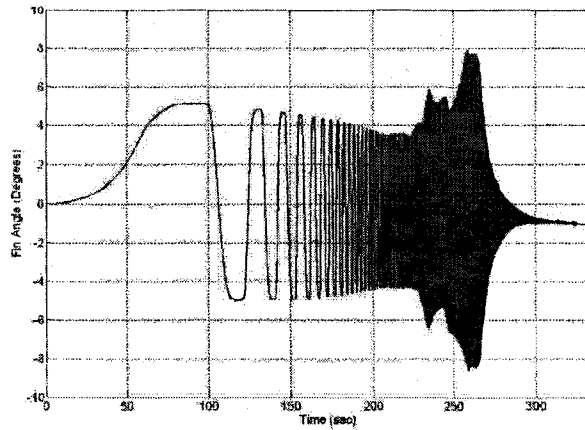


Figure 4.5: Fin Angle Output

of the aerodynamic moment due to angle of attack and fin deflection angle subjected to the interference effects of the projectile body. Calculations were performed over a range of angle of attack and canard deflection angles at a representative glide phase Mach number of 0.5. From these aerodynamic predictions, the canard normal force, normal force center of pressure and hinge moment were determined by integrating the pressure and shear forces over the canard surfaces. In the predictions, both the top and bottom canards were deflected to the same deflection angles in each computation and canard performance for both the upper and lower canard were determined. In the analysis presented here, the canards are modeled with a gap between the canard and the body, although no attachment hardware is modeled in the simulations. The canards are placed in the x-configuration with respect to the pitch-plane (the stable configuration with respect to roll). Flow symmetry across the pitch-plane is assumed.

The schematic of the tapered fin and also the predicted normal force center of pressure at $M=0.5$ for angle of attack of 0, 5, 10 degrees and canard deflections between -10 and 10 degrees is shown in Fig. 4.1. The canard normal force versus canard deflection angle for angles of attack of -10 to 10 degrees for the upper canard is shown in Figure 4.2. For zero degrees

angle of attack, the canard normal force varies linearly with canard deflection angle up to 10 degrees angle of attack. Linear variation of the canard normal force with canard deflection angle was also observed at higher angles of attack.

Figure 4.3 shows the computed aerodynamic hinge moments versus canard deflection angle for angles of attack of -10 to 10 degrees. Although the trend is generally decreasing with canard deflection angle, the variation is somewhat nonlinear with deflection angle. The curves of the Figure 4.3, can be linearized to describe the external moment and it can be accurately modeled as a linear function of the fin angle with a bias term and a reasonable model can be expressed as

$$m_a = m_{a0}(\alpha) + p_a(\alpha)\beta \quad (4.17)$$

$$= m_{a0}(\alpha) + p_a(\alpha)L^{-1}e^{*T}q \quad (4.18)$$

where $p_a(\alpha)$ is a polynomial in the angle of attack, α , $p_a(\alpha) = p_0 + p_1\alpha + \dots + p_k\alpha^k$ (k is a positive integer) and $e^{*T} \in \mathbb{R}^{2n}$ is a unit vector whose $(2n-1)^{th}$ element is one and rest are zero. The modified fin model including aerodynamic moment takes the form

$$M\ddot{q} + Kq = B_0u(t) + B_a m_a \quad (4.19)$$

where $B_a = (0, \dots, 0, 1, 0)^T \in \mathbb{R}^{2n}$.

A stall is a sudden reduction in the lift forces generated by aerofoil. This occurs when the critical angle of attack of the aerofoil is exceeded, typically about 14 to 16 degrees. The smart fin can operated upto 10° angle of attack in real-time. So, there is less possibility to fall in the stall effect. Still, studying stall effect of these fins and also including these effect in the mathmematical model is of interest in the future work.

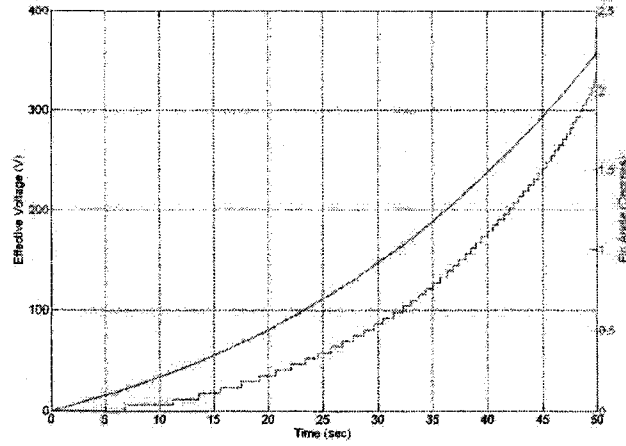


Figure 4.6: Zoomed view of 4.4 and 4.5

4.2 Model Identification

Model identification techniques are used to obtain a model of the smart fin prototype. An input excitation signal that is rich enough should be used to allow accurate representation of the fin dynamics. Using MATLAB Signal Processing Toolbox,[58], a logarithmic sweep chirp signal is generated and fed to the actuators. While other types of chirp signal are available, logarithmic sweep is selected as it could generate a large range of frequencies starting from a low frequency within a relatively short time. The input signal:

$$y_{chirp} = A \cos(\psi(t) + \phi_0) \quad (4.20)$$

$$\psi(t) = A2\pi \int_0^t f_0 \frac{f_i(t_g)}{f_0} \frac{t}{t_g} dt$$

The definition and values of parameters used in Equation 4.20 for the target sweep are shown in Table 4.1. The selected chirp signal (effective voltage in volts) is shown in Fig. 4.4. The response of the system for the above signal (fin angle in degrees) is shown in Fig. 4.5.

A combined zoomed view of Fig. 4.5 and Fig. 4.4 is shown in Fig. 4.6, which shows that the

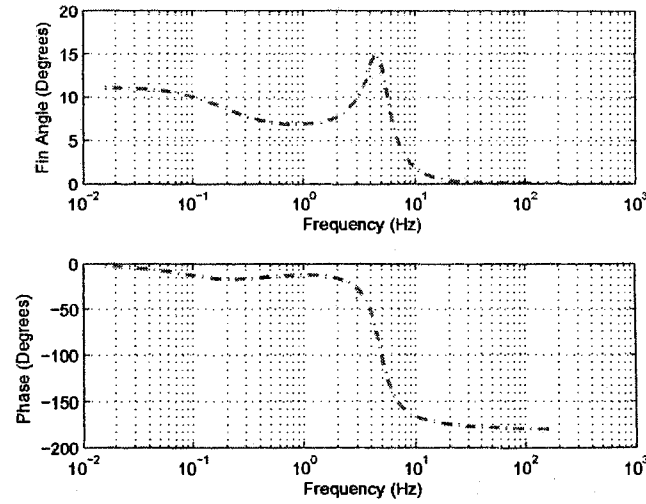


Figure 4.7: Bode plot of the identified smart fin model

fin exhibits a lag due to the hysteresis behavior of piezoceramic actuator. It is decided to avoid the complexities of creating a nonlinear model that can accurately represent the fin. Instead, a linear model that best fits the input and output data is used. The developed controllers should have the robustness to account for any inaccuracy in this model.

The effective voltage and fin angle signals of the fin as shown in Fig. 4.5 and Fig. 4.4 are fed to MATLAB System Identification Toolbox (V.6.0.1), [58], to obtain model of the system. Various experimental system identification techniques, including the robust quadratic prediction error criterion (ARMAX), are used to create the models of the smart fin system. However, it is found that the prediction error method algorithm with using a 3rd order model is found to give the best estimation of the smart fin system. The obtained model can approximate the first mode of the system. The resulting transfer function of the smart fin prototype is:

$$G(s) = \frac{\theta(s)}{V_e(s)} \quad (4.21)$$

$$= \frac{3.355s + 42.0717}{s^3 + 12.71s^2 + 1334s + 6656} \quad (4.22)$$

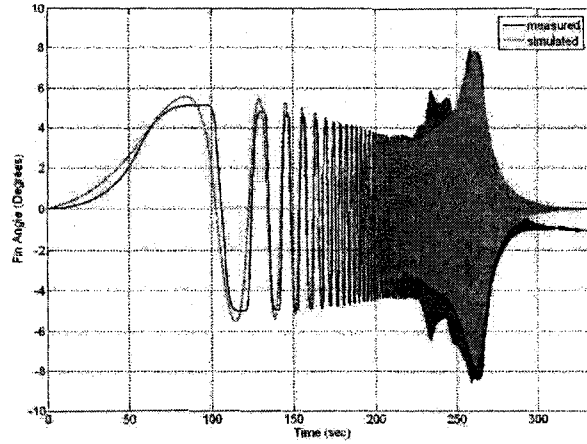


Figure 4.8: Comparison between measured and simulated data

where s is the Laplace variable, $\theta(s)$ is the in fin angle in degrees, and $V_e(s)$ is an effective voltage in volts, which is the average of absolute sum of two individual voltages V_1 and V_2 . The Bode plot of the smart fin system is shown in Fig. 4.7. The same input signal is fed into Equation 4.22. The resulting output of the simulation is compared to actual output as shown in Fig. 4.8. The correlation factor between measured and simulated data is found to be 65.4%. The variation in the results can be explained by the nonlinear nature of the MFC actuator.

4.3 Comparison: Mathematical Model and Identified Model

The comparison is done between two developed models i.e. mathematical model and identified model. The open-loop step response of the fin for the effective voltage 1000V is shown in Fig. 4.9. The developed two different models predicted almost similar response for the step signal. Therefore, we have the flexibility to use either model to design the controller for the rotation angle of the smart projectile fin.

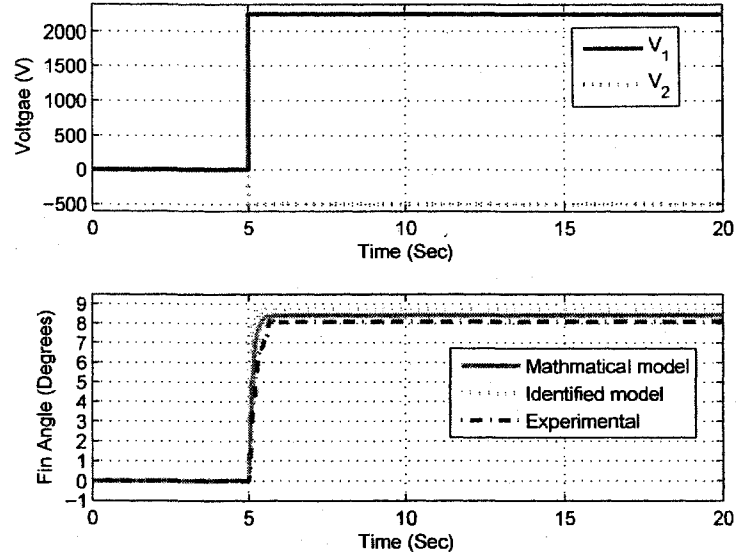


Figure 4.9: Open-loop Step Response of Smart Fin

Table 4.1: Characteristics of the Excitation Signal

Variable	Value
A (scale factor, Volt)	750
ϕ_0 (initial phase, Rad)	0.0
t_g (target time, sec)	335
f_0 (initial frequency, Hz)	0.003
$f_i(t_g)$ (target frequency, Hz)	100

CHAPTER 5

FUZZY LOGIC CONTROL

This chapter presents two kinds of fuzzy logic controller for controlling the rotation angle of the fin. One is based on genetic algorithm and other one is based on inverse dynamics of the smart fin.

5.1 A Structure for the Fuzzy Logic Controller

A PD-like fuzzy logic controller is proposed in this work. The controller uses errors of the fin angle, β , and its angular velocity, $\dot{\beta}$, with respect to reference time-history, β_r and $\dot{\beta}_r$ respectively, as the inputs to the controller. These errors are defined as e_β and $e_{d\beta}$ respectively in the remainder of this work. The proposed fuzzy logic controller determines the desired change in voltage required for both MFC actuators bonded each other to reach the desired fin angle trajectory, $\Delta u(t)$, which is added to the voltage of the previous sampling interval $u(t - \Delta t)$. Figure 5.1 shows the structure of the proposed fuzzy logic controller for the fin angle.

In this chapter, couple of controllers are designed. One controller is based on Genetic Algorithm (GA) and other one is based on inverse-dynamics.

5.2 GA-Based Fuzzy Logic Control

Five membership functions are used to describe each of the three variables: negative big (NB), negative small (NS), zero (Z), positive small (PS) and positive big (PB).

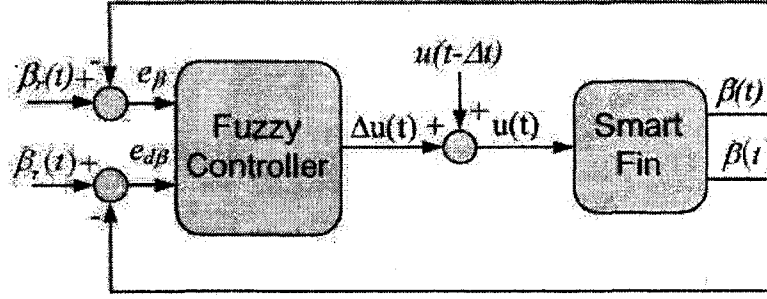


Figure 5.1: Structure of the Smart Fin Fuzzy Logic Controller

5.2.1 Rules for the Controller

The rules for the controller are based on intuition and observations of inertial systems. The goal of the fuzzy controller is to maintain the fin along a desired trajectory. The rules of the fin fuzzy controller, Table 5.1, are selected such that if the fin angle is approaching the correct position or if the fin angular velocity error belongs to the zero function, the controller will produce no change in voltage. Rules are selected such that the controller produces change in voltage only when the tip is moving away from the desired target position.

The degree of membership of a controller output can be related to those of the controller inputs by the following relationship,

$$\mu(y_j) = \min(\mu_A(X_1), \mu_B(X_2), \dots, \mu_C(X_m)) \quad (5.1)$$

The centroid method is used in this article for defuzzification. Discussion at the remainder of this work is limited to Gaussian curve membership functions, whose form is,

$$\mu(z, \sigma, c) = e^{-\frac{(z-c)^2}{2\sigma^2}} \quad (5.2)$$

The Gaussian curve membership function has the advantage of being described using only

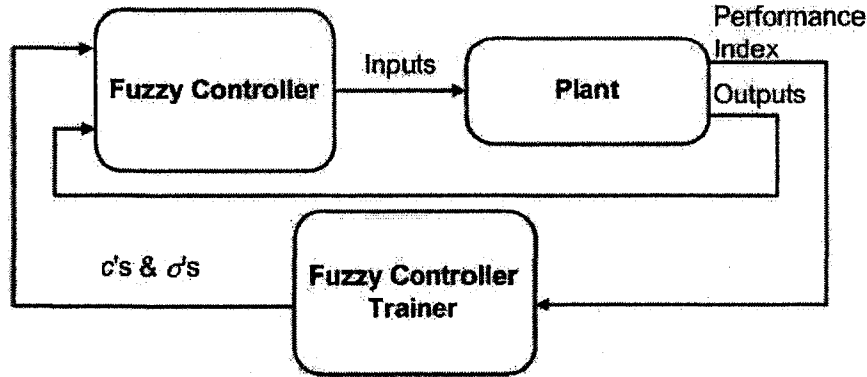


Figure 5.2: Block Diagram of the Algorithm used for Tuning Membership functions of Fuzzy Controllers

two parameters. These parameters are c that determines the center of the function while σ controls its shape.

5.2.2 Tuning of the Fuzzy Controller Using Genetic Algorithm

The performance of a fuzzy controller depends on the range of its input and output variables and shape of the membership functions. While a good estimate of these membership functions may be available through experience in some cases, such estimates may not be available or may be only obtained by operating the system extensively. An automated method to tune the membership functions of the fuzzy controller is therefore proposed.

Genetic Algorithms (GA's) can be useful to achieve this objective. Classical optimization algorithms, which start from a given point and proceed toward the minimum based on pre-defined criteria, suffer from the tendency to be trapped in a local minimum, especially for problems with a large degree of dimensionality. On the other hand, genetic algorithms are stochastic methods that are based on natural selection and genetics. While genetic algorithms can be effective in optimizing systems with a large number of variables and many local minima, they are computationally intensive. Hybrid genetic algorithms address this deficiency by combining genetic algorithm with traditional, nonlinear programming to improve

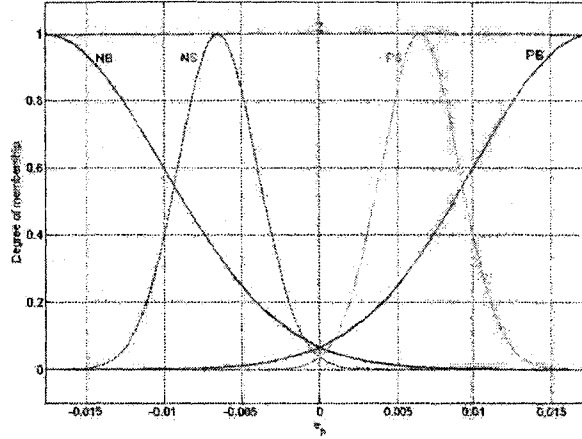


Figure 5.3: Membership Functions, e_β

performance. GA's have been successfully used to eliminate vibration of beams and plates by several investigators, such as, [35], [36], [32], [33], [34], [59], [37]. A hybrid GA is used in this work. The algorithm is labeled, Hybrid Fuzzy Simplex Genetic Algorithm (HFSGA) [39]. This algorithm accelerates the search while maintaining the ability of genetic algorithms to avoid being trapped at local minima.

A fuzzy controller may have many, or an infinite number of, "acceptable" designs. Evaluating the claim that a certain controller is good depends on some criterion that measures the performance of the system. Therefore, the tuning process starts by defining a performance index that measures the controller's performance. Different forms may be more appropriate for other problems. The performance index chosen in this case is

$$PI = \sum_{i=1}^{nt} (e_{\beta i}^2 + Q e_{d\beta i}^2) \quad (5.3)$$

where, nt is the total sampling time divided by sampling interval. Q is a weighing factor that is used to give more importance on angle or angular velocity errors.

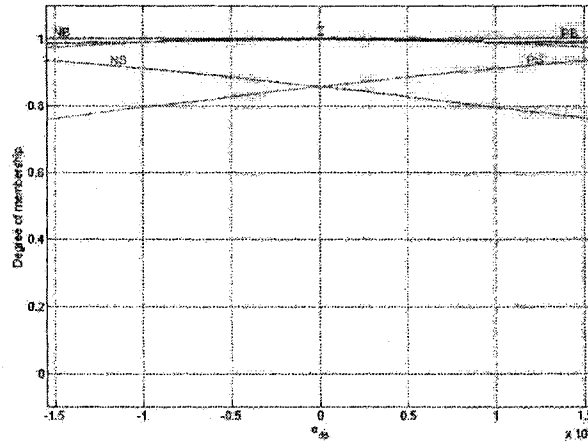


Figure 5.4: Membership Functions, e_{d3}

In the absence of gravity, it is fair to assume that membership functions are symmetrical. The problem is then modeled as having *fifteen* variables (genes) that correspond to the shapes (Z , PS , and PB) and centers of the membership functions (PS and PB) of: and and $\Delta u(t)$ respectively. Each variable is represented by real numbers. The objective is to minimize a performance index in the form of the above equation.

The Tuning process of the fuzzy logic controller can be represented by the block diagram of Fig. 5.2. The system has three blocks:

1. Plant: The system that will be controlled. It receives controller inputs and produces sensors outputs.
2. Fuzzy Controller Trainer: This trainer uses Hybrid Fuzzy Simplex Genetic Algorithm (HFSGA) to evaluate the system performance index. It suggests modifications of the membership functions to minimize this performance index. An overview of HFSGA is presented in the following section.
3. Fuzzy Controller: Fuzzy controller produces the inputs for the plant.

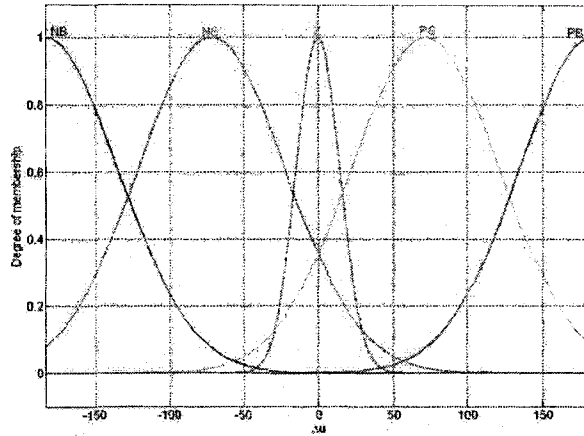


Figure 5.5: Membership Functions, Δu

5.2.3 Tuning the Smart Fin Fuzzy Controller Using Hybrid Fuzzy Simplex Genetic

Algorithm (HFSGA)

The model of Equation 4.22 and Table 5.1 is used to train the fuzzy controller. The desired angular rotation of the fin is from *zero* to -3 degrees within one-time step. The number of samples, nt , is equal to 1000 samples over the simulation period of fifteen seconds. Q is assigned a value of 0.1 based on several trials.

An initial population of 225 chromosomes is randomly generated. The algorithm selects 50 % of the population with the best fitness value as parents, as well as members, of next generation. The rest of the new population is generated by crossing over two randomly chosen parents using the weighted average operator. A mutation rate of 0.01 is selected. The positions of the mutated strings are included in an array of random integers that are selected from the array:

$[1, 2, \dots, Population_size * Numberofstrings]$. The values of these mutated strings are randomly generated. The member with the best fitness in each generation is used as the initial point in a search using Fuzzy Simplex algorithm. The controller was tuned for the case when

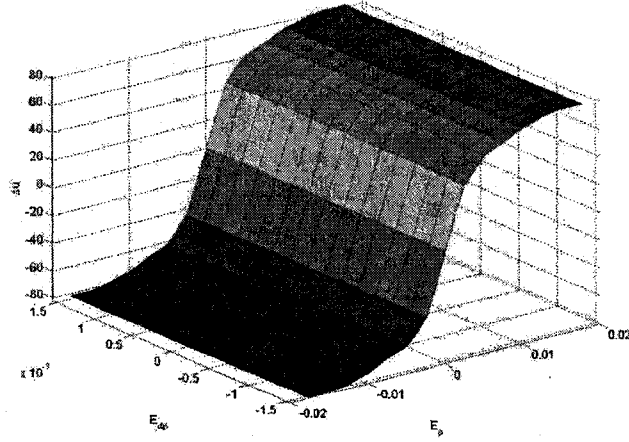


Figure 5.6: Surface of the Fuzzy Output Variables, Δu

angle of attack is equal to zero. The membership functions of the member with the best value of the performance index at the final generation are shown from Figs. 5.3 through 5.5. The surface of the fuzzy output variable, Δu , is shown in Fig. 5.6. Membership functions and surface of the controller has greater sensitivity to e_β than to $e_{d\beta}$ within the considered ranges of the angle and angular velocity that are under consideration.

5.2.4 Simulation Results

A computer program is developed to simulate the system with designed fuzzy logic controller. Figure 5.7 shows simulation results for the proposed controller, which results in 11 % overshoot and a zero steady state error after 1.5 seconds. Figure 5.8 shows the corresponding effective voltage of the controller.

5.2.5 Experimental Results

This section discusses the validation of the developed fuzzy logic controller by testing it within a subsonic wind tunnel under no-wind and wind conditions.

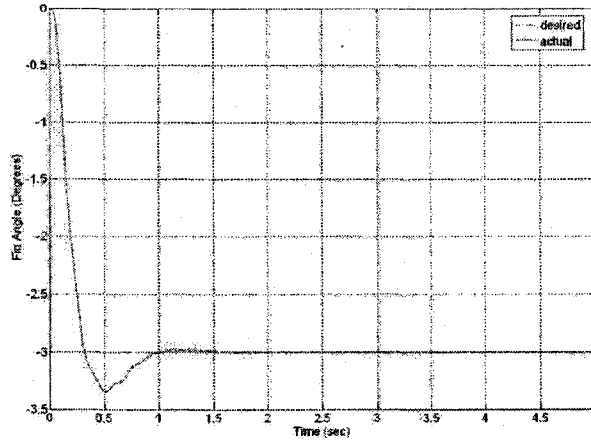


Figure 5.7: Simulated Fin Angle Response

Performance under no-wind conditions

The proposed fuzzy controller is verified for no-wind inside the wind tunnel. The reference fin angle, β_d , is set to be -3° . Experimental data is collected at every 0.015 second. The experimental results are shown in Fig. 5.9 and Fig. 5.10. The controller successfully accomplishes the desired fin angle with zero steady state error after 2.0 seconds with 6.8% overshoot. Figure 5.10 shows that steady state value of the required voltage needed to reach the desired fin angle is significantly below the value obtained during simulation, while the peak voltages in both cases are comparable. This difference may be explained by the higher level of non-linearity of the actuator at low frequencies as shown in Fig. 4.6 and Fig. 4.8.

Assessment of the Controller's Robustness

As the smart fin will be operated under different circumstances, the controller should be robust enough to reject the disturbances. Two experiments are conducted to assess the performance of the proposed controller. In the first experiment, a disturbance is created using a compression spring (spring constant 74.60 N/m) and XYZ stand as shown in Fig. 5.11. After the target angle, β_d , is reached, the XYZ stand is used to push the spring against the middle

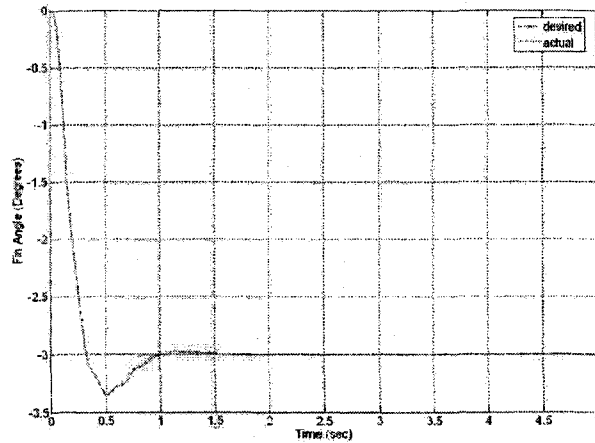


Figure 5.8: Simulated Effective Voltages to the MFC's

of the smart fin. As Figure 5.12 shows, the controller is able to overcome the disturbance and return the fin to the target angle within *five* seconds. Figure 5.13 indicates that the effective voltage reaches the saturation value ($-750V$) for a brief period while overcoming the disturbance. Figure 5.13 also shows that steady state voltage after the introduction of the disturbances is higher than in the case without disturbance as can be expected.

Performance under Wind Loading

The second experiment details the performance of the proposed controller in the wind tunnel under varying operating conditions. As stated earlier, model identification is conducted under no-wind conditions. It is assumed that the fuzzy controller is robust enough to handle disturbances caused by wind pressure that induce aerodynamic moments on the fin.

The smart fin is therefore tested under various angles of attack, α , Fig. 1.1. The following values of α are used: 15, 10, 5, 0, -5 , -10 , -15 degrees. A wind velocity of 40.23meter/second (90mph) is used to test the controller. The reference fin angle, β_d , is set to be -3° for all cases. The time histories of the fin angle for different angles of attack are shown in Figs. 5.14, 5.16, 5.18. The corresponding effective voltage results are shown in Figs. 5.15, 5.17, 5.19.

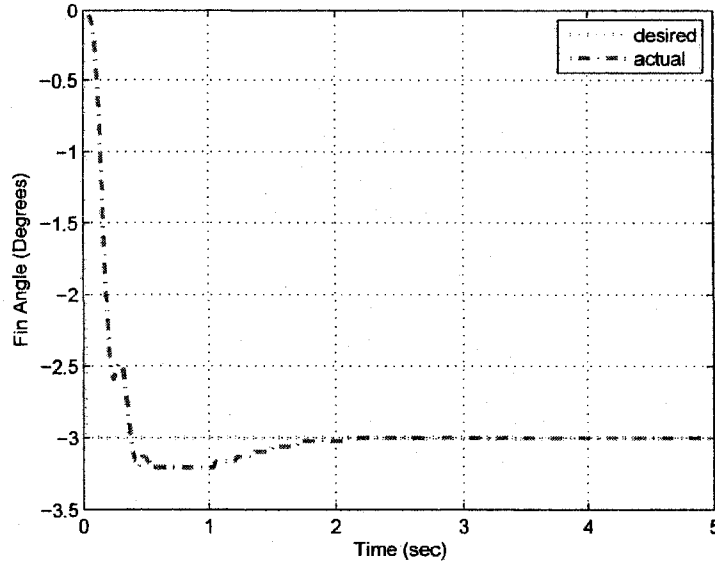


Figure 5.9: Fin Angle Response under No-Wind Conditions

The results are plotted in separate figures for clarity. The controller is able to successfully track the target angles even in the presence of aerodynamic disturbance. The results show that as the angle of attack increases, the response time and effective voltage required to reach the target angles increases. Target angle is reached in less than a second in all cases. The effective voltage to the MFC's indicates a gradual increase in power demands as the angle of attack increases. Effective voltage reaches saturation value ($-750V$) for momentarily in all cases except when angle of attack, α , is equal to 0, -5 , and -10 degrees.

5.2.6 Conclusions

The identified model is used to design a fuzzy logic controller for the fin. Hybrid Fuzzy Simplex Genetic Algorithm (HFSGA) is used to tune the performance of this controller by varying the ranges and shapes of the membership functions of its input and output variables. Several experiments are conducted inside and outside the wind tunnel to assess performance of the fuzzy logic controller. Results show that experimental results are comparable to sim-

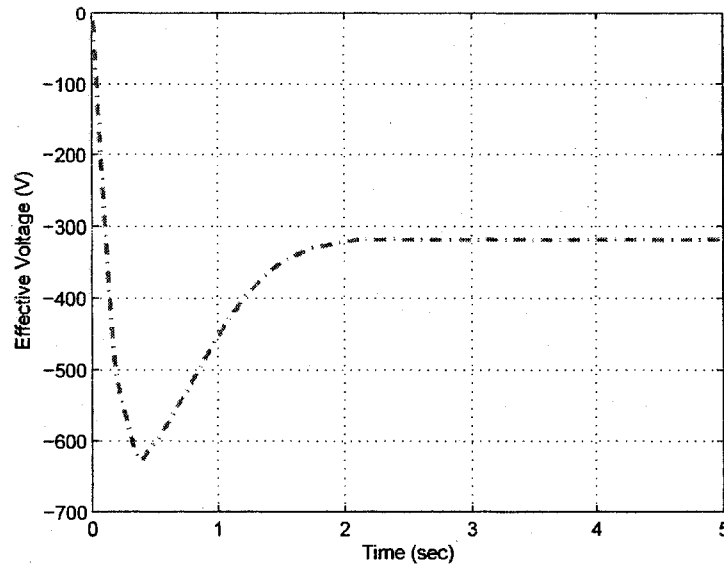


Figure 5.10: Effective Voltages to the MFC's under No-Wind Conditions

ulation. Results also show that the fuzzy controller is robust enough to overcome various operating disturbances and subsonic wind velocities.

5.3 Inverse Dynamics based Fuzzy Controller

Fuzzy logic control has an intuitive nature, which may work well in controlling simple systems. However, Smart fins offer several challenges. Seven membership functions are used to describe each of the three variables: negative big (NB), negative medium (NM), negative small (NS), zero (Z), positive small (PS), positive medium (PM), and positive big (PB).

5.3.1 Rules for the Fuzzy Logic Controller

The rules for the controller are based on a previous work, which showed that the control surface is more sensitive to changes in $e_\beta(t)$ than $e_{d\beta}(t)$. The rules of the fin fuzzy controller, Table 5.2, are selected such that if the fin angle is approaching the correct position or if the fin angular velocity error belongs to the zero function, the controller will produce no change

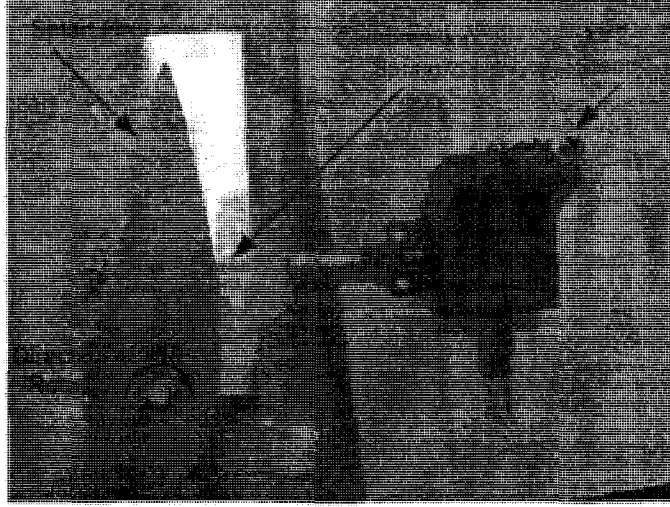


Figure 5.11: Top View of the Disturbance Test Setup

in voltage. The proposed rules attempt to use the strain energy of the beam to dampen vibrations. Rules are selected such that the controller produces change in voltage only when the tip is moving away from the desired target position.

5.3.2 Gaussian Membership Functions

The membership functions for all variables are symmetrical about the zero value of each variable. Membership functions for a variable an input or output variable of the controller, η , are arranged according to the following equations.

$$\sigma_{PB,\eta} = \gamma_{\eta} C_{PB,\eta} \quad (5.4)$$

$$C_{PM,\eta} = \delta_{\eta} C_{PB,\eta} \quad (5.5)$$

$$\sigma_{PM,\eta} = \delta_{\eta} \sigma_{PB,\eta} \quad (5.6)$$

$$C_{PS,\eta} = \delta_{\eta} C_{PM,\eta} \quad (5.7)$$

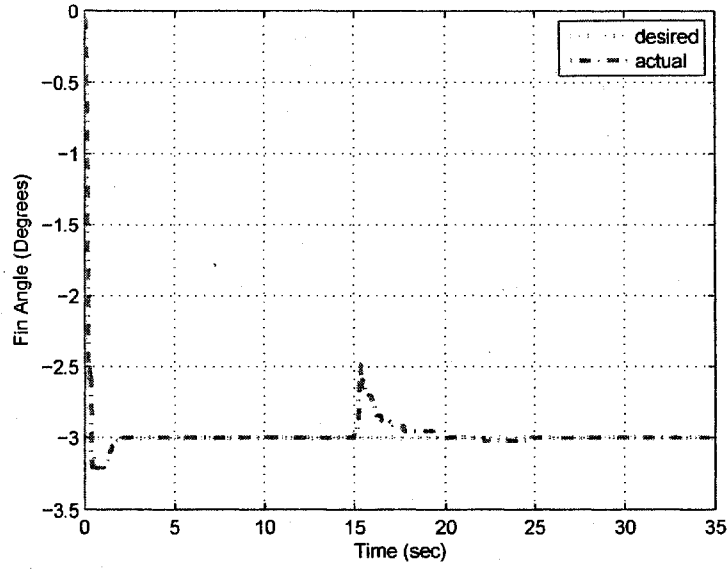


Figure 5.12: Fin Angle Response under Disturbance

$$\sigma_{PS,\eta} = \delta_{\eta} C_{PM,\eta} \quad (5.8)$$

$$C_{Z,\eta} = 0 \quad (5.9)$$

$$C_{Z,\eta} = \delta_{\eta} C_{PS,\eta} \quad (5.10)$$

where γ_{η} and δ_{η} are design parameters controlling the mean and the standard deviations of the Gaussian membership functions. These two variables in addition to $C_{PB,\eta}$ control the shape and distribution for other membership functions for a variable. These design parameters are to be selected by the user to achieve best performance. Due to symmetry of membership functions, equations similar to the above ones can be written for the NB , NM , and NS membership functions. Fig. 5.20 shows typical distribution of membership functions for input and output variables respectively.

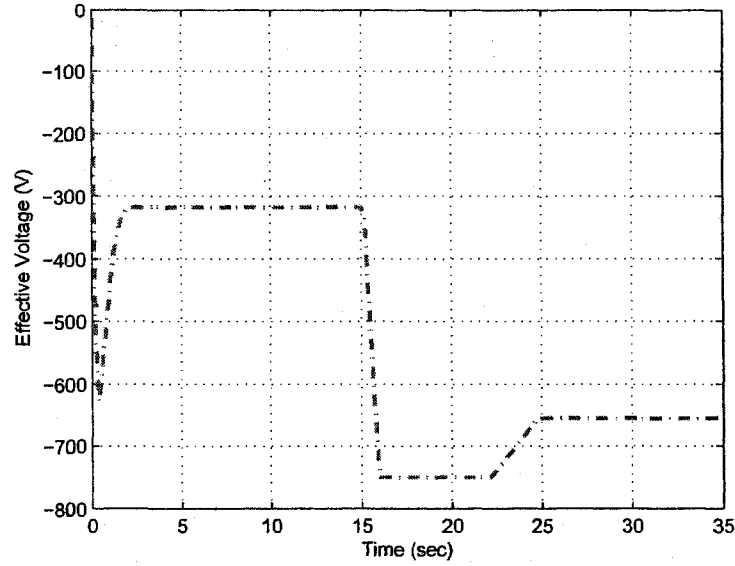


Figure 5.13: Effective Voltages to the MFC's under Disturbance

5.3.3 Defining the Ranges of the Variables using Inverse Dynamics

The proposed controller depends on the ranges of input and output variables. Instead of leaving these ranges static or empirically modify them, this work proposes a method for adjusting these ranges whenever the characteristics of the smart fin and its actuator or the desired path change. The ranges of input variables are chosen as a function of the desired fin rotation history motion and system parameters.

The process starts by identifying a desired fin angle history, β_d . In this work, bang-bang profile for a time of t_d with equal acceleration and deceleration periods, t_a , is used. The corresponding tip displacement of the piezoelectric actuator is,

$$w_{n+1d} = w_d(L) = \beta_d L \quad (5.11)$$

Using the deflection equations for a cantilever beam with concentrated moment at the

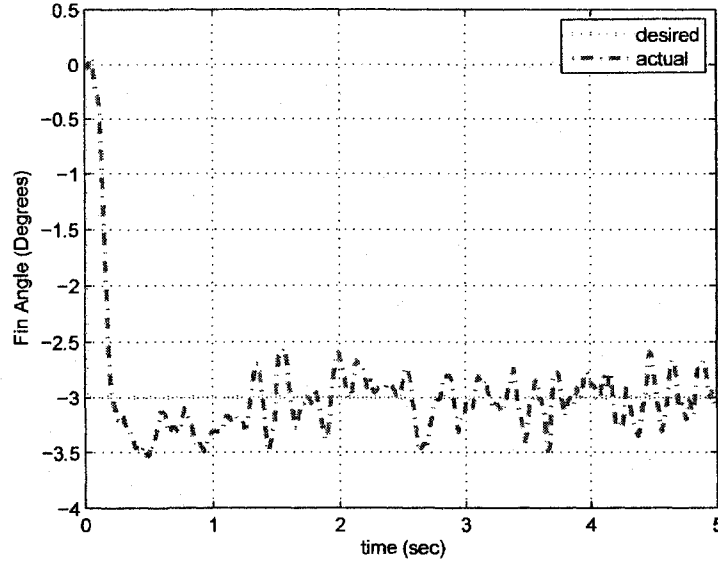


Figure 5.14: Fin Angle Response at Angle of Attack 0° and 40.23 m/s Wind Velocity

tip, the displacements and rotations of the other nodes can be described in terms of the displacement of tip (node n) as follows,

$$w_{id} = w_{n+1d} \frac{x^2}{L^2} \quad (5.12)$$

$$\phi_{i+1d} = w_{n+1d} \frac{2}{L} \quad (5.13)$$

$$\phi_{i+1d} = \phi_{n+1d} \frac{x}{L} \quad (5.14)$$

Based on the rearranging the dynamic equations of the smart fin, Eq. (4.19), the forces needed to produce a desired path, can be expressed as,

$$B_0(u_d(t)) = M\ddot{q}_d + Kq_d - A_Rq_d - B_R \quad (5.15)$$

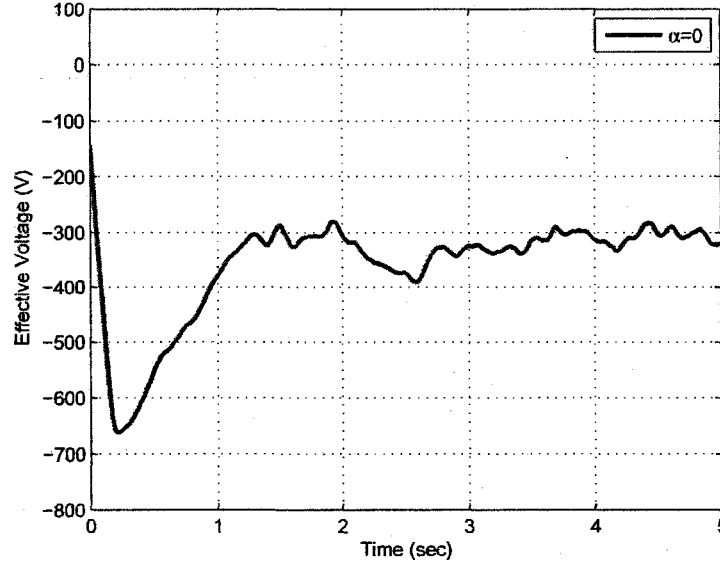


Figure 5.15: Effective Voltage to the MFC's under Angle of Attack 0° and 40.23 m/s Wind Velocity

where, $A_R = p_a(\alpha)L^{-1}e^{*T}$, $B_R = m_{a0}$

$$q_d = [w_{2d}, \phi_{2d}, \dots, w_{n+1d}, \phi_{n+1d}]^T \quad (5.16)$$

Since the elements of B_0 matrix are all zeros except the last row, Eq. (5.15) can be reduced to,

$$u_d(t) = \frac{1}{B_{0,2n}}(M_{2n}\ddot{q}_d + K_{2n}q_d - A_{2n}q_d - B_{2n}) \quad (5.17)$$

The change in desired voltage is,

$$\Delta u_d(t) = u_d(t) - u_d(t - \Delta t) \quad (5.18)$$

The maximum absolute value of $\Delta u_d(t)$ corresponds to the center of gravity of the PB

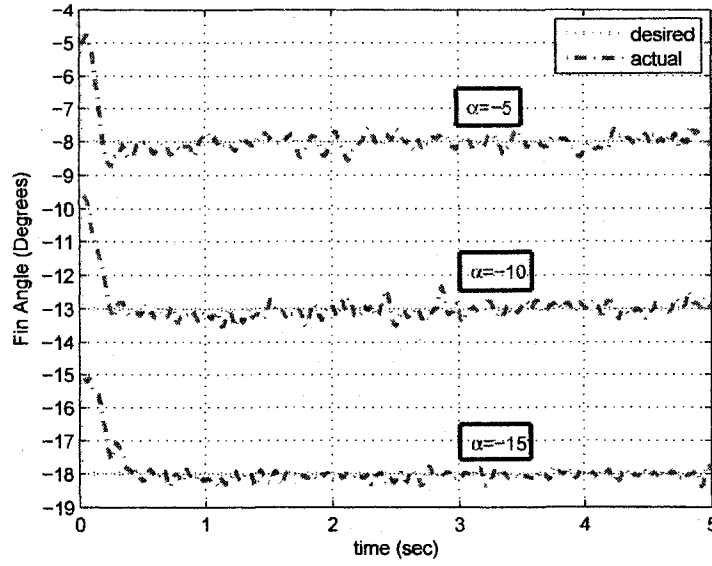


Figure 5.16: Fin Angle Response under negative Angles of Attack and 40.23 m/s Wind Velocity

membership function of Δu . For this output variable, the maximum value of the PB membership function, $C_{PB,\Delta u}$ can be calculated using the following equation:

$$CG_{PB,\Delta u} = \frac{\int_{-\infty}^{C_{PB,\Delta u}} \frac{-(x - C_{PB,\Delta u})^2}{2\sigma_{PB,\Delta u}^2} dx}{\int_{-\infty}^{C_{PB,\Delta u}} \frac{-(x - C_{PB,\Delta u})^2}{2\sigma_{PB,\Delta u}^2} dx} \quad (5.19)$$

Solving the above equation symbolically shows that,

$$C_{PB,\Delta u} = R_{\Delta u}(CG_{PB,\Delta u}) \quad (5.20)$$

where,

$$R_{\Delta u} = \frac{\sqrt{2\pi}}{\sqrt{2\pi} - 2\gamma_{\Delta u}} \quad (5.21)$$

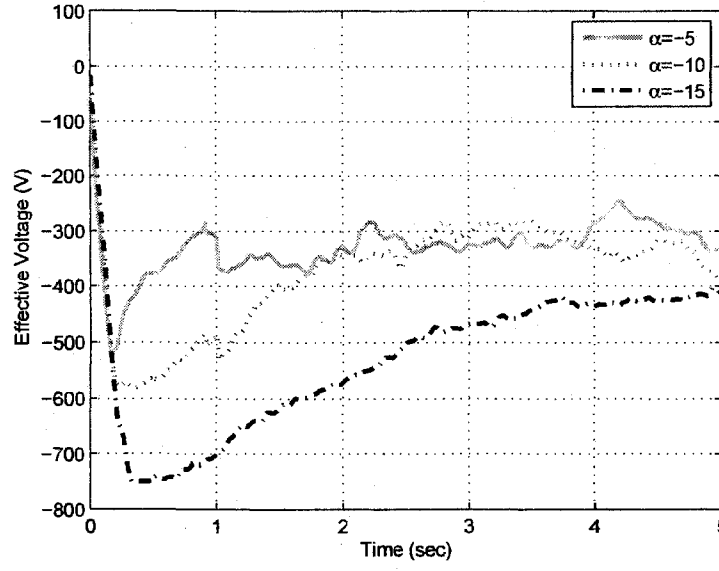


Figure 5.17: Effective Voltage to the MFC's under negative Angles of Attack and 40.23 m/s Wind Velocity

The ranges of the two controller inputs are,

$$C_{PB,e\beta} = R_{e\beta} \max(\beta_d) \quad (5.22)$$

$$C_{PB,e_{d\beta}} = R_{e_{d\beta}} \max(\dot{\beta}_d) \quad (5.23)$$

To evaluate the effectiveness of the proposed controller, the following performance index chosen in,

$$PI = \sum_{i=1}^{nt} (e_{\beta i}^2 + e_{d\beta i}^2) \quad (5.24)$$

where, nt is the total sampling time divided by sampling interval. Time to desired target, which is defined at the time instant when angle error is permanently less than 0.01 degree is also used to assess the performance of the controller.

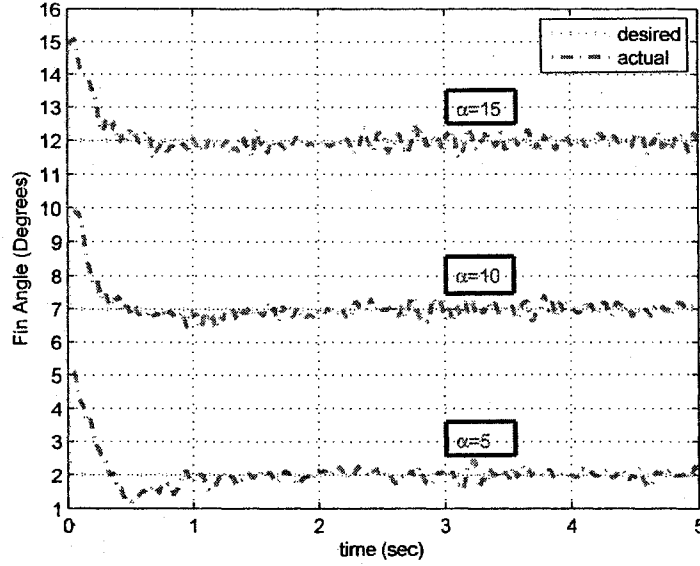


Figure 5.18: Fin Angle Response under positive Angles of Attack and 40.23 m/s Wind Velocity

5.3.4 Simulation Example

A computer program has been developed to simulate the dynamics of the fin and actuator. The mass moment of inertia of the fin, J_f , is equal to, $0.001 \text{ kg} - \text{m}^2$. The physical parameters and mechanical properties of the smart fin actuator and glass fiber used in this simulation are listed in Table 5.3 & 5.4 respectively. The smart fin characteristics are different from chapter 3 and also from the above controller [53]. Dimensional moments have been obtained from the CFD results presented previously are represented by following equation,

$$M_e = (-0.7097 |\alpha| - 0.1212)\beta - 0.189\alpha \quad (5.25)$$

where α and β are expressed in radians and the resulting moment is expressed in $\text{N} - \text{m}$.

The beam is modeled using five elements of equal length. The range of the angle of attack α and the fin angle β are both 10 degrees. The desired acceleration profile is bang-bang with

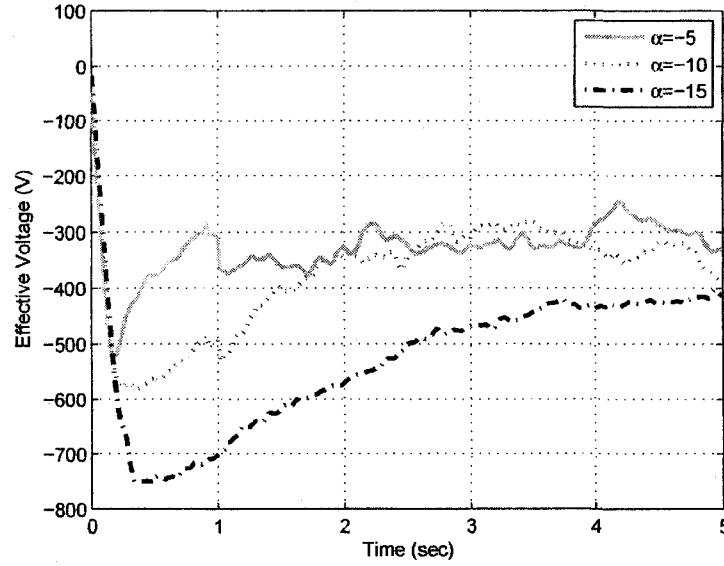


Figure 5.19: Effective Voltage to the MFC's under positive Angles of Attack and 40.23 m/s Wind Velocity

0.5 seconds each for acceleration and deceleration. The number of samples, nt , is equal to 400 samples over the simulation period of *twenty* seconds. It is assumed that voltage is zero at the beginning of the simulation. Initial fin angle is calculated based on deviation from the zero position due to the aerodynamic moment.

In this work $R_{e\beta}$ and $R_{ed\beta}$ are chosen as 0.005 and 0.20 respectively. $\gamma_{e\beta}$, $\gamma_{ed\beta}$, and $\gamma_{\Delta u}$ are chosen to be, 0.4, 0.4, and 0.4 respectively. Similarly, $\delta_{e\beta}$, $\delta_{ed\beta}$, and $\delta_{\Delta u}$ are chosen to be, 0.8, 0.8, and 0.8 respectively. These values are shown since they proved to result in a stable controller over large range of operating conditions and system parameters which will be shown later. Several case studies are considered as shown in Table 5.5.

The controller was successfully tested for the case studies of Table 5.5. The results, which are summarized in Table 5.6, show that the controller moves the fin toward the desired angle. Stable solutions are consistently produced in all cases. In each of these cases, a different

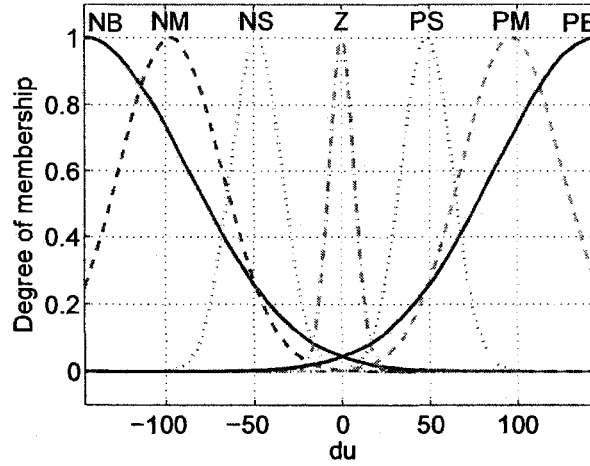


Figure 5.20: Membership Functions of Δu

controller was generated based on inverse dynamics and the motion characteristics in each case. Fig. 5.21 and Fig. 5.22 show the controller surface for Case C and Case F respectively. Comparing these two figures demonstrates that the range of $e_\beta(t)$ and $e_{d\beta}(t)$ decrease as the desired travel decreases while the desired time remains unchanged. A similar reduction is observed in the output of the controller. The results of Case C are shown in Fig. 5.23(a) and Fig. 5.23(b) while the results of Case F are shown in Fig. 5.24(a) and Fig. ?? respectively. The figures exhibit limited overshoot in both cases. The voltage signals in both cases are smooth.

To further evaluate the advantage of the proposed approach, Case C was repeated when the length of the fifth element was increased from 5 mm to 10 mm. The new control surface is shown in Fig. 5.25(a), which shows that the range of $e_\beta(t)$ and $e_{d\beta}(t)$ slightly increase, when compared to Fig. 5.21. As the flexibility of the actuator decreases, the output of the controller is automatically scaled up. The performance index increases from $2.399e - 005$ to $2.7295e - 005$. The results of this case are shown in Fig. 5.25(b) and Fig. 5.25(c) respectively.

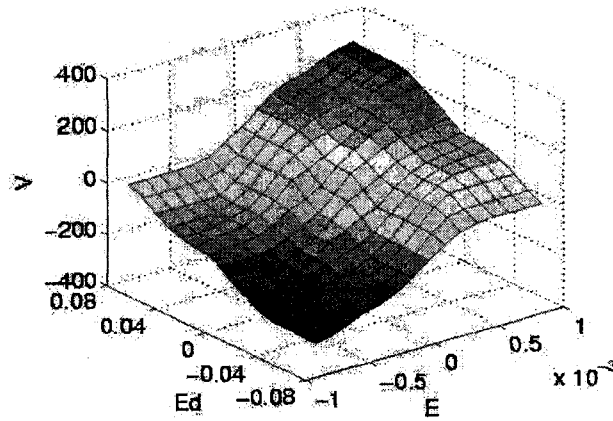


Figure 5.21: Control Surface Case C

5.3.5 Robustness of the Controller

To assess the robustness of the proposed controller, Case C of the previous section is subjected to disturbance by doubling the aerodynamic moment between 2 and 3 seconds. As expected, the controller produced some angular oscillations that were eliminated by 4.6 seconds, Fig. 5.26(a). The performance index increases from $2.399e-005$ to $1.2693e-004$. The corresponding voltage to the piezoelectric actuator exhibits some overshoot when compared to Case C, Fig. 5.26(b).

5.3.6 Conclusions

The mathematical model based on finite element approach is used to design a controller. This work presents a method for adjusting ranges of variables for the inputs and outputs of the fuzzy logic controller according to the system characteristics and desired motion using inverse dynamics equations. The relative shapes and distribution of membership functions with respect to each other are maintained fixed. The proposed method has the advantage of avoiding guessing acceptable ranges of the variables.

Results show that the controller can successfully function under various operating condi-

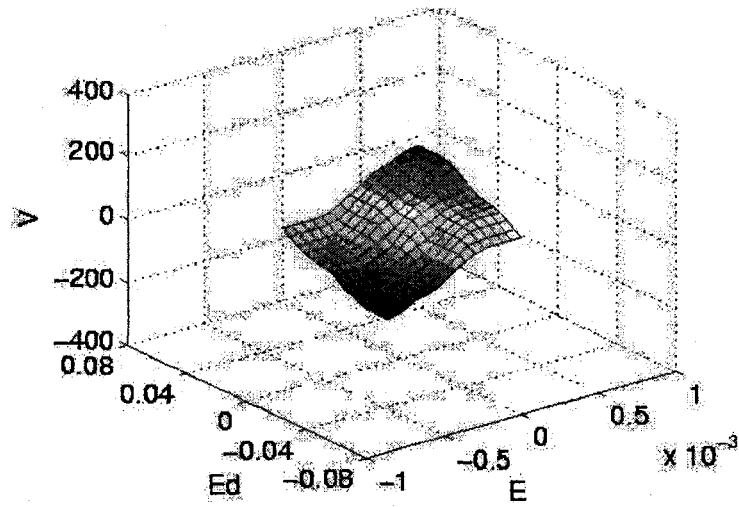
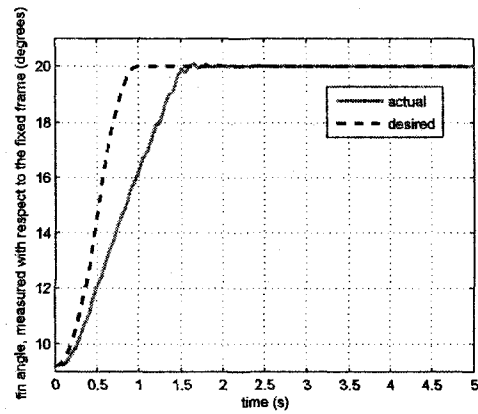


Figure 5.22: Control Surface Case F

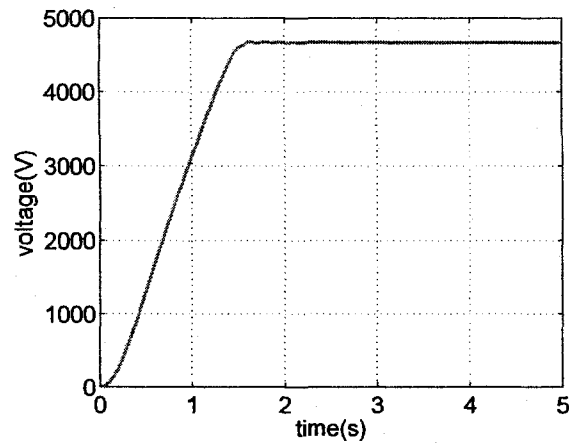
tions. The robustness of the controller is verified. The procedures presented in this work can be applied to other systems that are difficult to characterize.

Table 5.1: Rules for the fin fuzzy controller

$e_{\beta}(t) \Rightarrow$	<i>NB</i>	<i>NS</i>	<i>Z</i>	<i>PS</i>	<i>PB</i>
$e_{d\beta}(t) \Downarrow$					
<i>NB</i>	<i>NB</i>	<i>NS</i>	<i>Z</i>	<i>Z</i>	<i>Z</i>
<i>NS</i>	<i>NS</i>	<i>Z</i>	<i>Z</i>	<i>Z</i>	<i>Z</i>
<i>Z</i>	<i>Z</i>	<i>Z</i>	<i>Z</i>	<i>Z</i>	<i>Z</i>
<i>PS</i>	<i>Z</i>	<i>Z</i>	<i>Z</i>	<i>Z</i>	<i>PS</i>
<i>PB</i>	<i>Z</i>	<i>Z</i>	<i>Z</i>	<i>PS</i>	<i>PB</i>

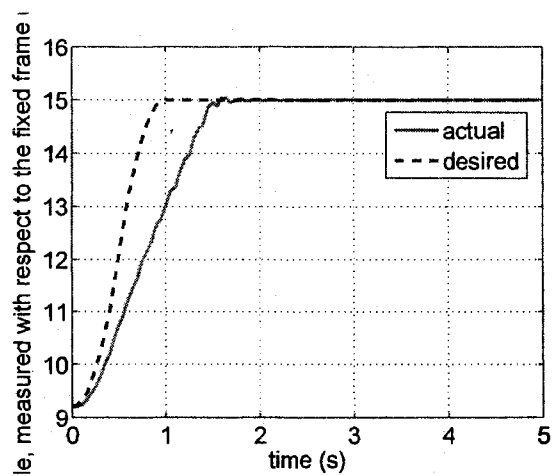


(a) Angle of the Fin Response Case C

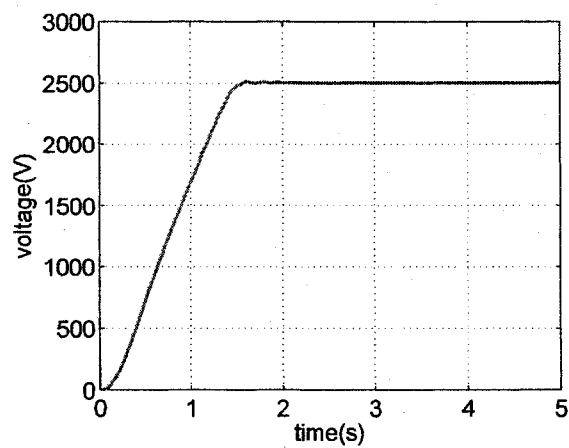


(b) Voltage to the Piezoelectric Actuator for Case C

Figure 5.23: Results for Case C

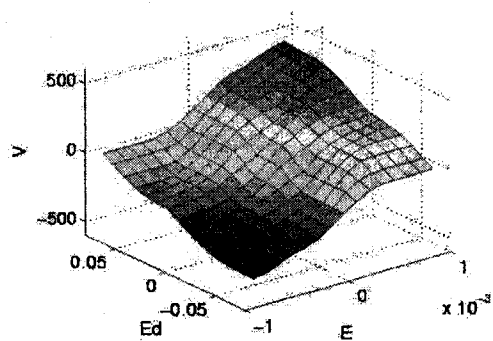


(a) Angle of the Fin Response Case F

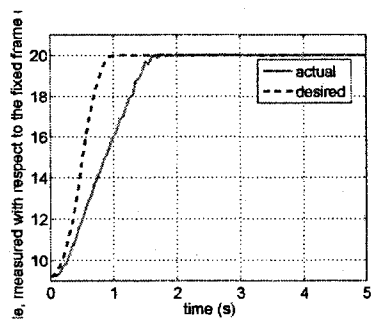


(b) Voltage to the Piezoelectric Actuator for Case F

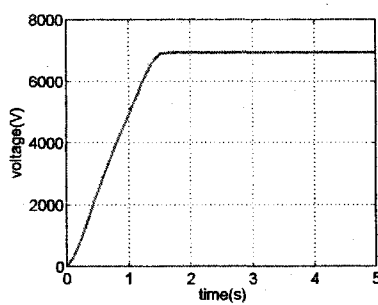
Figure 5.24: Results for Case F



(a) Control Surface Case C (Length of fifth element=10 mm)

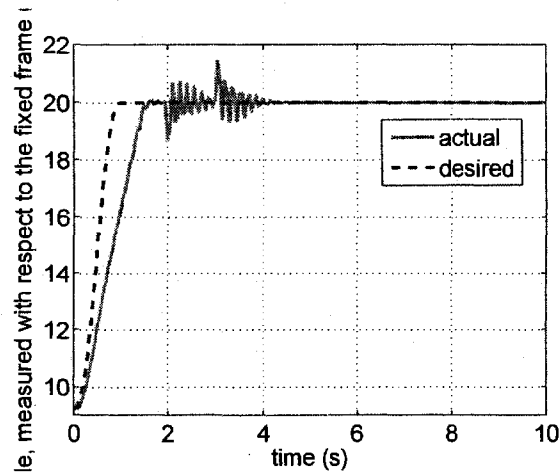


(b) Angle of the Fin Response Case C (Length of fifth element=10 mm)

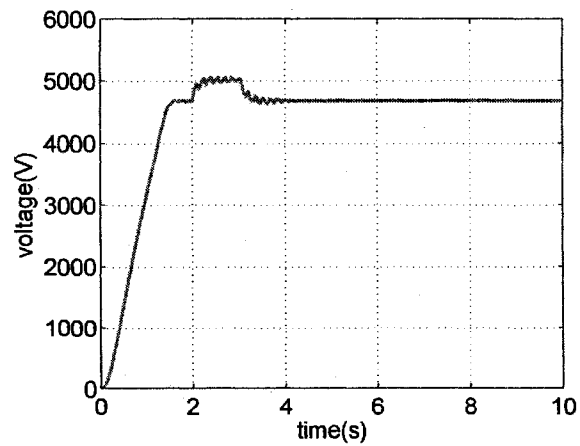


(c) Voltage to the Piezoelectric Actuator for Case C (Length of fifth element=10 mm)

Figure 5.25: Results for Case C (Length of fifth element=10 mm)



(a) Angle of the Fin Response Case C when Subjected to External Disturbance



(b) Voltage to the Piezoelectric Actuator for Case C when Subjected to External Disturbance

Figure 5.26: Results for Case C when Subjected to External Disturbance

Table 5.2: Rules for the fin fuzzy controller

$e_\beta(t) \Rightarrow$ $e_{d\beta}(t) \Downarrow$	<i>NB</i>	<i>NM</i>	<i>NS</i>	<i>Z</i>	<i>PS</i>	<i>PM</i>	<i>PB</i>
<i>NB</i>	NB	NM	NS	Z	Z	Z	Z
<i>NM</i>	NM	NS	Z	Z	Z	Z	Z
<i>NS</i>	NM	NS	Z	Z	Z	Z	PS
<i>Z</i>	NS	Z	Z	Z	Z	Z	PS
<i>PS</i>	NS	Z	Z	Z	Z	PS	PM
<i>PB</i>	Z	Z	Z	Z	PS	PM	PB

Table 5.3: Characteristics of the Smart Fin Actuator

Variable	Piezoelectric Actuator
L (mm)	25
ρ (kg/m^3)	7500
b (mm)	40
h (mm)	0.3
E_p (GPa)	30.34
d_{33} (m/V)	427.5e-12

Table 5.4: Characteristics of the Glass Fiber

Variable	Glass Fiber
L_1 (mm)	5
L_5 (mm)	5
ρ (kg/m^3)	1800
b (mm)	40
h (mm)	0.3
E_b (GPa)	1.2

Table 5.5: Typical Case Studies

Angle of attack α (degrees)	-10	0	10
	0.725 to 10 (A)	0.0 to 10 (B)	-0.789 to 10 (C)
Fin angle motion β (degrees)	0.725 to 5 (D)	0.0 to 5 (E)	-0.789 to -5 (F)
	0.725 to -10 (G)	0.0 to -10 (H)	-0.789 to -10 (I)

Table 5.6: Results of the Case Studies

Case Study	Performance Index (PI)	Time to Desired Target (seconds)
<i>A</i>	1.6231e-5	2.35
<i>B</i>	1.8912e-5	2.40
<i>C</i>	2.2443e-5	2.45
<i>D</i>	3.4997e-6	2.30
<i>E</i>	4.728e-6	2.10
<i>F</i>	6.6273e-6	2.30
<i>G</i>	2.2071e-5	2.40
<i>H</i>	1.8912e-5	2.35
<i>I</i>	1.6005e-5	2.35

CHAPTER 6

ADAPTIVE CONTROL

This chapter starts with state variable representation of the smart fin model. It also presents three kinds of adaptive control systems which can track the desired trajectory. All three adaptive controllers are designed for the control of fin angle and rejection of aerodynamic disturbance input. As smart fin is operated under various operating conditions, the designed adaptive controllers can modify the control law by itself to track the reference trajectory by overcoming the disturbances. For the purpose of controller design, it is assumed that the model parameters are not known. The input signal is the voltage applied to actuator and the output variable is chosen to be the rotation angle of fin for all three controllers.

6.1 State Variable Representation

As derived in Chapter 3, the modified fin model including the aerodynamic force takes the form

$$M\ddot{q} + Kq = B_0u(t) + B_a m_a \quad (6.1)$$

where $B_a = (0, \dots, 0, 1, 0)^T \in \mathbb{R}^{2n}$. Using (4.18) in (6.1) gives

$$\ddot{q} = -M^{-1}K_m q + M^{-1}B_0u(t) + M^{-1}e^*v(\alpha) \quad (6.2)$$

where $K_m = K - p_a(\alpha)L^{-1}e^*e^{*T}$.

M and K_m are positive definite symmetric matrices. As such there always exists a non-

singular matrix V such that

$$V^T M V = I_{2n \times 2n}, V^T K_m V = \Omega^2 \quad (6.3)$$

where $\Omega^2 = \text{diag}(\Omega_i^2)$, $i=1, \dots, 2n$. In general, frequency Ω_i may not be distinct, but numerical computation for the fin model shows that $\Omega_i \neq \Omega_j$, $i \neq j$. (Of course the adaptive law design of Section IV remains valid even when the frequencies are not distinct.)

Defining $\eta = V^{-1}q$, one obtains from (6.2) and (6.3)

$$\begin{aligned} \ddot{\eta} &= \Omega^2 \eta + V^T B_0 u(t) + V^T e^* v(\alpha) \\ &= \Omega^2 \eta + B_1 u(t) + F_1 v \end{aligned} \quad (6.4)$$

where $B_1 = V^T B_0 \in \mathbb{R}^{2n}$ and $F_1 = V^T e^*$. The model form, (6.4), has no damping. However, there is nonzero structural damping for any elastic body. As such it is common to introduce a dissipation term proportional to the rate $\dot{\eta}$. Introducing a damping term of the form $2D\dot{\eta}$, where $D = \text{diag}(\zeta_i)$, $i = 1, \dots, 2n$, $\zeta_i > 0$, one obtains the system

$$\ddot{\eta} = -2D\dot{\eta} - \Omega^2 \eta + B_1 u(t) + F_1 v \quad (6.5)$$

The fin angle in new coordinates becomes

$$\beta = L^{-1} e^{*T} q = L^{-1} e^{*T} V \eta = C_0 \eta \quad (6.6)$$

where $C_0 = L^{-1} e^{*T} V$.

Defining the state vector $x = (\eta, \dot{\eta})^T \in \mathbb{R}^{4n}$, a state variable representation of (6.5) takes

the form

$$\begin{aligned}\dot{x} &= \begin{bmatrix} 0_{2n \times 2n} & I_{2n \times 2n} \\ -\Omega^2 & -2D\Omega \end{bmatrix} x + \begin{bmatrix} 0_{2n \times 1} \\ B_1 \end{bmatrix} u + \begin{bmatrix} 0_{2n \times 1} \\ F_1 \end{bmatrix} v \\ &\equiv Ax + Bu + Fv\end{aligned}\tag{6.7}$$

6.2 Adaptive Control: Nussbaum Gain Based

In this section, an adaptive control system based on Nussbaum gain is designed. It is assumed that order of the model and its system matrices D , Ω , B_1 , C_0 and F_1 as well as the high frequency gain are not known. Furthermore, it is assumed that only the fin angle and angular rate are measurable. Let $y = \beta + \mu_0 \dot{\beta}$ be the controlled output variable, where $\mu_0 > 0$. Consider the reference trajectory generator of the form:

$$\mu_0 \dot{y}_m = -y_m + y^* \tag{6.8}$$

where $y^* = \beta^*$ is the target value of the fin angle. We are interested in designing an adaptive control system such that the $y(t)$ asymptotically tracks the reference trajectory y_m . Note that as y converges to y_m , β converges to β^* . The complete closed-loop system including the adaptive controller is shown in Fig. 6.1.

6.2.1 Control Law

A state variable representation of (??) can takes the form

$$\dot{x} = AX + Bu + d \tag{6.9}$$

where $d = [0_{1 \times 2n}, F_1^T v]^T$ and $B = [0_{1 \times 2n}, B_1^T]^T$.

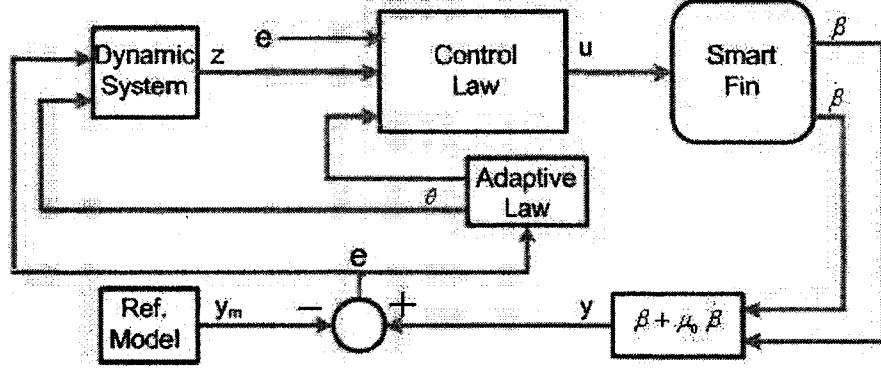


Figure 6.1: Structure of the Adaptive Control System

There exists a coordinate transformation (not needed for design) such that (6.7) takes the form

$$\dot{X}_1 = A_1 X_1 + b_{12} y + d_a \quad (6.10)$$

$$\dot{y} = a_2 X_1 + b_{22} y + k_p u + d_y$$

where $X_1 \in \mathbb{R}^{4n-1}$, $A_1 \in \mathbb{R}^{(4n-1) \times (4n-1)}$, $d_a \in \mathbb{R}^{4n-1}$ is a constant vector, and d_y is a constant. The parameter k_p is the high-frequency gain. Furthermore, introduce a new vector $z \in \mathbb{R}^{4n-1}$ as

$$z = X_1 + d_3 \quad (6.11)$$

where d_3 is yet to be selected. Then using (6.10) and (6.11) gives

$$\begin{aligned} \dot{z} &= A_1(z - d_3) + b_{12} y + d_a + \dot{d}_3 \\ \dot{y} &= a_2(z - d_3) + b_{22} y + k_p u + d_y \end{aligned} \quad (6.12)$$

Suppose we choose d_3 to satisfy

$$\dot{d}_3 = A_1 d_3 - d_a \quad (6.13)$$

that is

$$\begin{aligned} d_3(t) &= - \int_0^t e^{A_1(t-\tau)} d_a d\tau \\ d_3(0) &= 0 \end{aligned} \tag{6.14}$$

Then defining $d_y - a_2 d_3 = d_f$, (6.12) gives

$$\begin{aligned} \dot{z} &= A_1 z + b_{12} y \\ \dot{y} &= a_2 z + b_{22} y + k_p u + d_f \end{aligned} \tag{6.15}$$

Note that the zero dynamics of the system, when the output y is identically zero, have the representation of the form

$$\dot{z} = A_1 z \tag{6.16}$$

Since A_1 is Hurwitz, $z(t) \rightarrow 0$ as $t \rightarrow \infty$.

Now following [60], the derivation of the adaptive law using the Nussbaum gain is considered. In view of (6.8), the reference trajectory is of the form

$$y_m(t) = y^* + \delta(t) \tag{6.17}$$

where $\delta(t)$ is an exponentially decaying signal. Consider a signal $z_m(t)$ which satisfies

$$\dot{z}_m = A_1 z_m + b_{12} y_m \tag{6.18}$$

Defining $\tilde{z} = z - z_m$ and $e = y - y_m$, we obtain the error equation

$$\begin{aligned} \dot{\tilde{z}} &= A_1 \tilde{z} + b_{12} e \\ \dot{e} &= a_2 \tilde{z} + b_{22} e + k_p u + [a_2 z_m + b_{22} y_m + d_f - \dot{y}_m] \end{aligned} \tag{6.19}$$

Since A_1 is Hurwitz, according to (6.17) and (6.18), z_m converges to a constant vector and one has

$$a_2 z_m + b_{22} y_m + d_f - \dot{y}_m = k_0^* + e_m(t) \quad (6.20)$$

where k_0^* is a constant and $e_m(t)$ is an exponentially decaying signal. Using (6.20), (6.19) can be written as

$$\begin{aligned} \dot{\tilde{z}} &= A_1 \tilde{z} + b_{12} e \\ \dot{e} &= a_2 \tilde{z} + b_{22} e + k_p u + k_0^* + e_m(t) \end{aligned} \quad (6.21)$$

Of course, the matrices A_1 , b_{12} , a_2 and scalar parameters b_{22} , k_p , k_0^* are not known. Define a regressor vector w and a parameter vector θ^* as

$$\begin{aligned} w &= [e, 1]^T \in \mathbb{R}^2 \\ \theta^* &= \left[\frac{\mu}{|k_p|}, \frac{k_0^*}{|k_p|} \right]^T \in \mathbb{R}^2 \end{aligned} \quad (6.22)$$

where $\mu > 0$ is sufficiently large (yet to be determined). Let θ be the estimate of θ^* and $\tilde{\theta} = \theta - \theta^*$ be the parameter vector error. Since A_1 is a Hurwitz matrix, there exists a positive definite symmetric matrix P satisfying the Lyapunov equation

$$A_1^T P + P A_1 = -2I \quad (6.23)$$

For the derivation of the control law, consider a Lyapunov function

$$V(e, \tilde{z}, \tilde{\theta}) = \frac{1}{2}(\tilde{z}^T P \tilde{z} + e^2 + |k_p| \tilde{\theta}^T \Gamma^{-1} \tilde{\theta}) \quad (6.24)$$

where Γ is a positive definite symmetric matrix (denoted as $\Gamma > 0$). The derivative of V along the solution of (6.21) yields

$$\begin{aligned}\dot{V} = & \frac{1}{2}\tilde{z}^T[A_1^T P + P A_1]\tilde{z} + \tilde{z}^T P b_{12}e + e[a_2\tilde{z} + b_{22}e \\ & + k_p u + k_0^* + e_m(t)] + |k_p| \tilde{\theta}^T \Gamma^{-1} \dot{\theta}\end{aligned}\quad (6.25)$$

Now the control law and the adaptation law are chosen as

$$\begin{aligned}u &= N(z(t))\theta^T(t)w(t) \\ \dot{z}(t) &= \theta^T(t)w(t)e(t), \quad z(0) = z_0 \in \mathfrak{R} \\ N(z(t)) &= z^2(t) \sin(z(t)) \\ \dot{\theta} &= \Gamma w(t)e(t)\end{aligned}\quad (6.26)$$

where $N(z)$ is called the Nussbaum gain, which can take care of the sign of high-frequency gain k_p .

Substituting (6.26) in (6.25) gives

$$\begin{aligned}\dot{V} \leq & -\|\tilde{z}\|^2 + \|\tilde{z}\| (\|P b_{12} + a_2^T\|) |e| + b_{22}e^2 \\ & + k_p e N(z)\theta^T w + e k_0^* + e e_m(t) + |k_p| (\theta^T - \theta^{*T}) w e\end{aligned}\quad (6.27)$$

Substituting for $|k_p| \theta^{*T} w e = \mu e^2 + k_0^* e$ and using the inequalities

$$\begin{aligned} e e_m &\leq p_1 e^2 + \frac{e_m^2(t)}{4p_1} \\ \|\tilde{z}\| \|Pb_{12} + a_2^T\| \|e\| &\leq p_2 \|\tilde{z}\|^2 + \frac{\|Pb_{12} + a_2^T\|^2 e^2}{4p_2} \end{aligned} \quad (6.28)$$

where $p_1 > 0$ and $p_2 > 0$, (6.27) gives

$$\begin{aligned} \dot{V} &\leq -[1 - p_2] \|\tilde{z}\|^2 - [\mu - |b_{22}| - p_1 - \frac{\|Pb_{12} + a_2^T\|^2}{4p_2}] e^2 \\ &\quad + k_p N(z) \dot{z} + |k_p| \dot{z} + \frac{e_m^2}{4p_1} \end{aligned} \quad (6.29)$$

Choosing $p_2 = \frac{1}{2}$, $p_1 = \frac{1}{2}(\mu - |b_{22}|)$, one obtains

$$\begin{aligned} \dot{V} &\leq -\frac{\|\tilde{z}\|^2}{2} - [\frac{1}{2}(\mu - |b_{22}|) - \frac{\|Pb_{12} + a_2^T\|^2}{2}] e^2 \\ &\quad + k_p N(z) \dot{z} + |k_p| \dot{z} + \frac{e_m^2}{4p_1} \end{aligned} \quad (6.30)$$

For the choice of the gain μ

$$\mu > |b_{22}| + \|Pb_{12} + a_2^T\|^2 + \lambda \quad (6.31)$$

(6.30) yields

$$\dot{V} \leq -\frac{1}{2} \|\tilde{z}\|^2 - \frac{1}{2} \lambda e^2 + k_p N(z) \dot{z} + |k_p| \dot{z} + \frac{e_m^2(t)}{4p_1} \quad (6.32)$$

Integrating (6.32) both sides gives

$$V(e(t), \tilde{z}(t), \tilde{\theta}(t)) + \frac{1}{2} \int_0^t (\|\tilde{z}\|^2 + \lambda e^2) d\tau \leq \Pi(z(t)) \quad (6.33)$$

where

$$\begin{aligned}\Pi(z(t)) &= V(e(0), \tilde{z}(0), \tilde{\theta}(0)) + \epsilon_0 + z(t)(|k_p| + 2k_p \sin(z)) \\ &\quad + 2k_p \cos(z) - k_p z^2 \cos(z) - z_0(|k_p| + 2k_p \sin(z_0)) \\ &\quad - 2k_p \cos(z_0) + k_p z_0^2 \cos(z_0) \\ \epsilon_0 &= \int_0^\infty \frac{e_m^2(\tau)}{4p_1} d\tau\end{aligned}$$

For the computation of $\Pi(z)$,

$$\int N(z) \dot{z} dt = \int z^2 \sin(z) dz \quad (6.34)$$

$$= 2z \sin(z) - z^2 \cos(z) + 2 \cos(z) \quad (6.35)$$

has been used.

In view of (6.33), it follows that there exist a closed, bounded interval $[z^-, z^+]$ containing $\Pi(z_0)$ for which $\Pi(z^-)$ and $\Pi(z^+)$ are negative. But the left side of the (6.33) is always positive. As such $z(t)$ can not pass through z^- or z^+ , and therefore $z(t)$ is bounded. Then $V(t)$ is bounded which in turn implies that $e, \tilde{z}, \tilde{\theta} \in L^\infty$ and $e, \tilde{z} \in L^2$. It can be seen that all the signals in the closed-loop system are bounded. Then using Barbalat's lemma [60], one concludes that \tilde{z} and e converge to zero as $t \rightarrow \infty$.

6.2.2 Digital Simulation Results

The simulation results for the smart fin based on the theoretical model using the digital computer are presented in this section. MATLAB/SIMULINK tool are used to simulate the dynamics (including the adaptive control law) of the smart fin system. The mechanical and geometrical properties of the of the simulated model are shown in Table 3.1. The mass moment of inertia of the smart fin, J_f , is $0.0015 \text{ kg} - m^2$. The bimorph is modeled using *five* elements of equal length. A state-variable representation of the smart fin model of dimension of 20

is obtained for simulation. The aerodynamic moment (4.18) is chosen for different angles of attack of the projectile based on the CFD analysis. The parameters of the aerodynamic moment are estimated by a linear approximation of the data obtained by the CFD analysis. Those parameters of the aerodynamic moment are $m_{a0} = -0.0022, p_a = +0.0005$ for $\alpha = -5^\circ$, and $m_{a0} = -0.0028, p_a = +0.01$ for $\alpha = +5^\circ$. The value of Γ is chosen as $2000(I_{2 \times 2})$. The initial value of $\theta = (\theta_1, \theta_2)^T$ and z_0 are chosen as zero. Simulation is done using the above values for different reference commands and different angles of attack. The simulation results are given for the reference fin angle $\beta^* = -2^\circ$ at angles of attack $\alpha = 5$ and $\alpha = -5$, in Figure 6.2 and Figure 6.12. Simulation results show that the fin angle asymptotically converges to the target angle by adapting the estimated parameters θ_1 and θ_2 . The voltage required to rotate the fin at angle of attack $\alpha = 5$ is approximately $-146V$. In case of $\alpha = -5$, the voltage required is $-200V$. There is no overshoot in the results and the flexible modes reach steady state values, in both cases. The estimated parameters remain bounded and converge to certain constant values.

6.2.3 Experimental Results

The numerical simulation results of the previous section show that adaptive controller accomplishes fin angle control and rejects constant aerodynamic disturbance forces. But this control law cannot guarantee closed-loop stability in the presence of time-varying disturbance inputs encountered in wind tunnel tests and as such this control law must be modified to compensate for disturbances which are not constant. We point out that the derivation of system (6.15) from (6.10) remains valid if the terms d_a and d_v are time-varying; but now the disturbance input $d_f(t)$ is time-varying and unlike Section IV does not asymptotically tend to a constant value. To nullify the effect of $d_f(t)$ an additional signal is added in the control

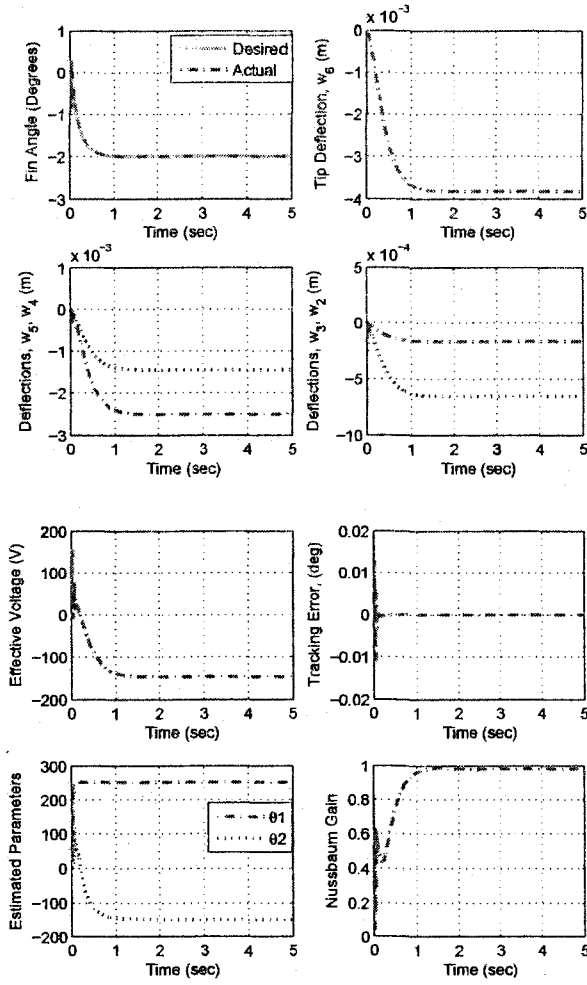


Figure 6.2: Fin Angle= -2° , Angle of Attack= 5°

law (6.26). Following [60], one can show that the modified control law takes the form:

$$\begin{aligned}
 u &= N(z)(\theta^T(t)w(t) + \text{sgn}[e(t)]D_0) \\
 \dot{z} &= \theta^T w e + D_0 |e| \\
 N(z(t)) &= z^2(t) \sin(z(t)) \\
 \dot{\theta} &= \Gamma w(t)e(t)
 \end{aligned} \tag{6.36}$$

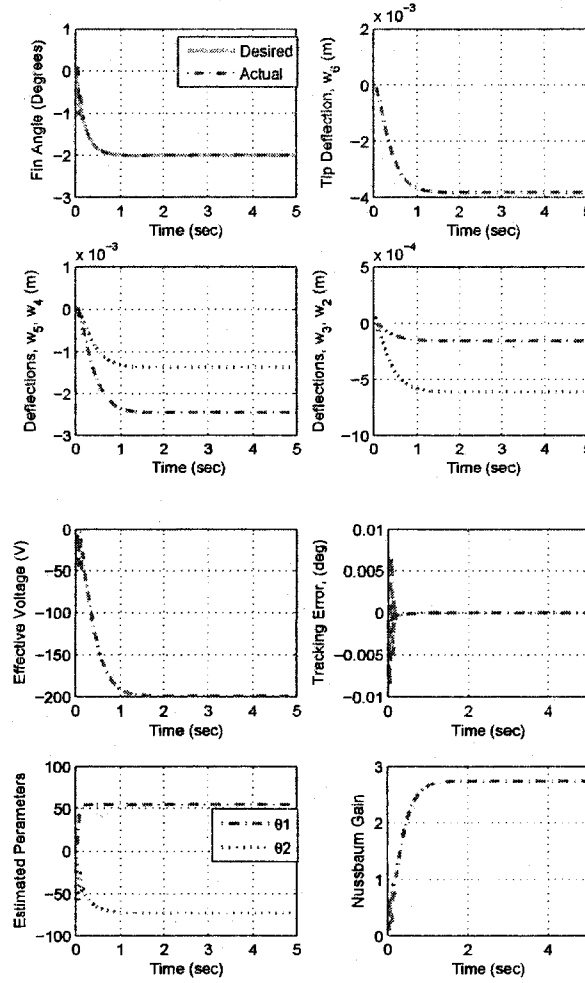


Figure 6.3: Fin Angle $=-2^\circ$, Angle of Attack $=-5^\circ$

where $D_0 > \sup |d_f(t)|$, $t \geq 0$ is a sufficiently large gain. It can be proven that in the closed-loop system, including control law (6.36), asymptotic fin angle tracking is accomplished. Although, the control law (6.36) can guarantee closed-loop stability and trajectory control, the wind tunnel tests show inferior transient responses caused by the nonlinearity of the Nussbaum gain. Therefore, experimental results are presented using a simplified control law obtained from (6.36), by replacing the Nussbaum gain as $N(z) = -\text{sgn}(k_p)$ [60]. The simplified control

law is given by [60]:

$$\begin{aligned} u &= -\text{sgn}(k_p)(\theta^T(t)w(t) + \text{sgn}[e(t)]D_0) \\ \dot{\theta} &= \Gamma w(t)e(t) \quad \Gamma = \Gamma^T > 0 \end{aligned} \tag{6.37}$$

where $D_0 \geq (\frac{1}{k_{pm}})\sup |d_f(t)|$, $t \geq 0$ and $k_{pm} \leq |k_p|$. The modified control law in (6.37) accomplishes boundedness of all signals and asymptotic tracking.

Performance Under No-Wind Conditions

The adaptive controller (6.37) is validated by wind tunnel tests. First, the fin control is considered for *zero* wind speed. The initial value of parameter vector $\theta(0) = (\theta_1(0), \theta_2(0))^T$ is chosen as zero. This is rather a worse choice of gains but is done to show the robustness property of the controller. The value of Γ is $0.1I_{2 \times 2}$. The reference fin angle is set to be $\beta^* = -2^\circ$ for real-time simulation. The feedback signal considered is of the form $y = \beta + \mu_0\dot{\beta}$, where μ_0 is set to be 0.1. The experimental data is collected at every 0.001 second. The rate of fin angle is obtained by digital differentiation. The experimental results are shown in Figure 6.13 for *zero* wind speed. The modified controller possesses the ability to track the target angle within 1.5 seconds by adapting the parameters θ_1 and θ_2 . The voltage required to reach the desired angle is $-290V$. The estimated parameters converge to constant values.

Performance Under Wind Loading

In order to examine the effect of the unknown aerodynamic moment in the real-time control and also to verify the robustness of the designed adaptive controller, experiments are conducted for wind speed 13.4 m/s in the UNLV's subsonic wind tunnel. The controller is tested for various angles of attack, $\alpha = (0, -5, -10)$. The same reference fin angle is used for all cases. The values of $\theta(0)$ and Γ used for wind speed *zero* case are retained. The value of D_0 is chosen as 100. The real-time simulation is carried out at a time step of 0.001 seconds. Test results are shown in Fig. 6.16. We observe that the controller is able to drive the fin

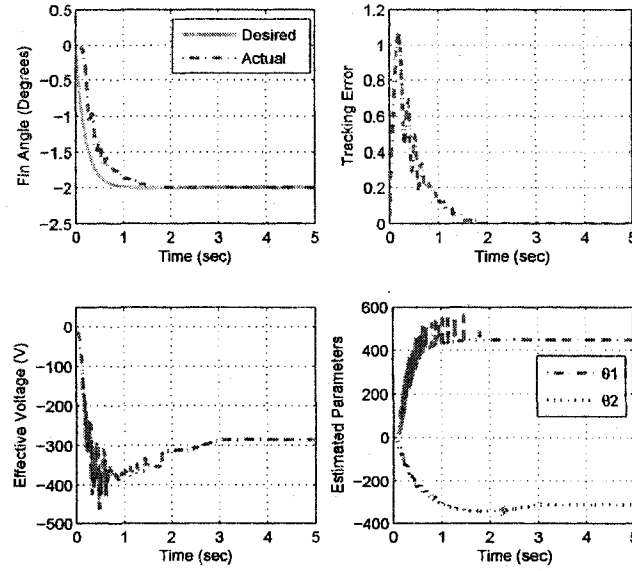


Figure 6.4: Experimental Results at zero Wind Speed

along the desired trajectory even in the presence of aerodynamic disturbance.

6.2.4 Summary: Digital Simulation Results and Wind Tunnel Test Results

This section presents the summary of digital computer simulation and wind tunnel test results. The same reference angle is chosen in both cases. The initial values of the parameter vector $\theta(0)$ is zero in both cases. Even though the worst scenario of $\theta(0) = 0$ is chosen in both cases, the closed-loop responses are good. Of course, some better transient response is possible by tuning these parameters properly. In both cases, the θ_1 converges to some positive value and θ_2 converges to a negative value. The controller tracks the reference fin angle trajectories and rejects the aerodynamic disturbance in both cases.

6.2.5 Conclusions

The model of the fin system includes the aerodynamic moment which is a function of the angle of attack of the projectile. A state variable model using finite element method is obtained. The dimension as well as the parameters of the model are assumed to be completely

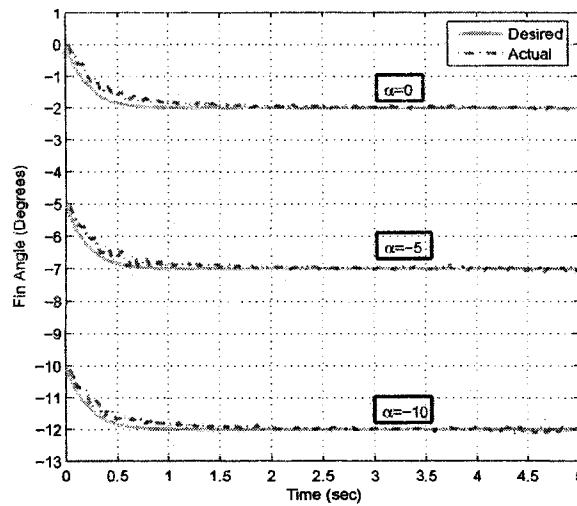


Figure 6.5: Fin Angle Response under Various Angles of Attack at Wind Speed 13.4 m/s

unknown for the controller design. An adaptive control based on Nussbaum gain is designed for the control of the fin rotation angle. The developed adaptive control system is independent of the sign of the high-frequency gain. Simulation results show that the designed control system accomplishes fin angle control in spite of uncertainties in the fin parameters and the aerodynamic coefficients. The designed controller is modified for closed-loop stability for real-time tests in the presence of time varying aerodynamics forces for real-time simulation. The modified adaptive controller is validated using the subsonic wind tunnel at the University of Nevada, Las Vegas. Experimental results show that the designed adaptive controller accomplishes fin angle control and also the proposed controller is robust enough in the presence of time-varying disturbance.

6.3 Adaptive Control: Servoregulator

This controller is based on previous work done in [50]. This section deals with an adaptive servoregulator is designed for the control of fin angle and the rejection of the disturbance

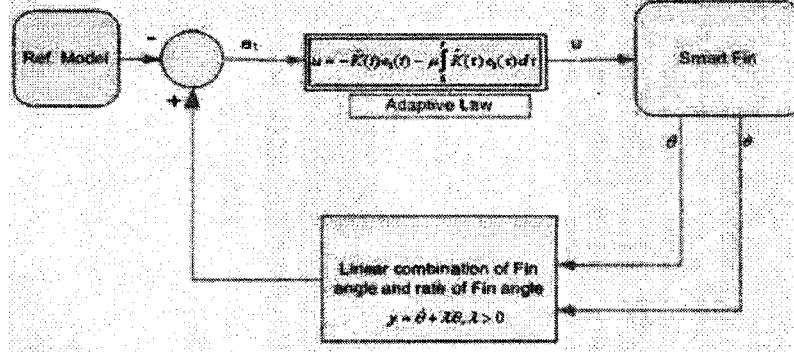


Figure 6.6: Structure of the Adaptive Servoregulator

input (aerodynamic moment). Similar to the above controller, it also assumes that order of the model and its system matrices D , Ω , B_1 , C_0 and F_1 are completely unknown. Furthermore, it is assumed that only the fin angle and angular rate are measurable. We are interested in designing an adaptive control system such that the fin angle asymptotically converges to any prescribed fin angle β^* , a constant, and rejects the constant disturbance input v . The structure of the adaptive servoregulator is shown in Fig. 6.6.

6.3.1 Control Law

We select the controlled output variable as

$$\begin{aligned}
 y &= (\dot{\beta} + \lambda\beta) \\
 &\equiv C_0\dot{\eta} + \lambda C_0\eta \\
 &\equiv Cx
 \end{aligned} \tag{6.38}$$

where $\lambda > 0$ is a design parameter. From 6.7 and 6.61, one obtains

$$\begin{aligned}
 \hat{y}(s) &= C(SI - A)^{-1}B\hat{u}(s) + C(SI - A)^{-1}F\hat{v}(s) \\
 &= \frac{n_p(s)}{d_p(s)}\hat{u}(s) + \frac{n_f(s)}{d_p(s)}\hat{v}(s)
 \end{aligned} \tag{6.39}$$

where s is the Laplace variable and u and v denote Laplace transforms of u and v respectively, and

$$\begin{aligned} n_p(s) &= C \text{adj}(SI - A)B \\ n_f(s) &= C \text{adj}(SI - A)F \\ d_p(s) &= \det(sI - A) \end{aligned} \tag{6.40}$$

It is easily seen that from Eq. 6.5 that

$$d_p(s) = \sum_{i=1}^2 n(s^2 + 2\zeta\Omega_i s + \Omega_i^2) \tag{6.41}$$

is a Hurwitz polynomial. Furthermore, computing the polynomial $n_p(s)$ for this model, one finds that it is a Hurwitz polynomial. Therefore, the transfer function $\frac{n_p(s)}{d_p(s)}$ is minimum phase.

The tracking error $e_1 = y - y_m$ is

$$e_1 = \frac{n_p(s)}{d_p(s)} \hat{u}(s) - \hat{y}_m(s) \tag{6.42}$$

where y_m is the constant reference trajectory. For a given angle of attack, the aerodynamic moment component v acts as a constant disturbance input and it must be rejected by the controller. In order to eliminate this unknown disturbance term v , let us filter each side of Eq. 6.64 with $\frac{s}{s+\mu}$, where $\mu > 0$. For constant signals v and y_m , one has $sv = 0$ and $sy_m = 0$. Therefore, the filtered equation (6.64) yields

$$\left(\frac{s}{s+\mu}\right)e_1 = \frac{n_p(s)}{d_p(s)}\left(\frac{s}{s+\mu}\right)\hat{u}(s) \tag{6.43}$$

We note that we have ignored the exponentially decaying signal in (6.43).

Defining the filtered input signal as

$$u_f(s) = \left(\frac{s}{s + \mu}\right)\hat{u}(s) \quad (6.44)$$

(6.43) can be expressed as

$$e_1 = \frac{(s + \mu)n_p(s)}{sd_p(s)}\hat{u}_f(s) \triangleq H(s)\hat{u}_f(s) \quad (6.45)$$

In view of (6.43), it is sufficient to derive a control law $u_f(t)$ such that the tracking error e_1 is regulated asymptotically to zero.

For the fin model, $H(s)$ is minimum phase because $n_p(s)$ is Hurwitz and $\mu > 0$. Moreover, by the choice of the output y , the transfer function has relative degree one. As such using a simple argument from the root-locus technique, it is easily seen that a negative feedback law of the form

$$u_f(t) = -K_e e_1 \quad (6.46)$$

can stabilize the system (6.43), where $K_e > 0$. Indeed, as K_e tends to ∞ , the root loci of the closed-loop poles converge to finite stable zeros of $H(s)$ and one of the pole tends to $-\infty$ along the asymptote with angle π . This is interesting, because it is an extremely simple control law and yet it accomplishes error regulation.

Consider a minimal realization of $H(s)$ given by

$$\begin{aligned} \dot{x}_a &= A_a x_a + B_a u_f \\ e_1 &= C_a x_a \end{aligned} \quad (6.47)$$

where A_a , B_a and C_a are appropriate matrices. Of course, these matrices are not required for

synthesis. Since $H(s)$ is minimum phase with relative degree one, it follows that there exists a gain $K^* > 0$ such that [61]

$$\begin{aligned} P(A - K^* B_a C_a) + (A - K^* B_a C_a)^T P &= -Q < 0 \\ P B_a &= C_a^T \end{aligned} \tag{6.48}$$

where P and Q are positive definite symmetric matrices. However, K^* is not known. Let \hat{K} be an estimate of K^* and consider an output feedback law

$$u_f = -\hat{K} e_1 \tag{6.49}$$

The goal is now to adaptively tune \hat{K} to accomplish error regulation. Using (6.49) in (6.64) gives

$$\dot{x}_a = (A_a - K^* B_a C_a) x_a + (K^* B_a C_a x_a - \hat{K} B_a e_1) \tag{6.50}$$

Defining the parameter error $\tilde{K} = K^* - \hat{K}$, (6.50) gives

$$\dot{x}_a = \bar{A} x_a + \tilde{K} B_a e_1 \tag{6.51}$$

where $\bar{A} = (A_a - K^* B_a C_a)$ is a Hurwitz matrix since (6.48) holds.

For the derivation of the adaptation law, consider a quadratic Lyapunov function

$$V = x_a^T P x_a + \gamma \tilde{K}^2 \tag{6.52}$$

where $\gamma > 0$. The derivative of V along the solution of (6.50) is given by

$$\dot{V} = x_a^T(PA_a + A_a^T P)x_a + 2x_a^T P\tilde{K}B_a e_1 + 2\gamma\tilde{K}\dot{\tilde{K}} \quad (6.53)$$

Using (6.48) in (6.53) and noting that $x_a^T P B_a = x_a^T C_a^T = e_1$ gives

$$\dot{V} = -x_a^T Q x_a + 2\tilde{K}(\gamma\dot{\tilde{K}} + e_1^2) \quad (6.54)$$

In order to eliminate \tilde{K} form, the adaptation law is chosen as

$$\dot{\tilde{K}} = -\dot{\tilde{K}} = -\gamma^{-1}e_1^2 \quad (6.55)$$

Substituting (6.55) in (6.54) gives

$$\dot{V} = -x_a^T Q x_a \leq 0 \quad (6.56)$$

Since $V(x_a, \tilde{K})$ is positive definite and $\dot{V} \leq 0$, x_a and \tilde{K} are bounded. Furthermore, invoking Barbalat's Lemma [62], one can establish that x_a tends to zero which in turn implies that $e_1 = C_a x_a$ converges to zero and β tends to β^* .

The control input $u(t)$ now can be obtained using (6.43). In view of (6.43), one has

$$\hat{u} = \left(\frac{s + \mu}{s}\right)\hat{u}_f \quad (6.57)$$

which yields

$$u(t) = u_f(t) + \mu \int_0^t u_f(\tau) d\tau \quad (6.58)$$

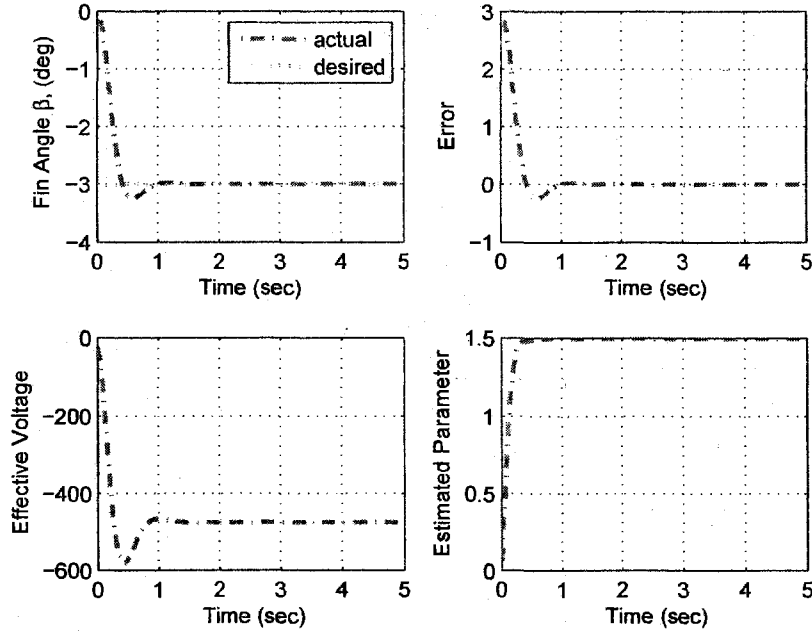


Figure 6.7: Simulation Results at zero Wind Speed

Using $u_f(t) = -\hat{K}(t)e_1(t)$ in (6.58) gives

$$u(t) = -\hat{K}(t)e_1(t) - \mu \int_0^t \hat{K}(\tau)e_1(\tau)(t)d\tau \quad (6.59)$$

We notice that for a constant \hat{K} , the control input simply uses proportional and integral feedback of the tracking error.

6.3.2 Simulation Results

This section presents the simulation results for the smart fin including the servoregulator. The initial value of \hat{K} is taken as *zero*. Simulation is done for various reference commands. Figure 6.7 show the simulation results for fin angle command of -3 degrees. It is observed that the fin angle asymptotically converges to the desired value in 1 second. The control input needed for the fin to deflect to angle $\theta = -3$ deg is $485V$. We observe that there is a overshoot

in the responses. Extensive simulation has been done using various command inputs. These results show that the regulator is effective to control of the fin angle in each case.

6.3.3 Experimental Results

The simulation results show that controller accomplishes fin angle control but this control law can not guarantee closed-loop stability because of identified model is linear and approximate representation of the non-linear smart fin system. The adaptation law must be modified to avoid parameter divergence. Therefore we have used σ modification yielding a modified adaptation law given by

$$\dot{\hat{K}} = \gamma^{-1}(e_1^2 - \sigma \hat{K}) \quad (6.60)$$

for the laboratory tests. It can be shown that in the presence of bounded disturbances, the modified law prevents parameter divergence but may yield a finite terminal tracking error.

Performance Under No-Wind Conditions

The reference fin angle is set to -3 deg during real-time simulation. For feedback the signal $\theta + 0.1\dot{\theta}$ is used. The initial value of \hat{K} is taken as *zero*. The value of σ is set to 0.01. The real-time simulation is carried at a time step of 0.001 s. Results are shown in Fig. 6.8. We observe asymptotic fin angle tracking is accomplished. The time taken to track the reference trajectory is approximately less than 2 s.

Performance Under Wind Loading

The designed adaptive controller is evaluated under varying operating conditions. The smart fin is tested under different angles of attack, $\alpha = (0, -5, -10)$, and wind speed of 40.23 m/s. The same desired angle is used for all cases. The value of \hat{K} is taken as *zero*. The real-time simulation is carried out at a time step of 0.001 seconds. Experimental results for fin angle control is shown in Fig. 6.9. The control input required to reach their target values

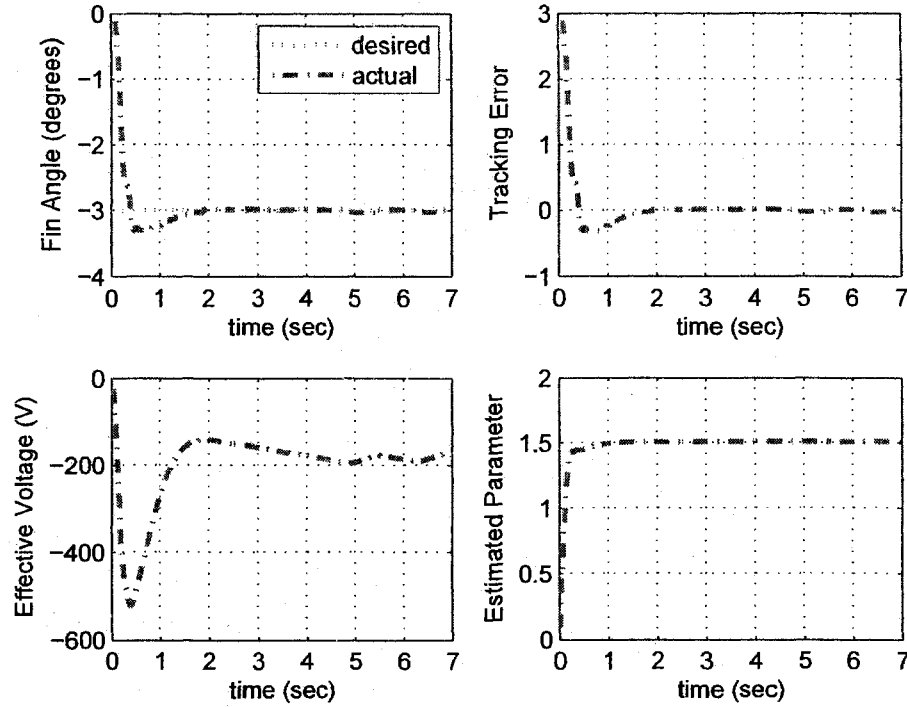


Figure 6.8: Experimental Results at zero Wind Speed

is shown in Fig. 6.10. The controller successfully drive the fin towards the desired trajectory by overcoming the aerodynamic disturbance.

6.3.4 Conclusions

An adaptive servoregulator is designed for the control of fin angle. Simulation and experimental results shows that the designed adaptive control system accomplishes precise fin angle control in spite of uncertainties in the fin parameters and the aerodynamic moment coefficients.

6.4 Adaptive Control: Fin Angle Feedback

This section deals with an adaptive controller based on only fin angle feedback information. For the derivation of control law, it is assumed system matrices D , Ω , B_1 , C_0 and F_1 are

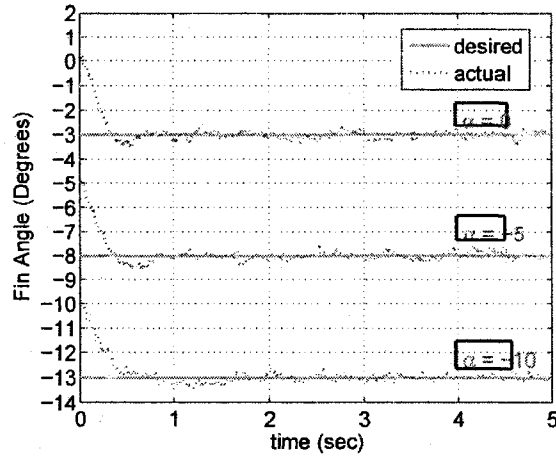


Figure 6.9: Fin Angle Response under Various Angles of Attack at Wind Speed 40.23 m/s

completely unknown, and only the fin angle is measured for feedback. Control using only the fin angle measurement is very practical since measurements of the flexible modes is not easy. Suppose that $\beta^*(t)$ is a given smooth bounded reference fin angle trajectory, we are interested in designing an adaptive control system such that the fin angle tracking error asymptotically satisfies $|\tilde{e}(t)| = |\beta(t) - \beta^*(t)| < \epsilon_0$, where the error bound ϵ_0 is any given positive real number, in spite of the action of disturbance input $v(t)$.

6.4.1 Control Law

We select the controlled output variable as

$$\begin{aligned} y &= \beta \\ &\equiv Cx \end{aligned} \tag{6.61}$$

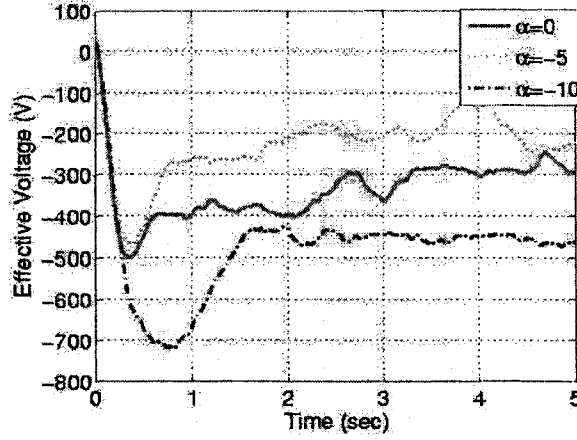


Figure 6.10: Effective Voltages to the MFC's under positive Angles of Attack and 40.23 m/s Wind Velocity

From (6.61), one obtains

$$\begin{aligned}
 \hat{y}(s) &= C(SI - A)^{-1}B\hat{u}(s) + C(SI - A)^{-1}F\hat{v}(s) \\
 &= \frac{n_p(s)}{d_p(s)}\hat{u}(s) + \frac{n_f(s)}{d_p(s)}\hat{v}(s) \\
 &= H(s)[\hat{u}(s) + \frac{n_f(s)}{n_p(s)}\hat{v}]
 \end{aligned} \tag{6.62}$$

where s is the Laplace variable and \hat{u} and \hat{v} denote Laplace transforms of u and v respectively; and

$$\begin{aligned}
 n_p(s) &= C[\text{adj}(SI - A)]B \\
 n_f(s) &= C[\text{adj}(SI - A)]F \\
 d_p(s) &= \det(sI - A) \\
 H(s) &= \frac{n_p(s)}{d_p(s)}
 \end{aligned} \tag{6.63}$$

It is easily seen from (6.4) that $d_p(s)$ is a Hurwitz polynomial. Computing the polynomial $n_p(s)$ for this model, one finds that it is a Hurwitz polynomial, Therefore the transfer function

$H(s)$ is minimum phase and its relative degree is 2.

We make the following assumptions for the purpose of control law derivation.

- **Assumption 1.** Only output variable (fin angle) $y(t)$ is measured for synthesis.
- **Assumption 2.** Reference signal $y^*(t)$ and its derivatives are smooth and bounded.
- **Assumption 3.** Disturbance v and its derivatives are bounded.
- **Assumption 4.** $H(s)$ is minimum phase and the high-frequency gain is positive.

The tracking error $e = y - y^* = \beta - \beta^*(t)$ is

$$\begin{aligned} e &= \frac{n_p(s)}{d_p(s)} [\hat{u}(s) - \frac{n_f(s)}{n_p(s)} \hat{v} - \frac{d_p(s)}{n_p(s)} \hat{y}^*(s)] \\ &= \frac{n_p(s)}{d_p(s)} [\hat{u}(s) + w(s)] \end{aligned} \quad (6.64)$$

where $y^* = \beta^*(t)$ is the time-varying reference trajectory and

$$w(s) = \frac{n_f(s)}{n_p(s)} \hat{v} - \frac{d_p(s)}{n_p(s)} \hat{y}^*(s)$$

is bounded function because n_p is stable polynomial. So, it is possible to revise the problem of output tracking of a reference trajectory $\beta^*(t)$ as stabilization problem of the model (6.64).

So, Let us choose the control law as

$$u(t) = -\chi(s)(\mu + k)\hat{e} \quad (6.65)$$

where number $k > 1$, $\chi(s) = (s + 1)$ and coefficient μ are chosen so that polynomial $\gamma(s) = d_p(s) + \mu n_p(s)\chi(s)$ is Hurwitz. The transfer function $H(s)$ is of relative degree 2, as such the

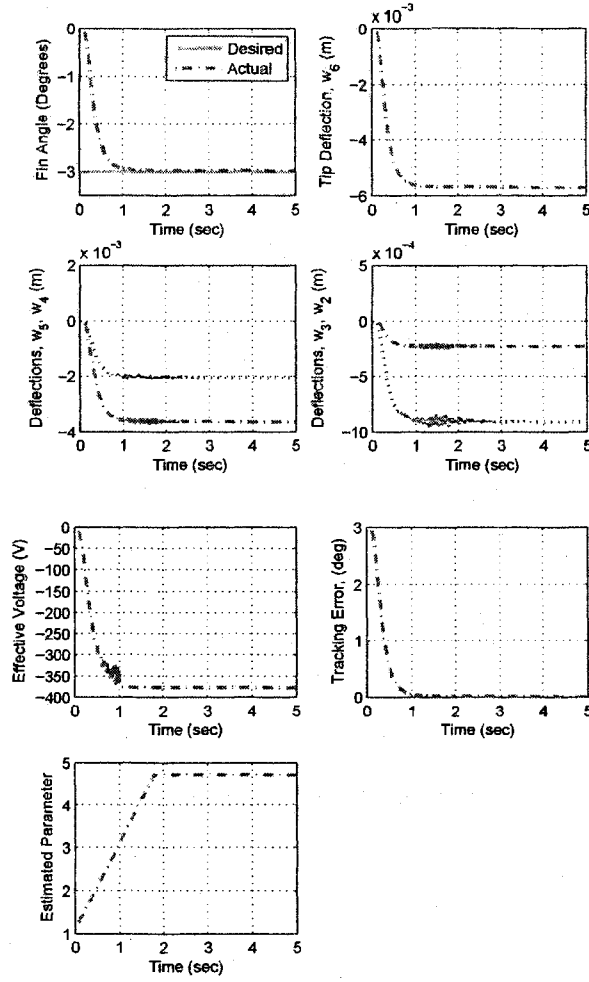


Figure 6.11: Simulated Fin Angle Response under no disturbance

signal $\hat{e}(t)$ is constructed using a first-order filter given by

$$\frac{d\hat{e}}{dt} = \sigma k_1 (e - \hat{e}) \quad (6.66)$$

where $\sigma > (\mu + k)$ and $k_1 > 0$. Note that for $e = 0$, $\hat{e}(0)$ is asymptotically stable.

Substituting (6.65) into (6.64), one obtains

$$\begin{aligned} e &= \frac{n_p(s)}{d_p(s)} (-\chi(s)(\mu + k)\hat{e} + w(t)) \\ &= \frac{n_p(s)}{d_p(s)} (-\chi(s)(\mu + k)e + \chi(s)(\mu + k)\varepsilon + w(t)) \end{aligned} \quad (6.67)$$

where $\varepsilon = e - \hat{e}$.

Let us rewrite the (6.67) in the following way

$$d_p(s)e + \mu n_p(s)\chi(s)e = n_p(s)\chi(s)((\mu + k)\varepsilon - ke + w'(t)) \quad (6.68)$$

where $w'(t) = \frac{1}{\chi(s)}w(t)$

By simplifying the equation (6.68)

$$e = \frac{\psi(s)}{\gamma(s)} (-ke + (\mu + k)\varepsilon + w'(t)) \quad (6.69)$$

where $\psi(s) = n_p(s)\chi(s)$, and $\gamma(s) = d_p(s) + \mu n_p(s)\chi(s)$.

The state-space representation of Eq. (6.69)

$$\begin{aligned} \dot{x}_a &= A_a x_a + B_a (-ke + (\mu + k)\varepsilon + w'(t)) \\ e_1 &= C_a^T x_a \end{aligned} \quad (6.70)$$

where A_a , B_a and C_a are appropriate matrices. It has been shown in [63] that there exists a $\mu > 0$ such that the transfer function, $H_a = C_a^T(sI - A_a)^{-1}B_a$ is strictly positive real. Exploiting the SPR property of $H_a(s)$, it has been established in [63] such that there exists $\sigma > \mu + k$ such that all trajectories of the system are bounded and that for a choice of

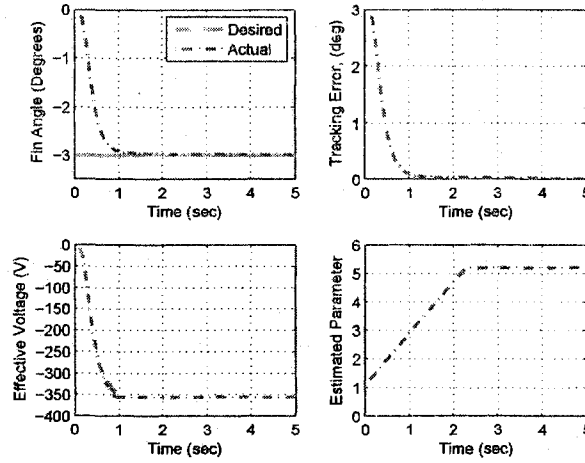


Figure 6.12: Simulated Fin Angle Response at Angle of Attack = -5°

parameter k , tracking error asymptotically satisfies $|\tilde{e}(t)| = |y(t) - y^*(t)| < \epsilon_0$, where the ϵ_0 is the prescribed error bound. The matrices A_a , B_a and C_a are not required for synthesis. For the complete proof for closed loop stability, one can refer to [63].

The control input $u(t)$ now can be obtained using Eq. 6.65. In view of Eq. 6.65, one has

$$\begin{aligned}
 u &= -(s+1)(\mu+k)\hat{e} \\
 &= -(\mu+k)[\dot{\hat{e}} + \hat{e}] \\
 &= -(\mu+k)[\sigma k_1(e - \hat{e}) + \hat{e}]
 \end{aligned} \tag{6.71}$$

Since the parameters of the system are unknown, the value of the k is not known. Let \tilde{k} be an estimate of $k + \mu$. For tuning \tilde{k} , we can use the algorithm proposed by Bobstov and Nikolaev [64].

$$\frac{d\tilde{k}}{dt} = \lambda(t) \tag{6.72}$$

where $\tilde{k}(0) > 1$ and based on the tracking error ϵ_0 , the function $\lambda(t)$ is calculated in the

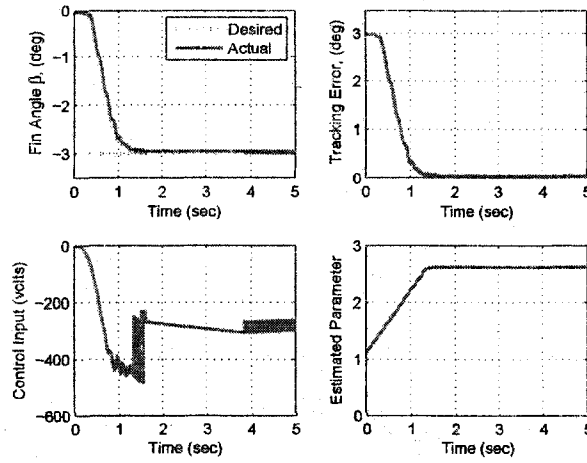


Figure 6.13: Fin Angle Response under No-Wind Conditions

following way

$$\lambda(t) = \begin{cases} \lambda_0 & \text{for } |e| > \epsilon_0, \\ 0, & \text{for } |e| \leq \epsilon_0 \end{cases} \quad (6.73)$$

where $\lambda_0 > 0$. The value of σ is set to $\sigma_0 \tilde{k}^2$, where $\sigma_0 > 0$.

The adaptive version of control law (6.71) is obtained by using the estimate of \tilde{k} for $k + \mu$ in (6.71). Using the estimate \tilde{k} in (6.71) gives

$$\begin{aligned} u &= -(s + 1)\tilde{k}\hat{e} \\ &= -\dot{\tilde{k}}\hat{e} - \tilde{k}\dot{\hat{e}} - \tilde{k}\hat{e} \end{aligned} \quad (6.74)$$

Using the tuning law (6.73) and estimation equation (6.66) in (6.74) gives

$$u = -\lambda(t)\hat{e}(t) - \tilde{k}[\sigma k_1(e - \hat{e})] - \hat{e} \quad (6.75)$$

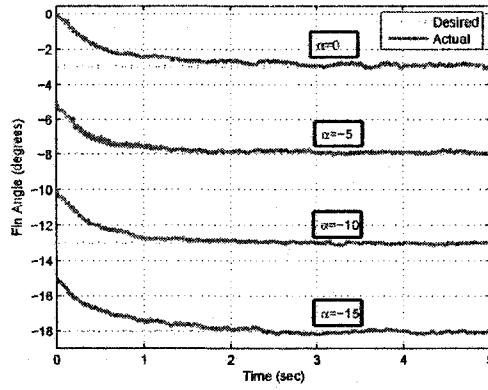


Figure 6.14: Fin Angle Response under Various Angles of Attack at Wind Speed 40.23 m/s

6.4.2 Simulation Results

The simulation results for the smart fin based on the theoretical model using the digital computer (including the adaptive control law) are presented in this section. The mechanical and geometrical properties of the of the simulated model are shown in Table 3.1. The mass moment of inertia of the smart fin, J_f , is 0.001 kg-m^2 . The bimorph is modeled using the *five* elements of equal length. A state-variable representation of the smart fin model of dimension of 20 is obtained for simulation. The aerodynamic moment (4.18) is chosen for different angles of attack of the projectile based on the CFD analysis. The parameters of the aerodynamic moment are estimated by a linear approximation of the data obtained by the CFD analysis. Those parameters of the aerodynamic moment are $m_{a0} = -0.0022, p_a = +0.0005$ for $\alpha = -5^\circ$, and $m_{a0} = -0.0028, p_a = +0.01$ for $\alpha = +5^\circ$. The value of ϵ_0 and σ is chosen as 0.05 and 5 respectively. The initial value of $\tilde{k}(0)$ is set to be 1.1. Simulation is done using the above values for different reference commands at no disturbance and also at different angles of attack.

The simulation results are given for the reference fin angle $\beta^* = -3^\circ$ at no aerodynamic moment acting on the fin and at angle of attack, $\alpha = -5$, in Figure 6.11 and in Figure 6.12 respectively. Simulation results show that the fin angle asymptotically converges to the

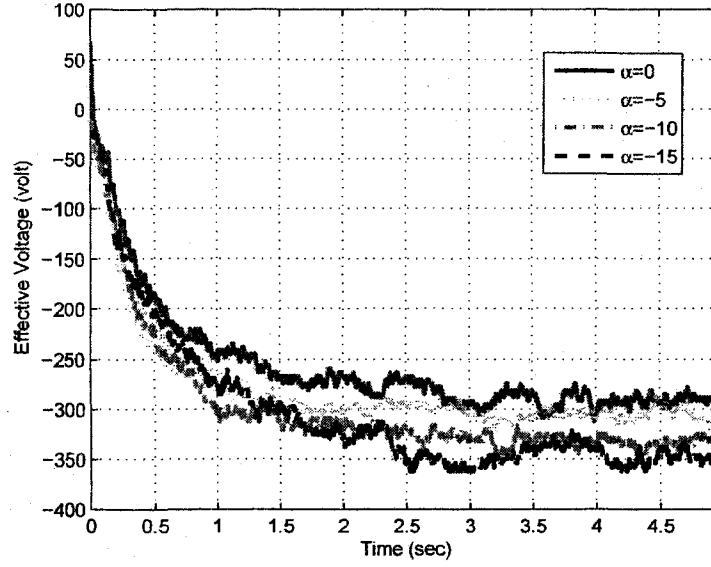


Figure 6.15: Effective Voltage to the MFC's under various Angles of Attack and 40.23 m/s Wind Velocity

target angle by adapting the estimated parameter \tilde{k} . The voltage required to rotate the fin is approximately $-375V$. In case of $\alpha = -5$, the voltage required is $-350V$.

There is no overshoot in the results and the flexible modes reach steady state values. The estimated parameter remain bounded and converge to certain constant values.

6.4.3 Experimental Results

This section discusses the validation of the developed controller by testing it within a subsonic wind tunnel under no-wind and wind conditions.

Performance Under No-Wind Conditions

The adaptive controller, Eq. 6.75, is validated by first testing it within the wind tunnel for zero wind speed. The reference fin angle is set to $\beta^* = -3^\circ$ during real-time simulation. The values of ϵ_0 , σ and $\tilde{k}(0)$ are chosen similar to simulation results. The experimental simulation is carried out at a time step of 0.001 sec. Results are shown in Fig. 6.13. The chattering in

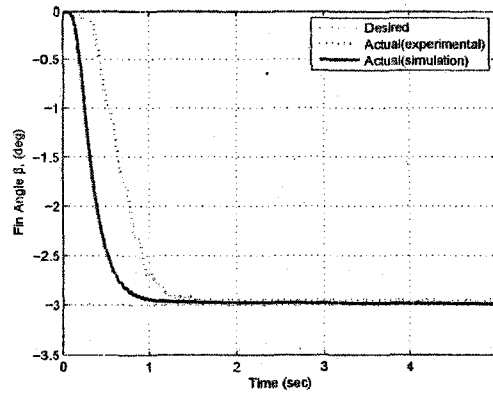


Figure 6.16: Comparison: Fin Angle Responses at No Disturbance

control input can explained by accuracy of the encoder and can avoid by tuning the estimated parameter. Results show that controller has the capability of tracking the prescribed fin angle trajectory. The time taken to track the reference trajectory is approximately 1.5 sec.

Performance Under Wind Loading

As the smart fin will be operated under different circumstances, the controller should be robust enough to reject the disturbances. Wind tunnel experiments are conducted to assess the performance of the designed adaptive controller. The smart fin is tested under various angles of attack, $\alpha = 0^\circ, -5^\circ, -10^\circ, -15^\circ$. The reference fin angle is set to be $\beta^* = -3^\circ$ for all cases. The initial value of parameter $\tilde{k}(0)$ is set to 1.1. The value of σ is chosen to be 10. The experimental data is collected at every 0.001 second. The experimental results are shown in Figure 6.16 for wind speed 40.23 m/s. The corresponding effective voltage results are shown in Fig. 6.15. The controller possesses the ability to track the target angle within 1.5 seconds by adapting the parameter \tilde{k} and it can reject the aerodynamic wind pressure.

Comparison: Simulation and Test Results at No Disturbance

This section presents the comparison between digital computer simulation and test results. The same reference angle is chosen in both cases. The initial value of parameter $\tilde{k}(0)$ is set to

1.1 in both cases. In both cases, the \tilde{k} converges to positive certain value. The controller can track the desired target angles in both cases.

The time taken to track the reference trajectory in case of computer simulations is faster compared to test results. This can be explained by the fact that the theoretical finite element model does not include amplifier and sensor dynamics. The voltage required to reach the target angle is not same in both cases because the theoretical (ideal) model of the Section III is only an approximate representation of the physical fin system.

6.4.4 Conclusions

An adaptive controller is designed to control the rotation angle of a smart projectile fin. A piezoelectric bimorph is used to actuate the fin. The model of the fin system includes the aerodynamic moment which is a function of angles of attack of the projectile. A state variable model using finite element method was obtained. For the purpose of design, the dimension as well as the parameters of the model were assumed to be completely unknown. Moreover, only the fin angle is used for controller synthesis. An adaptive controller is designed for control of fin rotation angle. Simulation and wind tunnel test results show that the designed adaptive control system accomplishes fin angle control in spite of uncertainties in the fin parameters and the aerodynamic coefficients.

CHAPTER 7

SALIENT FEATURES OF DEVELOPED ALGORITHMS

Five kinds of control algorithms are developed in this work based on fuzzy logic and adaptive techniques to control the rotation angle of the smart projectile fin. They are:

1. Fuzzy Logic Control: GA-Based (FLC-GA)
2. Fuzzy Logic Control: Inverse Dynamics Based
3. Adaptive Control: Nussbaum Gain Based
4. Adaptive Control: Servoregulator (Adaptive Servo)
5. Adaptive Control: Only Fin Angle Feedback (Adaptive Feedback)

The major advantage of fuzzy logic controllers is that it requires less complex mathematical modeling because the controller rules are especially based on the knowledge of the system behavior and the experience of the control engineer. The GA-Based controller uses HFSGA to tune the performance of this controller by varying the ranges and shapes of the membership functions of its input and output variables. Several experiments are conducted inside and outside the wind tunnel to assess performance of this controller. Results also show that the fuzzy controller is robust enough to overcome various operating disturbances and subsonic wind velocities.

Inverse dynamics based controller presents a novel approach for automatically creating fuzzy logic controllers for the fin. A method for adjusting ranges of the variables for the

inputs and outputs of the fuzzy logic controller according to the system characteristics and desired motion using inverse dynamics equations is presented. This method has the advantage of avoiding guessing acceptable ranges of the variables. Simulation results show that the proposed controller can successfully drive smart fin under various operating conditions. This controller has to be implemented in real-time to check the performance.

As smart fin is operated under various operating conditions, the designed control law has to be modified by the controller itself to reject the disturbances and also to track the desired trajectory. The adaptive control has that capability by adapting the estimated parameters to operating environment. Moreover, for the fuzzy controller, the designer has to develop a number of if-then rules which often are not easy to obtain for the design of the fuzzy controller.

The Nussbaum gain adaptive control system does not require the knowledge of high-frequency gain. The fin angle and its derivative are used for the synthesis of the controller. This controller requires tuning of two gains and it can reject the aerodynamic disturbance without any adaptive law modification. The fin angle converges to the desired value generated by the command generator in the closed-loop system. Computer simulation results based on theoretical model show that the designed adaptive control system accomplishes fin angle control in spite of the uncertainties in the fin parameters and the aerodynamic coefficients. The numerical simulation results show that adaptive controller accomplishes fin angle control but this control law cannot guarantee closed-loop stability, because the theoretical fin model is only approximate representation of the physical model. The adaptive law must be modified for closed-loop stability in the presence of unmodeled dynamics and external disturbance inputs. Although, control law can guarantee closed-loop stability and trajectory control, wind tunnel tests show inferior transient response caused by the nonlinearity of the Nussbaum gain. The modified adaptive controller is tested in the UNLV subsonic wind tunnel at different wind

speed to validate the controller. Test results show that the proposed adaptive controller tracks the desired fin angle even in the presence of aerodynamic disturbance.

An adaptive servoregulator has been developed to control the smart fin angle. A linear combination of the fin angle and fin's angular rate is chosen as the controlled output variable similar to above controller. Here the controller requires tuning of only single gain, this controller is capable of rejecting the constant aerodynamic disturbance torque without any adaptive law modification. In the closed-loop system, the fin angle asymptotically converges to the target fin angle generated by a command generator. This adaptation law must be modified to avoid the parameter divergence for real-time simulation. The modification of the adaptation rule may sometimes give terminal tracking error. The developed controller is tested at different operating environment. Test results show that this controller is robust enough to overcome the disturbances and accomplishes fin angle.

7.1 Comparative Analysis of the Fin Angle Response of Fuzzy Logic and Adaptive Controllers

This section presents the comparative analysis of the developed controllers in this work. An adaptive servoregulator requires tuning of only single gain to improve the performance of the controller but this controller needs the knowledge of the sign of high-frequency gain. Moreover, it cannot guarantee asymptotic tracking of the fin angle in the presence of time-varying disturbance torque.

An adaptive controller based on Nussbaum gain does not require the knowledge of the high-frequency gain and it can handle the time-varying disturbance, but this controller requires two gain parameters to tune the performance of the controller. This controller can able to track the up to -2° desired fin angle and also it can able to reject the disturbance only up to

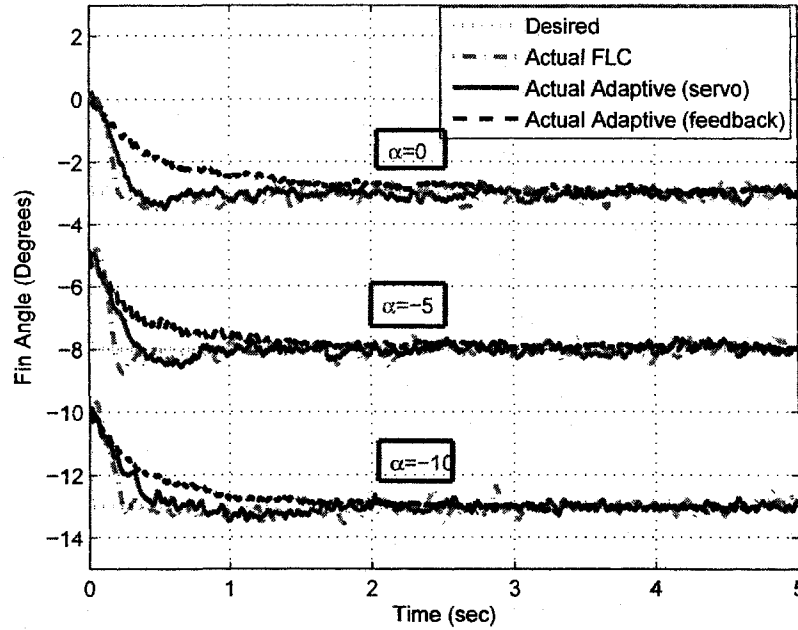


Figure 7.1: Fin Angle Responses for the Controllers (FLC-GA, Adaptive Servo, Adaptive Feedback) for Various Angles of Attack ($\alpha = 0^\circ, -5^\circ, -10^\circ$) at 40.23 m/s Wind Velocity

14.23m/s wind velocity during real-time simulation.

An adaptive controller based on only fin angle feedback requires only one gain parameter for tuning the controller and also only fin angle feedback is needed for controller design. Thus we can save a rate sensor. This is important when space spacing is essential in small aerial vehicles.

Fuzzy controller based on GA can track the desired fin angle and also reject the aerodynamic wind force but the designer has to develop a number of if-then rules which often are not easy to obtain for the design of the controller. A fuzzy controller based on inverse dynamics does not have a test result in this work.

The controllers FLC-GA, Adaptive Servo, Adaptive Feedback are tested at a wind speed of 40.23 m/s for various angles of attack, $\alpha = (0^\circ, -5^\circ, -10^\circ)$, at conditions similar to each

other. The same reference trajectory is used for all cases. The fin angle responses for three controllers are compared in Fig. 7.1. While the response for FLC-GA controller is faster to the other controllers, the controller Adaptive Servo and Adaptive Feedback produces less deviation after steady state from the steady state target of the fin angle as compared to FLC-GA controller. The controller Adaptive Feedback has less transient response when compared to other controllers.

CHAPTER 8

CONCLUSIONS

This dissertation considered the control of rotation angle of a smart projectile fin. These fins, which are deployed when the projectile reaches the apogee, are used to either steer the projectile toward its target or to stabilize it. The smart fin has a rigid hollow aero-shell that rotates around an axle, which is fixed within the body of the projectile. The cantilevered piezoelectric bimorph actuator is completely enclosed within the aero-shell of the fin.

The complete details of the actuator used in this work is discussed in second chapter. This chapter also gives the various configurations of actuators which can give the maximum deflection. The piezoelectric bimorph with no substrate found to be best configuration to achieve more fin angle.

The third chapter discussed the configuration of the smart fin. It also included the prototype of the fin, which is developed using rapid-prototyping machine. It is also presented the complete test setup for the real-time tests in the laboratory and in the wind tunnel to validate the developed controllers in real-time.

In the fourth chapter, two different models for the smart fin system are derived, i.e mathematical model based on finite element approach and identified model based on experimental data. The mathematical model includes the aerodynamic moment, which is function of the angle of attack of the projectile. MATLAB System Identification Tool Box is used to obtain a identified model of the smart fin system based on experimental data that is acquired by exciting the system using a chirp signal. Comparison is done between two models on the basis

of open-loop step response of the smart fin system. The results show that both models are comparable to the test results.

The fifth chapter considered the fuzzy logic control for the smart fin. Two fuzzy controllers are developed in this work. One is based on Genetic Algorithm that uses third order linear model. HFSGA is used to tune the performance of this controller by varying the ranges and shapes of the membership functions of its input and output variables. Results show that the fuzzy controller is robust enough to overcome various operating disturbances and subsonic wind velocities. Second controller is based on inverse dynamics that uses the mathematical model. A method for adjusting ranges of the variables for the inputs and outputs of the fuzzy logic controller according to the system characteristics and desired motion using inverse dynamics equations is presented. This method has the advantage of avoiding guessing acceptable ranges of the variables. Results show that this controller can successfully function under various operating conditions.

Finally in chapter 6, various adaptive controllers are designed for the control of the fin angle and the rejection of disturbance input. For the purpose of design of these controllers, the dimension as well as the parameters of the model are assume to be completely unknown. A linear combination of the fin angle and fin's angular rate is chosen as the controlled output variable for two adaptive controllers. Other adaptive controller uses only fin angle for feedback. Computer simulations showed that in the closed-loop system, the fin angle is precisely controlled in spite of uncertainties in the system parameters and aerodynamic moment coefficients. Experimental results show that the designed adaptive controllers accomplishes fin angle control.

The salient features of the designed algorithms in this research work are discussed in chapter seven. The comparison is also done in this chapter. It is found to be each controller has

it's own advantages and disadvantages depending upon the operating environment. Finally, the future work of this research is discussed in chapter 9.

CHAPTER 9

FUTURE WORK

The piezoelectric actuators are well suited elements in high precision positioning applications such as scanning probe microscopy (SPM), scanning tunneling microscopy (STM), optical alignments, diamond turning machines, active vibration control of rotor bearing systems [65]. These actuators are used to meet the requirements of high resolution in displacement. However, the existence of nonlinear multi-path hysteresis in piezoelectric material complicates the control of a piezoelectric actuator in precision applications. So, there is a need to develop the hysteresis model of the smart fin, actuated by piezoelectric actuator, to improve the tracking performance of the controller. The typical hysteresis of the smart fin system is shown in Fig. 9.1. The developed controllers, as discussed in chapter 5 and chapter 6, have controllers have less tracking performance for tracking sinusoidal reference trajectory because these are based on linear model of the system.

One of the future work includes modeling of a piezoelectrically actuated smart fin hysteresis and design a controller based on hysteresis model to track the sinusoidal reference trajectory with minimum error based compared to earlier designed controllers.

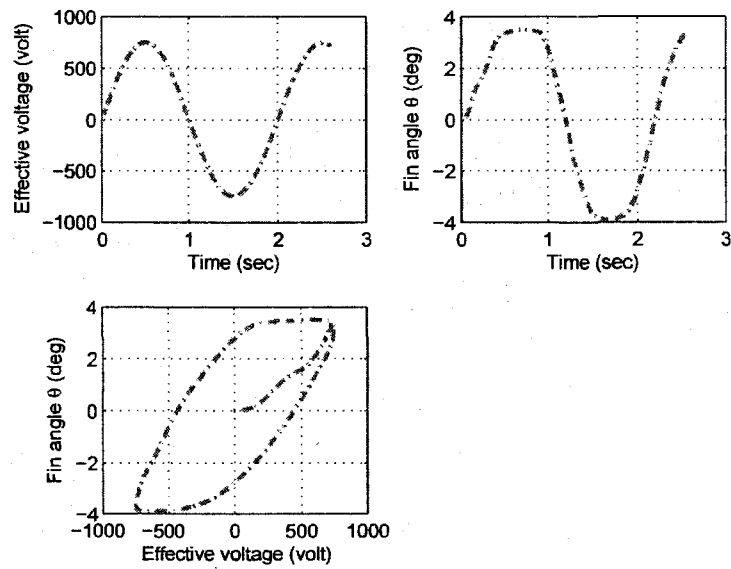


Figure 9.1: Hysteresis of smart fin. The plot shows sinusoidal response of the System with $0.5Hz$ frequency voltage signal

BIBLIOGRAPHY

- [1] A. Bent, "Active fiber composite material systems for structural control applications," *SPIE's 6th International Symposium on Smart Structures and Materials*, 1999.
- [2] W. Wilkie, R. Bryant, J. High, R. Fox, R. Hellbaum, A. Jalink, B. Little, and P. Marick, "Low-cost piezoelectric actuator for structural control applications," *SPIE 7th Annual International Symposium on Smart Structures and Materials*, 2000.
- [3] R. C. Batra and K. Ghosh, "Deflection control during dynamic deformations of a rectangular plate using piezoceramic elements," *AIAA Journal*, vol. 33, no. 8, pp. 1547–1548, 1995.
- [4] C. Niezrecki, D. Brei, S. Balakrishnan, and A. Moskalik, "Piezoelectric actuation: State of the art," *Articles*.
- [5] D. J. Cappelleri and M. I. Frecker, "Optimal design of smart tools for minimally invasive surgery," *Proceedings of Optimization in Industry II*, 1999.
- [6] G. Y. Zhou and Q. Wang, "Design of a smart piezoelectric actuator based on a magnetorheological elastomer," *Institute of Physics Publishing (Smart Material. Structures)*, vol. 14, pp. 504–510, 2005.
- [7] C. C. Lin, C. Y. Hsu, and H. N. Huang, "Finite element analysis on deflection control of plates with piezoelectric actuator," *Composite Structure*, vol. 35.
- [8] F. Lowrie, "Finite element modeling of electroceramics," *NPL Reporst CMMT (A) 150*, 1999.
- [9] J. Mathew, B. Sankar, and L. Cattafesta, "Finite element modeling of piezoelectric actuators for active flow control applications," *AIAA*, 2001.
- [10] Z. Q. Qu, "An efficient modeling method for laminated composite plates with piezoelectric sensors and actuators," *Institute of Physics Publishing (Smart Material. Structures)*, vol. 10, pp. 807–723, 2001.
- [11] M. C. Reaves and L. G. Horta, "Piezoelectric actuator modeling using msc/nastran and matlab," *NASA/TN*, vol. 212651, 2003.
- [12] M. Brissaud, S. Ledren, and P. Gonnard, "Modelling of a cantilever non-symmetric piezoelectric bimorph," *Journal of Micromechanics and Microengineering*, vol. 13, pp. 832–844, 2003.
- [13] Q. Li, M. L. nad J. Mei, and W. Clark, "A study of displacement distribution in a piezoelectric heterogeneous bimorph," *Journal of Mechanical Design*, vol. 126, pp. 757–763, 2004.

- [14] G. L. C. M. de Abreu, J. F. Ribeiro, and J. V. Steffen, "Finite element modeling of a plate with localized piezoelectric sensors and actuators," *Journal of Braz. Soc. of Mech. Sc. and Eng.*, vol. 2, pp. 117–125, 2004.
- [15] R. Barrett, "Active plate and missile wing development using directionally attached piezoelectric elements," *AIAA Journal*, vol. 32, no. 3, pp. 601–609, 1994.
- [16] P. E. Frederick, "Development of a piezoelectric servo-flap actuator for helicopter rotor control," *MIT Libraries*, 1994.
- [17] A. August and S. Joshi, "Preliminary design of smart structure fins for high-speed missiles," *Proceedings of SPIE - The International Society for Optical Engineering*, vol. 2721, pp. 58–65, 1996.
- [18] O. Rabinovitch and J. Vinson, "On the design of piezoelectric smart fins for flight vehicles," *Smart Materials and Structures*, vol. 12, pp. 686–695, 2003.
- [19] O. Bilgen, K. Kochersberger, E. C. Diggs, A. J. Kurdila, and D. Inman, "Morphing wing aerodynamic control via macro-fiber-composite actuators in an unmanned aircraft," *AIAA Conference and Exhibit*, 2007.
- [20] S. B. Choi, C. C. Cheong, and C. H. Lee, "Position tracking control of a smart flexible structure featuring a piezofilm actuator," *Journal of Guidance, Control and Dynamics*, vol. 19, no. 6, 1996.
- [21] S. B. Choi and C. H. Lee, "Force tracking control of a flexible gripper driven by piezoceramic actuator," *Journal of Dynamic Systems, Measurement, and Control*, no. 119, pp. 439–445, 1996.
- [22] S. B. Choi, H. K. Kim, S. C. Lim, and Y. P. Park, "Position tracking control of an optical pick-up device using piezoceramic actuator," *Mechatronics*, vol. 11, no. 15, pp. 691–705, 2001.
- [23] H. Jung, J. Y. Shim, and D. Gweon, "Tracking control of piezoelectric actuators," *Institute of Physics Publishing (Nanotechnology)*, vol. 12, 2001.
- [24] Q. Lu, Z. Peng, F. Chu, and J. Huang, "Design of fuzzy controller for smart structures using genetic algorithms," *Institute of Physics Publishing (Smart Material. Structures)*, vol. 12, pp. 979–987, 2003.
- [25] M. P. Patel, J. Lopera, and T. T. Ng, "Active boattailing and aerodynamic control fins for maneuvering weapons," *AIAA Flow Control Conference*, 2004.
- [26] L. N. Iogru and H. Baruh, "Refined analysis of the piezoelectric pseudo-active control for helicopter blades vibration," *47th AIAA/ASME/ASCE/AHS/ASC Structures, Structural Dynamics, and Materials Conference*, 2005.
- [27] T. Bailey and J. E. Hubbard, "Distributed piezoelectric-polymer active vibration control of a cantilever beam," *J. of Guidance, Control, and Dynamics*, vol. 8, no. 5, pp. 605–611, 1985.
- [28] A. Baz and S. Poh, "Performance of an active control system with piezoelectric actuator," *Journal of Sounds and Vibration*, vol. 126, no. 2, pp. 327–343, 1988.

- [29] M. K. Kwak and D. Sciulli, "Fuzzy-logic based vibration suppression control experiments on active structures," *Journal of Sound and Vibration*, vol. 191, pp. 15–28, 1996.
- [30] K. Jorabchi and A. Yousufi-Koma, "A neural network controller for vibration suppression of a smart fin," *AIAA/ASME/ASCE/AHS/ASC Structures, Structural Dynamics and Materials Conference*, vol. 11, pp. 7604–7612, 2006.
- [31] W. Yim and S. N. Singh, "Variable structure adaptive control of a cantilever beam using piezoelectric actuator," *Journal of Vibration and Control*, vol. 6, pp. 1029–1043, 2000.
- [32] I. Zeinoun and F. Khorrami, "An adaptive control scheme based fuzzy logic and its application to smart structures," *Smart Material Structures*, vol. 3, pp. 266–276, 1994.
- [33] D. Beale and S. Lee, "The applicability of fuzzy control for flexible mechanisms," *ASME*, vol. 84, pp. 203–209, 1995.
- [34] S. Choi and M. Kim, "New discrete-time, fuzzy-sliding-mode control with applications to smart structures," *Journal of Guidance, Control and Dynamics*, vol. 20, pp. 857–864, 1997.
- [35] K. Cohen, R. Yaffe, T. Weller, and J. Ben-Asher, "Experimental studies on adaptive fuzzy control of a smart structure," *Journal of Vibration and Control*, vol. 8, pp. 1071–1083, 2002.
- [36] A. Ganguli, S. Jhawar, and P. Seshu, "Shape control of curved beams using piezoelectric actuators," *Proceedings of SPIE - The International Society for Optical Engineering*, vol. 5062, no. 1, pp. 297–304, 2002.
- [37] M. Sharma, S. P. Singh, and B. L. Sachdeva, "Theoretical and experimental investigation of fuzzy logic based active vibration control of beams," *Proceedings of the ASME Design Engineering Technical Conference*, vol. 5, pp. 2109–2117, 2003.
- [38] M. Trabia and W. Yim, "Fuzzy logic control of projectile fin angle using piezoelectric actuator," *ASME Dynamic Systems and Control Division*, vol. 73, pp. 613–618, 2004.
- [39] M. Trabia, "A hybrid fuzzy simplex genetic algorithm," *ASME Journal of Mechanical Design*, vol. 126, pp. 969–974, 2004.
- [40] M. Trabia and X. Lu, "A fuzzy adaptive simplex search optimization algorithm simplex genetic algorithm," *ASME Journal of Mechanical Design*, vol. 123, pp. 216–225, 2001.
- [41] M. Trabia, S. Parimi, and W. Yim, "Inverse dynamics-based fuzzy logic control of a projectile smart fin," *ASME 20th Biennial Conference on Mechanical Vibration and Noise*, 2005.
- [42] W. Yim, S. N. Singh, and M. Trabia, "Adaptive control of projectile fin angle using piezoelectric beam actuator," *Proceedings of SPIE - Smart Structures and Materials*, 2004.
- [43] D. C. Hyland, J. L. Junkins, and R. W. Longman, "Active control technology for space structures," *Journal of Guidance, Control and Dynamics*, no. 16, pp. 801–821, 1993.

- [44] H. Kaufmann, I. Barkana, and K. Sobel, *Direct Adaptive Control Algorithms*. Springer-Verlag, New York, 1998.
- [45] I. H. Mufti, "Model reference adaptive control for large structural systems," *AIAA Journal of Guidance, Control and Dynamics*, pp. 507–509, 1987.
- [46] A. M. Annaswamy and D. J. Clancy, "Adaptive control and stabilization of elastic spacecraft," *IEEE Transactions on Aerospace and Electronic Systems*, vol. 35, pp. 115–122, 1999.
- [47] A. Kelkar and S. Joshi, "Control of nonlinear multibody flexible space structures," *Springer, New York*, 1996.
- [48] S. N. Singh and R. Zhang, "Adaptive output feedback control spacecraft with flexible appendages by modelling error compensation," *Acta Astronautica*, no. 54, pp. 229–243, 2004.
- [49] S. N. Singh and A. D. Araujo, "Adaptive control and stabilization of elastic spacecraft," *IEEE Transactions on Aerospace and Electronic Systems*, no. 35, pp. 115–122, 1999.
- [50] S. Mani, S. Singh, S. K. Parimi, W. Yim, and M. Trabia, "Adaptive rotation of a smart projectile fin by piezoelectric beam actuator," *Journal of Vibration and Control*, 2005.
- [51] J. Arters, J. Vinson, T. Bogetti, P. Weinacht, W. Drysdale, and O. Rabinovitch, "Preliminary design of piezo-activated composite sandwich fins for projectile maneuverability," *46th AIAA/ASME/ASCE/AHS/ASC Structures, Structural Dynamics, and Materials Conference*, 2005.
- [52] A. Hickman, J. Vinson, T. Bogetti, P. Weinacht, W. Drysdale, and O. Rabinovitch, "Continued efforts in the development of piezo-activated composite sandwich fins," *47th AIAA/ASME/ASCE/AHS/ASC Structures, Structural Dynamics, and Materials Conference*, 2006.
- [53] M. Trabia, W. Yim, P. Weinacht, and V. Mudupu, "Control of a projectile smart fin using an inverse dynamics-based fuzzy logic controller," *ASME 21th Biennial Conference on Mechanical Vibration and Noise*, 2007.
- [54] R. B. Williams, "Nonlinear Mechanical and Actuation Characterization of Piezoceramic Fiber Composites," PhD Dissertation, Virginia Tech, Blacksburg, VA, March 2004.
- [55] N. W. Hagood and A. A. Bent, "Development of piezoelectric fiber composites for structural actuation," *34th AIAA/ASME/ASCE/AHS/ASC Structures, Structural Dynamics, and Materials Conference*, pp. 3625–3638, 1993.
- [56] Smart-Material, "<http://www.smart-material.com/smart-choice.php?from=products>," 2007.
- [57] D. L. L. Tao, *A first course in the finite element method using algor*. PWS Pub. Co, 1997.
- [58] MATLAB, <http://www.mathworks.com/access/helpdesk/help/toolbox/ident/>.

- [59] Y. Shen and A. Homaifar, "Vibration control of flexible structures with pzt sensors and actuators," *Journal of Vibration and Control*, no. 7, pp. 417–451, 2001.
- [60] G. Tao, *Adaptive Control Design and Analysis*. Wiley-IEEE Press, 2003.
- [61] A. L. Fradkov, I. V. Miroshnik, and V. O. Nikiforov, "Non linear and adaptive control of complex systems," *Kluwer Academic Publishers*, 1999.
- [62] M. Vidyasagar, "Non linear systems analysis," *SIAM Publications*, vol. 8, 2002.
- [63] A. Bobstov, N. Nikolaev, and O. Slita, "Adaptive control of liberation angle of a satellite," *Mechatronics*, no. 17, pp. 271–276, 2007.
- [64] A. Bobstov and N. Nikolaev, "Design of the control of nonlinear systems with functional and parameter uncertainties," *Automat Rem Contr*, vol. 66, no. 1, pp. 108–118, 2005.
- [65] K. Uchino, "Piezoelectric actuator and ultrasonic motors," *Norwell (MA): Kluwer Academic Publishers*, 1997.

VITA

Graduate College
University of Nevada, Las Vegas

Venkat Mudupu

Local Address:

15000 Park Row, 537
Houston, TX 70084

Home Address:

16-1-419/1
Reddy Street
Saidabad
Hyderabad, India 500059

Degrees:

Bachelor of Technology, Production Engineering, 2001
Jawaharlal Nehru Technological University, Hyderabad, India

Master of Engineering, Automation & Robotics, 2004
Osmania University, Hyderabad, India

Publications:

V. Mudupu, M. Trabia, W. Yim, P. Weinacht, "Design and Validation of Fuzzy Logic Control For A Smart Projectile Fin with A Piezoelectric Macro-Fiber Composite Actuator" Smart Mater. Struct. (17), April, 2008.

V. Mudupu, S. Singh, W. Yim, "Adaptive Control of A Smart Projectile Fin with Unknown High-Frequency Gain By Piezoelectric Actuation" ASME International Mechanical Engineering Congress and Exposition, Nov. 11-15, 2007, Seattle, Washington.

V. Mudupu, M. Trabia, W. Yim, P. Weinacht, "Design and Validation of Fuzzy Logic Control For A Smart Projectile Fin" ASME International Mechanical Engineering Congress and Exposition, Nov. 11-15, 2007, Seattle, Washington.

V. Mudupu, M. Trabia, W. Yim, P. Weinacht, "GA-Based Fuzzy Logic Control For A Smart Fin of A Projectile" ASME 21st Biennial Conference on Mechanical Vibration and Noise (VIB), Sept. 4-7, 2007, Las Vegas, Nevada.

M. Trabia, W. Yim, P. Weinacht, V. Mudupu, "Control Of A Projectile Smart Fin Using an Inverse Dynamics-Based Fuzzy Logic Controller" ASME 21st

Biennial Conference on Mechanical Vibration and Noise (VIB), Sept. 4-7, 2007, Las Vegas, Nevada.

V. Mudupu, S. Singh, and W. Yim, "Theoretical and Experimental Adaptive Control of a Smart Projectile Fin with Unknown High-Frequency Gain" under review for the Journal of IEEE/ASME Transactions on Mechatronics.

V. Mudupu, M. Trabia, W. Yim, M. Sa'adeh, "Modeling Of A Piezoelectrically Actuated Smart Projectile Fin Hysteresis" 3rd International Conference On Mechatronics, Dec. 18-20, 2008, Kuala Lumpur, Malaysia.

Dissertation Title:

Experimental and Theoretical Control Of A Smart Projectile Fin Using Piezoelectric Bimorph Actuator

Dissertation Examination Committee:

Chairperson, Dr. Woosoon Yim, Ph.D.

Chairperson, Dr. Mohamed B. Trabia, Ph.D.

Committee Member, Dr. Brenden J. O'Toole, Ph.D.

Committee Member, Dr. George F. Mauer, Ph.D.

Committee Member, Dr. Samir Moujaes, Ph.D.

Graduate Faculty Representative, Dr. Sahjendra N. Singh, Ph.D.